Performance prediction for turbomachines

Martin Christopher Gunton

PERFORMANCE PREDICTION FOR TURBOMACHINES

by Martin Christopher Gunton
Ph.D. Thesis, University of Durham, 1981

A B S T R A C T

In this computer-aided study, existing methods of determining the fluid flow in axial flow turbomachines are examined, and the Consistent Loss Model of Bosman and Marsh is here applied to both duct flow and intrablade applications of the Streamline Curvature technique. The resulting equations are presented in a form similar to that of the conventional equations, thus providing for easy modification of existing Streamline Curvature method computer programs.

Interpretation of the equations shows that the mean flow through a blade row passage cannot follow a parabolic path between the blade inlet and outlet flow angles, as is commonly assumed, but must maintain as continuous the streamwise derivative of angular momentum. Procedures are described to design three-dimensional blade shapes from basic aerofoil data, and to derive realistic intrablade mean stream surfaces, including allowances for flow deviation and secondary flow.

Numerical techniques are presented which have been developed for closely-spaced intrablade calculation grids, to obtain faster convergence than by conventional schemes in Streamline Curvature calculations. The computer program is intended for analysing multi-stage axial flow compressors; tests are presented of simple analytical cases and experimental data for isolated rows of blades, of a 'swan-necked' duct, and of a three-row experimental compressor.

Three-dimensional flow calculation methods are reviewed with reference to the limitations inherent in applying them to axial flow turbomachines. Suggestions are made for future work.

PERFORMANCE PREDICTION FOR TURBOMACHINES

by

Martin Christopher Gunton, B.Sc., A.M.I.Mech.E.

Thesis submitted for the degree of Doctor of Philosophy

of the University of Durham

Department of Engineering Science
University of Durham

1981

CONTENTS

LIST OF FIGURES

PERFORMANCE PREDICTION FOR TURBOMACHINES

Declaration

The material offered in this thesis is the work solely of the author. None of the material has previously been submitted by the author for any degree in this or any other university.

A C K N O W L E D G E M E N T S

The author expresses his gratitude to Professor H. Marsh, of the Department of Engineering Science at the University of Durham, for his encouragement and expert guidance throughout the studies reported here. He would also like to thank Dr. D. G. Gregory-Smith, of the same Department, for many useful discussions and for making available a computer program to perform secondary flow calculations.

Periods spent at Rolls-Royce Limited, Derby, and liaison at other times, have been directed with interest by Dr. R. Hetherington (now at the Cranfield Institute of Technology) and Dr. P. Stow. The author thanks them for their support and for furnishing information on the Company's computing methods.

The computing content of the work has been conducted at the Computer Unit of the University of Durham, and Messrs. B. Lander and R. Sheehan are thanked for their assistance when things have been going awry.

The project has been funded by a Co-operative Award in Science and Engineering, from the Science Research Council and Rolls-Royce Limited.

"Thank you" too to Miss Christine Plummer for her typing of the manuscript.

NOMENCLATURE

A	Calculation grid aspect ratio
B	Flow blockage factor
C	Streamline curvature (units: length^{-1})
C_p	Specific enthalpy per degree
C_v	Specific internal energy per degree
$\underline{D}$	Dissipative loss force
$\underline{F}$	Body force
I	Rothalpy: $I = h_o - \omega r V_u$
K, L	Property functions in equation 3.1
M	Mach number
N	Co-ordinate on S2 stream surface, normal to flow; number of blades
Q	Energy transfer by heat
R	Gas constant
S	Co-ordinate on S2 stream surface, in flow direction
T	Absolute temperature
$\underline{U}$	Blade speed: $\underline{U} = \underline{\omega} r$
$\underline{V}$	Absolute fluid velocity
$\underline{W}$	Blade-relative fluid velocity: $\underline{W} = \underline{V} - \underline{U}$
a	Speed of sound; length along blade chord to point of maximum camber
b	Blade maximum camber
c	Blade chord
e	2.1828
f	General function; circumferential force component: $f = F_u + D_u$
f'	Optimum relaxation factor
h	Enthalpy
$\underline{j}$	Unit vector in θ direction
k	General constant; constant in blade design logarithmic spiral: $k = \cot \tau$
m	Meridional co-ordinate
$\dot{m}$	Mass flowrate
n	Co-ordinate normal to both N and S
p	Pressure
q	General property; co-ordinate on conical blade design surface

r	Radial co-ordinate
s	Entropy; blade pitch
t	Time; blade thickness
z	Axial co-ordinate
Δ	A finite change
Ω	Angular velocity in solid-body-rotational flow
α	Absolute flow angle: $\tan \alpha = V_u/V_z$
α'	Blade angle on constant-radius section
β	Blade-relative flow angle: $\tan \beta = W_u/W_z$
γ	Isentropic index
δ	A small change; flow deviation at blade exit
ϵ	Flow angle: $\tan \epsilon = V_r/V_z$
ζ, η	Co-ordinates of conformal mapping in blade design
θ	Circumferential co-ordinate
λ, μ	Angles on intrablade stream surface defined by equation 3.8. N.B. $\tan \mu = - \tan \beta - \tan \epsilon \tan \lambda$
$\underline{\nu}$	Unit vector in n direction
ξ	Vorticity
π	3.14159...
ρ	Density
σ	Angle on conical blade design surface: $\tan \sigma = \tan \alpha' \cos \epsilon$
τ	Blade stagger angle
υ	Blade camber angle
φ	Sweepback angle of calculation station; Angle in blade design logarithmic spiral exponent $\varphi = \theta \sin \epsilon$
ψ	Stream function
$\underline{\omega}$	Rotor angular velocity

Suffixes

d	Datum value
m	Meridional component
r	Radial component
u	Circumferential component
z	Axial component
o	Stagnation value; datum value in blade design

1	Blade entry condition
2	Blade exit condition
max	Maximum value
min	Minimum value
$\underline{\ }$	(Underline) Vector quantity

Superscripts

*	Howell's nominal operating condition
',",etc.	First, second, etc. derivatives
$\overline{\ }$	(Overline) Passage-averaged value
$\sim$	(Tilda) Mass-averaged value

Operators

∇	The del operator
$\frac{D}{D}$	Derivative with space and time along streamline
$\frac{d}{d}$	Derivative
$\frac{\partial}{\partial}$	Partial derivative
$\frac{\partial}{\partial}$	Special partial derivative following stream surface

Other symbols are used locally as defined in the text.

CHAPTER 1

Introduction

1.1 The Context Of The Present Work

The development of the gas turbine aero-engine over the last forty years has demanded theoretical and technological advances in many fields, including aerodynamics. Research effort directed at aero-engines has benefitted the design of other types of turbomachine, such as land-based steam, gas or water turbines, water pumps and air compressors. The work described here is a study of the fluid flow through the rotating or stationary blade rows of axial-flow turbomachines in general, but with application to the aero-engine multi-stage compressor in mind.

The analysis of turbomachinery flow used in early design methods, during and after the second world war, was necessarily simple since calculating machines available were mechanical and so very slow. The usual method used was the Simple Radial Equilibrium analysis for compressible flow. The culmination of manual calculation techniques, in the late 1940's,was the Actuator Disc Theory of Hawthorne and Horlock, generally limited to incompressible flow, which was also one of the first flow models to be used on electronic computers.

In the early 1950's, Wu conceived a very complete theoretical treatment of the fluid mechanics and thermodynamics of turbomachinery; it could be implemented only in very limited form until the 1960's, by which time computers had been developed with greatly increased storage capability, and much higher running speeds. One method developed in that decade to employ part of Wu's analysis was the Streamline Curvature technique, produced by Silvester and Hetherington at Rolls-Royce Limited, and by workers in the U.S.A. such as Novak, or Smith. The main alternative method, using the same flow model as Streamline Curvature, is the Matrix Through-Flow approach developed at the National Gas

Turbine Establishment by Marsh. The term "through-flow" has come to indicate the capability of performing flow calculations within rows of blades, and not only in the lengths of duct between them. A different formulation of the problem from that in the two methods just named, is used in the Time-Marching method of Denton, which allows solutions to be found for transonic flows.

Development in the 1970's of computers with further increased speed and storage has made possible the use of more advanced flow models. The present state of the art allows the calculation of three-dimensional flow fields, to varying degrees of realism, for centrifugal impellers or other single row machines. The available computing power now approximately matches the present understanding of fluid behaviour, indicating that new research developments in fluid mechanics may now be usefully called for. A more full historical survey is given in Chapter 2.

Improved flow modelling may be considered either as a means of reducing the development time required in an aero-engine design, or as a path towards achieving better engine performance.

1.2 Scope And Application

Present methods of calculating fluid flow within turbomachine ducts and rows of blades are examined, and improvements made in certain respects:

(i) An improved analysis with a consistent model for flow losses was proposed by Horlock (1971) and developed by Bosman and Marsh (1974) for the Matrix Through-flow solution technique. The analysis is here applied to the alternative and widely-used Streamline Curvature method.

(ii) Calculation methods are presented for locations within blade rows using the consistent loss model analysis and the Streamline Curvature technique. The blade shape is generated in

full from basic aerofoil data, but the flow surface used for calculation allows for exit flow angle deviation, and is shaped to maintain as continuous the streamwise derivative of angular momentum at blade entry and exit.

(iii) Provision is made for flow angle adjustments within the blade rows resulting from secondary flows, the changes being calculated separately by a computer program due to Gregory-Smith (1977).

(iv) The commonly-used finite difference numerical technique is employed, but with empirically-developed procedures to provide faster convergence of the solution than conventional Streamline Curvature methods.

(v) The applicability of recently-developed three-dimensional calculation methods to axial-flow turbomachines is assessed briefly.

Application is to machines of the axial-flow type, and although both turbines and compressors may be analysed, the multi-stage axial-flow compressor is modelled rather than the turbine because, of the two, compressor design is found to be the more sensitive; the fluid flow against increasing static pressure can result in such phenomena as the separation of the flow from blade surfaces. Some of the overall assumptions made in the analysis, for example that of adiabatic flow (no energy transfer by heat through duct walls or blade surfaces), are reasonably applied to compressors but not to turbines, in which gas temperatures are much higher and cooling of blades and duct walls is often required.

Mathematical analysis of the aerothermodynamics of turbomachines may be used in two major ways: one is to predict the performance of a machine at the design stage, to optimise performance with the least

development work; the second is in the analysis of experimental results from machines under test. The present work is biased towards the design application. A computer program has been written in the PL/1 language to demonstrate the new analysis.

1.3 Principle of Operation of Axial-Flow Compressors and Turbines

The fluid flow in an axial-flow turbomachine, whether a compressor or turbine, has components of velocity parallel to the axis of rotation and in the tangential direction, but usually little radial velocity.

Fluid passing through an annular row of curved blades is deflected tangentially and by Newton's second law of motion, the rate of change of angular momentum of the fluid produces an opposite torque reaction on the row of blades.

Shaft work is produced in a turbine rotor, which turns because of the torque acting on its blades. There is in this case an accompanying drop in the total enthalpy in the fluid, usually appearing as drops in both temperature and pressure.

In a non-rotating - stator - blade row the torque does no work, so in the absence of flow losses there is no change of total enthalpy; stators are used to effect changes in fluid angular momentum and other properties, for subsequent entry to compressor rotors or turbines.

A compressor rotor is driven by a powered shaft to impart tangential and axial velocity to the fluid. The power is absorbed by the fluid as increased total enthalpy. In the following stator, the tangential velocity component is reduced greatly and part of the kinetic energy converted to a rise in static pressure.

A pair of blade rows, rotor and stator, is called a stage, and the ratio of the enthalpy change in the rotor to the enthalpy change in the stage is called the degree of reaction of the stage.

CHAPTER 2

Development of Flow Calculation Methods

2.1 Velocity Triangles

Techniques for flow calculation have generally been limited by the amount of calculation which could be performed in a reasonable time, and early methods for steam turbine design used simple models suitable for hand calculation.

Because of the annular shape of turbomachine flow passages, tangential velocity components and flow angles vary with radius, as do the values of other properties of the flow. In machines such as high pressure axial-flow steam turbines, the ratio of the inner to outer radii of blade rows - the hub:tip ratio - is often close to unity, and the flow conditions vary little across the blade span.

A simple two-dimensional design procedure applied at mid-span was found to be sufficiently accurate. Representing velocity vectors as lines in geometrical constructions, as in Figure 2.1, it is possible to calculate unknown flow angles, or other velocities, required for designing blade shapes. In particular this method gives a clear visualisation of the effect of rotor blade speed on the fluid entry and exit to and from rotors.

2.2 Radial Equilibrium Theory

By the 1940's attempts were made to devise three-dimensional methods to cater for the new interest in gas turbines with lower hub:tip ratios, but usable techniques were still those requiring relatively little calculation.

The classical method developed was the Radial Equilibrium Design of Cohen and White (1943), described by Horlock (1966), based on an

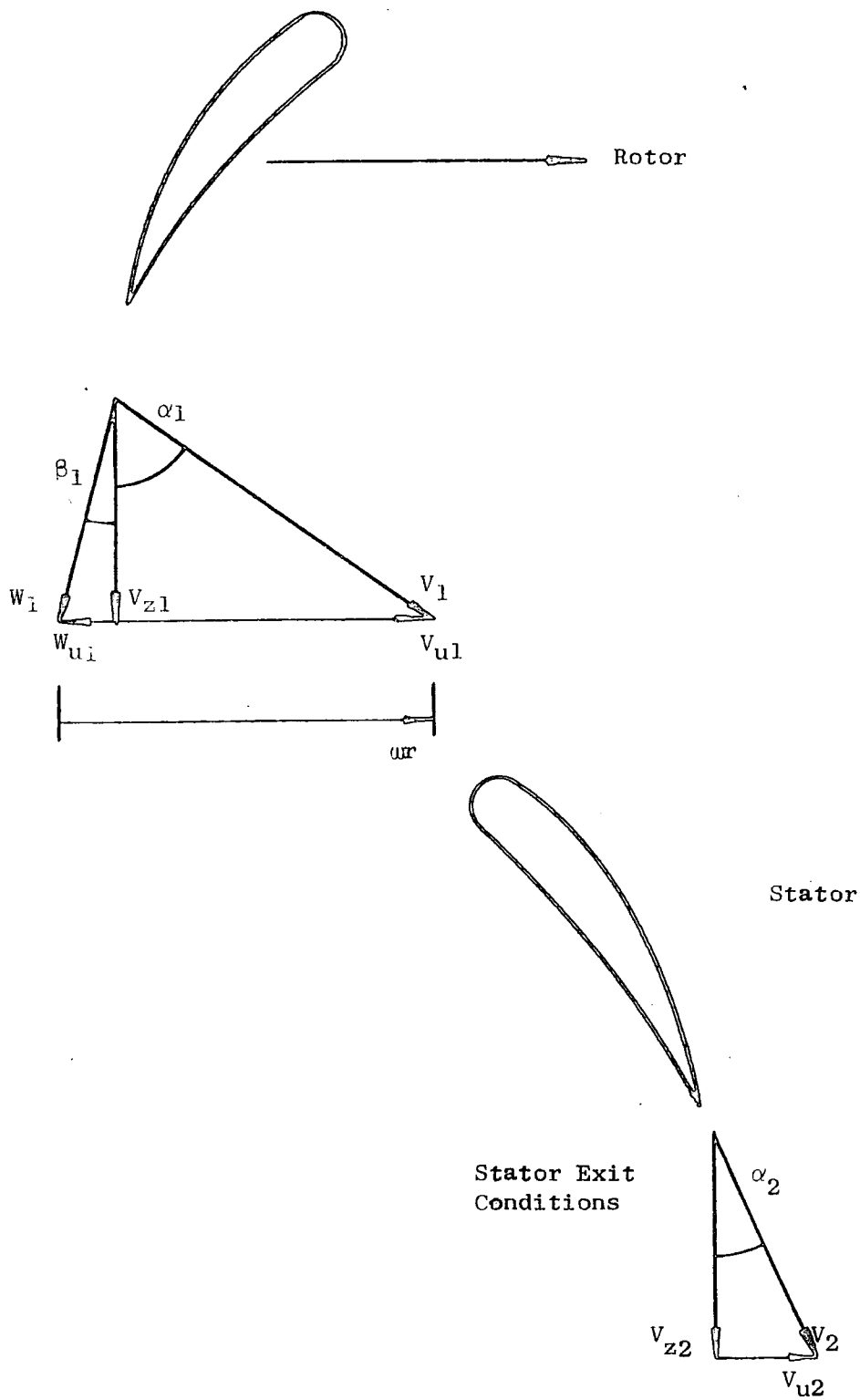

FIGURE 2.1: VELOCITY TRIANGLES

application of Newton's second law of motion in the radial direction, at points just upstream and downstream of blade rows. It is necessary to assume that at the calculation points the streamlines are straight, and parallel to the machine axis, i.e. that the radial velocity is zero and unchanging with axial distance.

Given a radial distribution of streamlines upstream of a blade row, and the variation of inlet and outlet flow angle, the equation

$$\frac{1}{\rho}\frac{dp}{dr} = \frac{V_u^2}{r}$$

may be used to find the density distribution at outlet, and the velocity and streamline positions. This equation is valid for compressible flow provided that the radial velocity is zero.

For a blade row with 'free vortex' circumferential velocity distributions at inlet and outlet - i.e. rV_u = constant with radius - there is no net shift of the streamlines, and such blade designs were commonly used because of the ease of aerodynamic design, though they are poor mechanically because of the large twist necessary on the blade shape.

In general, changes in fluid density are accompanied by flaring of the sides of the duct to vary the annulus flow area and maintain axial velocities, but this introduces significant radial velocities so that the assumption of zero radial velocity at calculation planes is no longer valid. Another objection to the radial equilibrium method is that it cannot model interference of the flow caused by adjacent rows of blades, because it is assumed that all radial motion occurs within blade rows, whereas in most turbomachines of low hub:tip ratio appreciable flow redistribution can be measured outside blade rows for distances comparable to the chord length.

2.3 Actuator Disc Theory

The major defects of radial equilibrium analysis were tackled in the Actuator Disc Theory comprehensively descibed by Horlock (1978). Here the blade row is represented by an infinitely thin disc, rotating or stationary, positioned where the real blade row would be, and it is imagined that a step-change in tangential velocity occurs across the disc. The effect of neighbouring blade rows is included in the theory but there are drawbacks - the radial velocity is still assumed to be small, and the flow must have small vorticity. The method works for compressible flow, but only if the duct walls are of constant radius, despite attempts to allow flared walls, for the following reason:

Referring to Figure 2.2, suppose that at point 1 compressible fluid is flowing close to the machine wall with velocity components V_z, V_r, V_u. A step-change in V_u occurs as the flow passes through the actuator disc, and so there is a sudden change in density. For continuity of mass flow rate, there must be a change in V_z so that the product ρV_z remains constant. V_r is invariant, there being no radial forces allowed in the actuator disc theory. Hence the flow angle ε changes abruptly, and the predicted flow no longer follows the casing geometry; indeed, it may be calculated as passing right through it!

2.4 Wu's General Theory

Wu (1952) published a theory for calculating the full three-dimensional flow field in turbomachines. At the time adequate computers did not exist to solve problems by his approach, but since then several methods of solution have been based on this analysis, which is summarised below.

The three-dimensional flow pattern of an inviscid fluid can be found by solving the following equations:

(i) Flow Continuity -

$$\frac{\partial \rho}{\partial t} + \nabla \cdot (\rho \underline{W}) = 0 \quad \text{if no fluid is entering or leaving} \qquad (2.1)$$

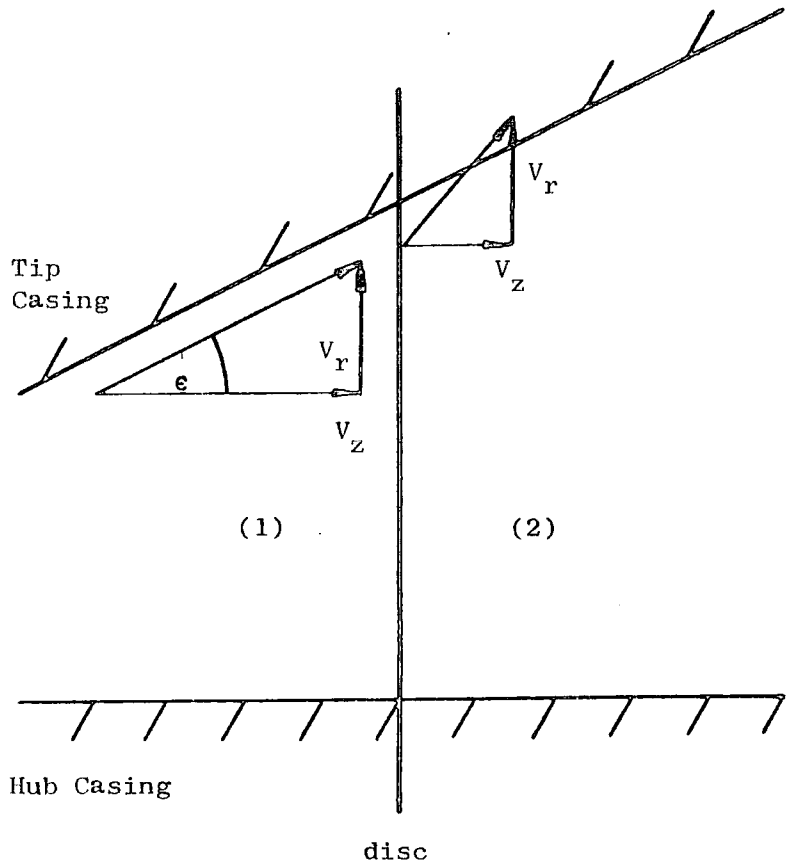

FIGURE 2.2: COMPRESSIBLE FLOW THROUGH ACTUATOR DISC IN FLARED DUCT

(ii) Motion - Newton's second law

$$\frac{D\underline{W}}{Dt} - \underbrace{\omega^2 r}_{\text{centripetal acceleration}} + \underbrace{2\underline{\omega} \times \underline{W}}_{\text{Coriolis acceleration}} = -\frac{1}{\rho}\nabla p \qquad \ldots (2.2)$$

From the first and second laws of thermodynamics the right hand side may be expressed as

$$-\frac{1}{\rho}\nabla p = -\nabla I + T\nabla s .$$

This law of motion gives three equations when expanded into three-dimensional co-ordinates, such as the cylindrical set r, θ, z, one in each co-ordinate direction.

(iii) Energy

$$\frac{DI}{Dt} = 0 \qquad \ldots (2.3)$$

if the flow is adiabatic.

This means that the rothalpy (see Appendix A) is constant along a streamline.

(iv) State

One of several forms; a suitable one is:

$$\frac{\rho}{\rho_o} = \left(\frac{h}{h_o}\right)^{\frac{1}{\gamma-1}} e^{(s_o - s)/R} \qquad \ldots (2.4)$$

where the suffix $_o$ denotes some reference value.

The assumption in (iii) of adiabatic flow is widely used and is reasonable for compressor applications, though less so for turbines. If there is a heat input of Q per unit mass per unit time, then $\frac{DI}{Dt} = Q$. Smith (1966) considers non-zero Q, but notes that the effects of heat addition on the radial equilibrium equation are expected to be small. Irreversibility will here be introduced into the equations of motion by including a frictional force against the direction of fluid flow.

It is required to find the three velocity components, V_z, V_r and V_u, and the fluid properties ρ, h and s. The velocity components and any two of the fluid properties may be found from the five equations (i) to (iii). The equation of state, (iv), shows the relationship between ρ, h and s so that the third of them may be found.

The three equations of motion and the energy equation can be combined to give an equation which states that in reversible adiabatic flow the entropy of the fluid remains constant along a streamline, but in irreversible flow it varies in some empirical way. Any four of these five equations (energy, entropy and three of motion) may then be used, the fifth being automatically satisfied.

If the frictional force modelling the flow losses is assumed to act in the (-z) direction, i.e. axially upstream, then by choosing the surplus equation above to be that of motion in the z direction, it is unnecessary to evaluate the frictional force.

The derivation of energy equation 2.3 is based on adiabatic flow, and in flow with losses its application along streamlines is valid only if the fluid is not heat-conducting. However, the mass flow averaged rothalpy in the flow field is constant if there is no external heat source, and equation 2.3 is used as a workable approximation along streamlines. These points are explained more fully in Appendix A.

2.5 Time-Dependence and Axial Symmetry

Equation 2.2 contains components in all three coordinate directions, and also time-dependence. A simplifying premise proposed by Wu (1952) is that the flow is taken as steady, so that all time derivatives vanish. This assumption is reasonable for an isolated row of blades with steady inlet flow conditions. However, circumferential variations of properties at exit from a blade row, as generally occur, will appear as unsteady flow to a downstream row of blades moving relative to the first row.

The assumption of steady flow is incorporated in many numerical methods based on Wu's (1952) analysis, but in any example with relative motion of blade rows, it must be coupled for consistency with another assumption that either all circumferential variation of properties is mixed out in the flow length between adjacent rows of blades, or that the flow pattern is axially symmetrical, when no circumferential variations of flow exist anywhere.

Between adjacent pairs of blades in a blade row, some general property, say q, varies circumferentially, typically in a repeating sawtooth pattern. A constant value of q may be approached by considering a row with very many blades, the thickness of each being greatly reduced to maintain the original thickness/pitch ratio. The sawtooth profile is now much reduced in scale, but it should be appreciated that the 'ripple' does not disappear, and the circumferential gradient of q is unchanged. As the number of blades tends to infinity, each exerts an infinitessimal force on an infinitessimal amount of fluid, thus producing a deflection of the flow.

In axisymmetric flow there are no such circumferential gradients, and no blades to effect change in angular momentum. Fluid is therefore redirected by a circumferentially-uniform 'body force' $\underline{F}$, introduced into the equations of motion, acting perpendicularly to the flow and thus it has components in the three coordinate directions. Ratios of the components are related to various flow angles. $\underline{F}$ is zero where there are no blades, as in duct flow.

The distinction between the many-bladed and the axisymmetric flow models is discussed by Horlock and Marsh (1971). Practical axisymmetric flow may be imagined in mercury flowing through a tube in a magnetic field, while conducting electricity, swirling flow being produced by magnetohydrodynamic forces.

2.6 Stream Surfaces

Wu (1952) proposes that the three-dimensional flow solution be obtained by combining sets of two-dimensional flows which lie on relative 'stream surfaces' through which no flow passes. There are two kinds of stream surface, illustrated in Figure 2.3, and denoted S1 and S2. Type S1 surfaces intersect with a z-plane, either upstream or about midway through a blade row, to form a circular arc. Type S2 surfaces form radial lines at one such intersection.

The assumption of axisymmetric flow implies that all S2 surfaces are identical, and a solution is required for only one S2 surface, called the 'mean' S2 stream surface. It also implies that the S1 surfaces are surfaces of revolution, with no twist in the circumferential direction. In duct flow these assumptions are quite satisfactory, but within blade rows the blade surfaces form flow boundaries, and in general the suction side of one blade has a different shape from the pressure side of its neighbour.

The notional shape of the mean S2 surface in a blade row is a matter of some debate - see Chapter 9 and also Horlock and Marsh (1971) - but in the present work it is based on the shape of the design camber surface of the blades in the row, with modifications for trailing edge flow angle deviation, and for blending of the circumferential curvature of the streamlines at entry and exit; the necessity for this is demonstrated in Chapter 4. The blade force $\underline{F}$ acts perpendicularly to the mean S2 surface everywhere.

For duct flow, angular momentum is conserved along a streamline if there are no flow losses, or else changes in angular momentum may be related to losses via entropy as mentioned in Section 2.4. Hence changes in flow direction are defined from the equations of motion. Within a blade row the fluid is assumed to follow the mean stream surface, whose

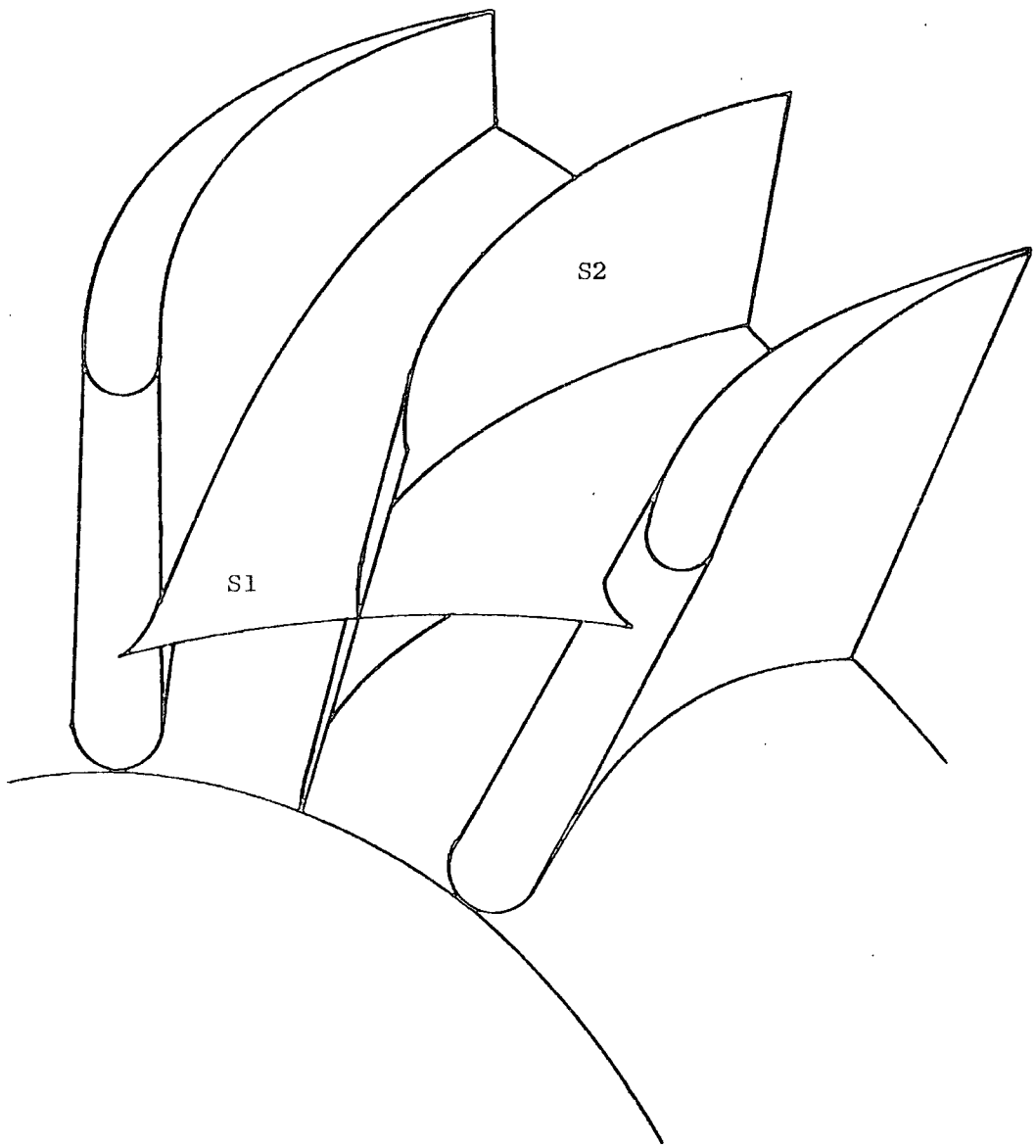

FIGURE 2.3: WU STREAM SURFACES TYPES S1 AND S2

geometry will usually depart from free-flow paths, and so over-ride considerations of conserving angular momentum. There is thus a geometrical condition relating the velocity components at any point within a blade row, and so a second of the six original equations in the analysis may be replaced. Since all θ-derivatives are here assumed to be zero, the circumferential equation of motion is the one to eliminate, so that the only equation of motion remaining is that in the radial direction. Such a substitution cannot be made in the duct flow analysis, as there is no geometrical constraint on flow direction.

2.7 Numerical Solutions Based on Wu's Theory

Two different methods of solution of the above-described formulation of the problem were developed, one by workers such as Silvester and Hetherington (1966) at Rolls-Royce Limited, and another by Marsh (1968) at the National Gas Turbine Establishment. Both obtain information about the overall flow pattern, but do so by different numerical techniques. For a comparison of the two see Marsh (1970).

Marsh's (1968) Matrix Through-Flow method uses the stream function as the main unknown, with the boundary conditions that the non-dimensional stream function is zero on the duct wall at the machine hub, and unity on the wall by the blade tips. Starting from a guessed pattern of intermediate stream function values, the radial equation of motion is expressed as a quasi-linear differential equation in stream function:

$$\frac{\overline{\partial^2 \psi}}{\partial r^2} + \frac{\overline{\partial^2 \psi}}{\partial z^2} = q(r,z) \quad .$$

This equation is solved iteratively by a finite difference method, manipulation of numbers being performed by matrices. The bar superscript over derivatives denotes the special derivative following a stream surface as described in Appendix B.

Silvester and Hetherington's (1966) method is known as the Streamline Curvature technique because although the main unknown is a fluid velocity term, it is necessary to perform the sensitive calculation of the slope and curvature of the streamlines at calculation points. The radial equation of motion is again used, this time cast into a form like:

$$W_m \frac{\partial W_m}{\partial r} + W_m^2 K(r) + L(r) = 0$$

This equation is solved iteratively, starting from an initial estimate of the functions K(r) and L(r). The procedures developed to reach a converged solution are the concern of Chapter 6.

It may be noted that the degree of swirl in duct flow has no effect on the choking of the flow which occurs as the fluid reaches sonic speed. Thus for duct flow the limiting case is of the meridional Mach number reaching unity. For intrablade flow, the flow channel is defined by the blade surfaces, and choking occurs when the overall relative Mach number is unity. Both the matrix through flow and the streamline curvature methods raise problems in transonic flow. In the matrix through-flow approach, the function $q(r,z)$ involves density terms, for which there are two possible solutions, one for relative Mach number less than unity (subsonic), the other for supersonic flow. The terms K(r) and L(r) in the streamline curvature method contain denominators of $(1 - M_m^2)$, which would result in a division by zero at $M_m = 1$. Thus both techniques are in general applied to subsonic meridional flows only.

CHAPTER 3

Mathematical Analysis For The Streamline Curvature Method, With An Improved Loss Model

3.1 Loss Measurement

Real fluid flow in turbomachines is irreversible, flow losses occurring because of skin friction at metal surfaces (in ducts and on blades), turbulent mixing in wakes downstream of blade rows and fluid friction in areas of shear flow. If the flow is assumed to be adiabatic, but irreversible then it is not isentropic, and entropy changes may be found using the formula

$$s_2 - s_1 = C_p \ln\left(\frac{T_{o2}}{T_{o1}}\right) - R \ln\left(\frac{p_{o2}}{p_{o1}}\right)$$

This relationship of thermodynamic properties may be applied between two points not necessarily on the same streamline. However, in adiabatic flow with C_p constant, $T_{o2} = T_{o1}$ following a streamline in duct or stator flow.

Changes in total pressure are derived from experimental results or largely empirically from known behaviour of similar designs, and it must be borne in mind when applying the following analysis that numerical data to be used in assessing the effects of flow losses are obtained experimentally, from such devices as pressure probes downstream of rows of blades.

The greatest pressure losses in practice occur within blade rows and in the downstream mixing-out of circumferential flow variations built up inside the blade row. Duct losses are found to be small, but are included in the analysis in this chapter. Wall boundary layers are not specifically modelled here, but may be included after a fashion by using high loss values on the hub and tip walls.

3.2 The Loss Model

The equations of motion set out in Section 2.4 do not include any representation of flow losses, except that the elimination of the equation of motion in the axial direction allows the presence of a force acting in the exactly opposite direction, without any component of it appearing in the remaining equations of motion.

It is more realistic to represent flow losses by a dissipative force, $\underline{D}$, as proposed by Horlock (1971), acting against the local relative velocity vector, i.e. in the $(-\underline{W})$ direction. There is often a considerable circumferential component in $\underline{W}$, so the fluid path is very different from the axial direction and, because of spiralling along ducts, path lengths are rather greater than the axial distances covered.

Following the analysis of Bosman and Marsh (1974), a rectangular co-ordinate system is chosen as illustrated in Figure 3.1 with two axes along and across the stream, in its surface (S and N directions) and the third (n direction) normal to the surface. The body force $\underline{F}$ which is necessary for axisymmetric inviscid flow to follow a prescribed stream surface shape, as within blade rows, then acts along the n-axis with no components in the S or N directions. The force $\underline{D}$ acts in the (-S) direction with no components in the N or n directions. Hence the equation of motion in the N direction contains neither body force nor dissipative force components.

The (N, n, S) co-ordinates may be applied to Wu's type S1 or S2 surfaces, but for this axisymmetric treatment of the problem, only the mean S2 surface is considered. Within rotating blade rows, the force $\underline{D}$ is assumed to oppose the flow relative to the moving surface, so the S co-ordinate is aligned to the relative velocity vector $\underline{W}$, not to $\underline{V}$, the absolute velocity vector.

Hong (1980) criticises the dissipative force approach to modelling losses, concluding that the force does not follow the direction of

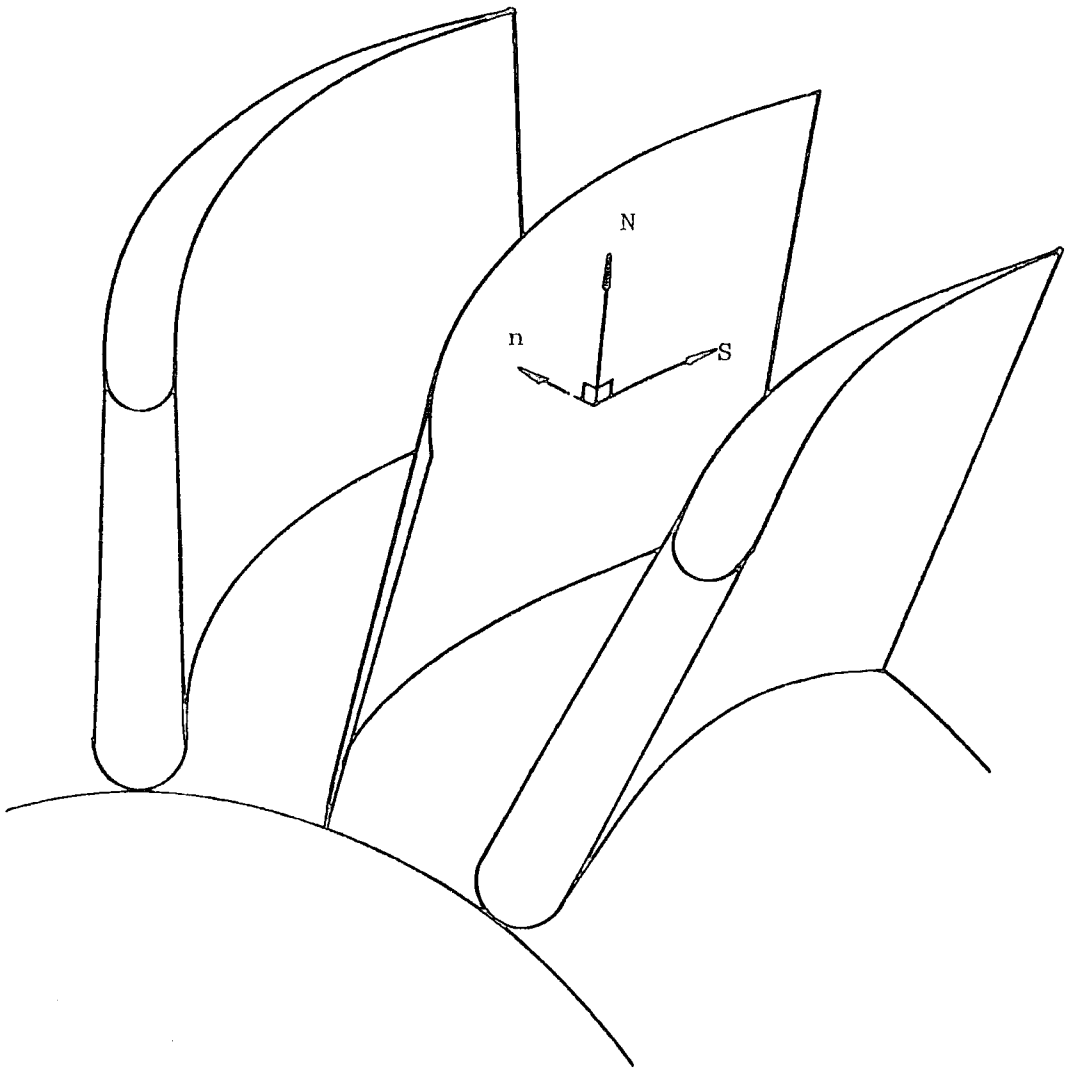

FIGURE 3.1: (N,n,S) CO-ORDINATES ON S2 STREAM SURFACE

($-\underline{W}$), though this appears to be reasoned from general rheological considerations. He models the dissipative force as a tensor, not a vector, and fluid tensor analysis allows the generation of shears perpendicular to the primary shear. Such behaviour is characteristic of non-Newtonian fluids, but the loss model proposed here, utilising the force vector $\underline{D}$, is valid for Newtonian fluids such as air.

3.3 Intrablade Flow - Formulation of N-direction Equation of Motion

Bosman and Marsh (1974) set out an application of the improved loss model to the equations for the matrix through-flow analysis, and obtained equations of motion in the (N, n, S) co-ordinates similar to those in the conventional (r, θ, z) co-ordinates.

In this section it will be shown that the concept can be manipulated into a form suitable for the streamline curvature technique, resulting in equations of motion which differ from those ordinarily used. The (N, n, S) co-ordinates at any point change their orientation as calculations proceed. Expressing the N-direction equation of motion in terms of (r, θ, z) co-ordinates allows the use of a co-ordinate system which does not shift from iteration to iteration as the calculated flow direction changes.

The form of the radial equilibrium equation derived by Silvester and Hetherington (1966), Smith (1966) and Novak (1967) is summarised by Marsh (1970) as:

$$W_m \frac{\partial W_m}{\partial r} + W_m^2 K(r) + L(r) = 0. \quad \ldots(3.1)$$

We desire a very similar form to this for the N-direction equilibrium equation.

Initially following the analysis of Bosman and Marsh (1974), the three equations of motion in the r, θ, and z directions including the dissipative force $\underline{D}$ are:

$$\frac{W_u}{r}\left[\frac{\partial(rV_u)}{\partial r} - \frac{\partial V_r}{\partial \theta}\right] - W_z\left[\frac{\partial V_r}{\partial z} - \frac{\partial V_z}{\partial r}\right] = \frac{\partial I}{\partial r} - T\frac{\partial s}{\partial r} - D_r \qquad (3.2a)$$

$$\frac{-W_r}{r}\left[\frac{\partial(rV_u)}{\partial r} - \frac{\partial V_r}{\partial \theta}\right] + \frac{W_z}{r}\left[\frac{\partial V_z}{\partial \theta} - \frac{\partial(rV_u)}{\partial z}\right] = \frac{1}{r}\frac{\partial I}{\partial \theta} - \frac{T}{r}\frac{\partial s}{\partial \theta} - D_u \qquad (3.2b)$$

$$W_r\left[\frac{\partial V_r}{\partial z} - \frac{\partial V_z}{\partial r}\right] - \frac{W_u}{r}\left[\frac{\partial V_z}{\partial \theta} - \frac{\partial(rV_u)}{\partial z}\right] = \frac{\partial I}{\partial z} - T\frac{\partial s}{\partial z} - D_z \qquad (3.2c)$$

These equations are to be solved on the mean stream surface and may be expressed in terms of the special derivatives defined in Appendix C, without discarding the θ-derivative terms, which will appear in the components of the body force $\underline{F}$, as also shown in Appendix C.

$$\frac{W_u}{r}\frac{\bar{\partial}(rV_u)}{\partial r} - W_z\left[\frac{\bar{\partial}V_r}{\partial z} - \frac{\bar{\partial}V_z}{\partial r}\right] = \frac{\bar{\partial} I}{\partial r} - T\frac{\bar{\partial} s}{\partial r} - F_r - D_r \qquad (3.3a)$$

$$-\frac{W_r}{r}\frac{\bar{\partial}(rV_u)}{\partial r} - \frac{W_z}{r}\frac{\bar{\partial}(rV_u)}{\partial z} = -F_u - D_u \qquad (3.3b)$$

$$W_r\left[\frac{\bar{\partial}V_r}{\partial z} - \frac{\bar{\partial}V_z}{\partial r}\right] + \frac{W_u}{r}\frac{\bar{\partial}(rV_u)}{\partial z} = \frac{\bar{\partial} I}{\partial z} - T\frac{\bar{\partial} s}{\partial z} - F_z - D_z \qquad (3.3c)$$

where $$\underline{F} = \frac{-1}{\rho r \nu_u}\frac{\partial p}{\partial \theta}\underline{\nu}$$

The force vector $\underline{F}$, being normal to the mean stream surface, is therefore normal to $\underline{W}$ and $\underline{D}$, and so

$$\left.\begin{aligned} W_r F_r + W_u F_u + W_z F_z &= 0 \\ D_r F_r + D_u F_u + D_z F_z &= 0 \end{aligned}\right\} \qquad \ldots (3.4)$$

Also, since the dissipative force vector $\underline{D}$ is assumed to oppose the velocity vector $\underline{W}$,

$$\frac{D_r}{W_r} = \frac{D_u}{W_u} = \frac{D_z}{W_z} \qquad \ldots (3.5)$$

The equation of motion in the N-direction contains no components of $\underline{F}$ or $\underline{D}$, since $\underline{F}$ and $\underline{D}$ (and $\underline{W}$) are perpendicular to the N-direction. Put another way,

$\underline{F} \times \underline{W}$ lies in the N-direction.

Using equations 3.4 and 3.5 it is possible to form

(3.3a) $(W_z F_u - W_u F_z)$ + (3.3b) $(W_r F_z - W_z F_r)$ + (3.3c) $(W_u F_r - W_r F_u)$

which contains no net components of $\underline{F}$ or $\underline{D}$ and is thus the equation of motion in the N-direction. Expanding, and noting that $W_r = V_r$ and $W_z = V_z$, results in

$$W^2 F_u \left[\frac{\partial V_r}{\partial z} - \frac{\partial V_z}{\partial r}\right] = W_u \left[F_z \frac{\partial I}{\partial r} - F_r \frac{\partial I}{\partial z}\right] - F_u \left[V_z \frac{\partial I}{\partial r} - V_r \frac{\partial I}{\partial z}\right]$$

$$- T W_u \left[F_z \frac{\partial s}{\partial r} - F_r \frac{\partial s}{\partial z}\right] + T F_u \left[V_z \frac{\partial s}{\partial r} - V_r \frac{\partial s}{\partial z}\right]$$

$$- \frac{W^2}{r}\left[F_z \frac{\partial (r V_u)}{\partial r} - F_r \frac{\partial (r V_u)}{\partial z}\right] \qquad \ldots (3.6)$$

This equation can be simplified by introducing two local angles λ and μ which define the local geometry of the mean stream surface, (Figure 3.2):

$$\left.\begin{aligned} \tan \lambda &= \frac{v_r}{v_u} = \frac{F_r}{F_u} \\ \tan \mu &= \frac{v_z}{v_u} = \frac{F_z}{F_u} \end{aligned}\right\} \qquad \ldots (3.7)$$

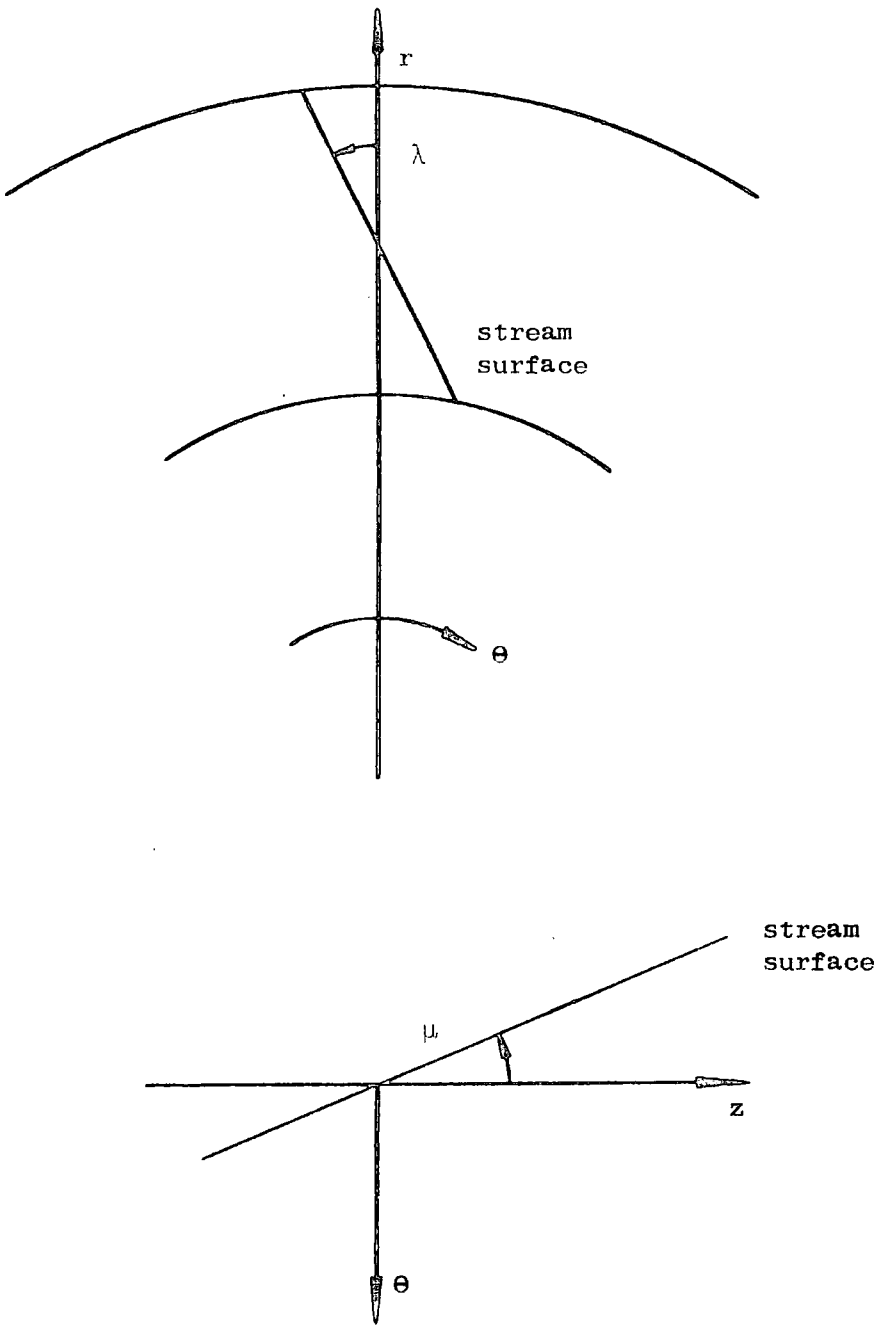

Angles marked are positive

FIGURE 3.2: FLOW ANGLES λ AND μ

Note that in the sign convention adopted (Appendix D), μ and α are of opposite signs.

From equation 3.4 the velocity components are related by:

$$W_r \tan \lambda + W_u + W_z \tan \mu = 0 \qquad \ldots (3.8)$$

which is the geometrical condition for the flow to follow the stream surface.

The continuity equation may be written as

$$\frac{\overline{\partial}(\rho B r V_r)}{\partial r} + \frac{\overline{\partial}(\rho B r V_z)}{\partial z} = 0,$$

where B is proportional to the local angular thickness of the stream surface. In the through-flow analysis, B is the ratio of the local circumference available for fluid flow to the total circumference, and although termed the 'blockage factor' is a measure of the unblocked flow area. In duct flow B = 1, but where there are blades of finite thickness, it is less than unity.

A stream function ψ may then be defined, where

$$\left.\begin{aligned} \frac{\overline{\partial}\psi}{\partial r} &= \rho B r V_z \\ \frac{\overline{\partial}\psi}{\partial z} &= -\rho B r V_r \end{aligned}\right\} \qquad \ldots (3.9)$$

For steady adiabatic flow, the energy equation

$$\frac{DI}{Dt} = 0$$

shows that the rothalpy I remains constant along a streamline. The rothalpy is therefore a function of ψ alone, so that

$$\left.\begin{aligned} \frac{\overline{\partial} I}{\partial r} &= \frac{dI}{d\psi} \frac{\overline{\partial}\psi}{\partial r} \\ \frac{\overline{\partial} I}{\partial z} &= \frac{dI}{d\psi} \frac{\overline{\partial}\psi}{\partial z} \end{aligned}\right\} \qquad \ldots (3.10)$$

Departing from the analysis of Bosman and Marsh (1974), equation 3.6 is divided by F_U and substitutions made for $\tan\lambda$ and $\tan\mu$:

$$W^2\left[\frac{\partial V_r}{\partial z}-\frac{\partial V_z}{\partial r}\right] = W_u\left[\tan\mu\,\frac{\partial I}{\partial r}-\tan\lambda\,\frac{\partial I}{\partial z}\right]-\left[V_z\frac{\partial I}{\partial r}-V_r\frac{\partial I}{\partial z}\right]$$

$$-TW_u\left[\tan\mu\,\frac{\partial s}{\partial r}-\tan\lambda\,\frac{\partial s}{\partial z}\right]+T\left[V_z\frac{\partial s}{\partial r}-V_r\frac{\partial s}{\partial z}\right]$$

$$-\frac{W^2}{r}\left[\tan\mu\,\frac{\partial(rV_u)}{\partial r}-\tan\lambda\,\frac{\partial(rV_u)}{\partial z}\right].$$

Combination of Rothalpy Terms

The terms involving rothalpy may be combined as follows:

$$W_u\left[\tan\mu\,\frac{\partial I}{\partial r}-\tan\lambda\,\frac{\partial I}{\partial z}\right]-\left[V_z\frac{\partial I}{\partial r}-V_r\frac{\partial I}{\partial z}\right]$$

$$=\frac{\partial I}{\partial r}\left[W_u\tan\mu-V_z\right]-\frac{\partial I}{\partial z}\left[W_u\tan\lambda-V_r\right]$$

$$=\frac{dI}{d\psi}\rho B r V_z\left[W_u\tan\mu-V_z\right]+\frac{dI}{d\psi}\rho B r V_r\left[W_u\tan\lambda-V_r\right]$$

using equations 3.9 and 3.10

$$=\frac{dI}{d\psi}\rho B r\left[-V_z^2+V_z W_u\frac{F_z}{F_u}+V_r W_u\frac{F_r}{F_u}-V_r^2\right]$$ using equation 3.7

$$=\frac{dI}{d\psi}\rho B r\left[-V_z^2-V_r^2-W_u^2\right]$$ using equation 3.4

$$=\frac{-dI}{d\psi}\rho B r W^2.$$ since $W_r = V_r$; $W_z = V_z$.

Entering this single rothalpy term we obtain:

$$W^2\left[\frac{\partial V_r}{\partial z}-\frac{\partial V_z}{\partial r}\right]=-\frac{dI}{d\psi}\rho B r W^2-TW_u\left[\tan\mu\,\frac{\partial s}{\partial r}-\tan\lambda\,\frac{\partial s}{\partial z}\right]$$

$$+T\left[V_z\frac{\partial s}{\partial r}-V_r\frac{\partial s}{\partial z}\right]-\frac{W^2}{r}\left[\tan\mu\,\frac{\partial(rV_u)}{\partial r}-\tan\lambda\,\frac{\partial(rV_u)}{\partial z}\right] \quad \ldots(3.11)$$

The meridional direction, co-ordinate m, is the streamline path projected onto a (r, z) plane of constant θ, so that

$$W_m^2 = W_r^2 + W_z^2$$

without any component of circumferential velocity. For the general property q the special derivatives are related by

$$W_m \frac{\bar{\partial} q}{\partial m} = W_r \frac{\bar{\partial} q}{\partial r} + W_z \frac{\bar{\partial} q}{\partial z}$$

The left hand side of equation 3.11 may then be expressed as:

$$W^2 \left[\frac{W_m}{W_z} \frac{\bar{\partial} V_r}{\partial m} - \frac{W_r}{W_z} \frac{\bar{\partial} V_r}{\partial r} - \frac{\bar{\partial} V_z}{\partial r} \right]$$

Introducing the streamline slope angle ϵ and radius of curvature C, where

$$\frac{1}{C} = - \frac{\partial \epsilon}{\partial m} ,$$

the left hand side of equation 3.11 may then be written as

$$W^2 \left[- \frac{W_m^2 \cos\epsilon}{W_z C} + \frac{W_m}{W_z} \frac{\bar{\partial} W_m}{\partial m} \sin\epsilon - \frac{W_r}{W_z} \frac{\bar{\partial} W_r}{\partial r} - \frac{\bar{\partial} W_z}{\partial r} \right] \quad \ldots(3.12)$$

The last two terms in the bracket combine to give

$$\frac{W_r}{W_z} \frac{\bar{\partial} W_r}{\partial r} + \frac{\bar{\partial} W_z}{\partial r} = \frac{W_m}{W_z} \frac{\bar{\partial} W_m}{\partial r}$$

Evaluation of $\bar{\partial} W_m / \partial m$

The term in expression 3.12 involving $\bar{\partial} W_m / \partial m$ may be evaluated following the analysis of Marsh (1970) from the equations of continuity and energy as follows.

The equation of continuity is

$$\frac{\bar{\partial}}{\partial r}(r B \rho W_r) + \frac{\bar{\partial}}{\partial z}(r B \rho W_z) = 0 .$$

$$\therefore W_r \frac{\bar{\partial}}{\partial r}(r B \rho) + r B \rho \frac{\bar{\partial} W_r}{\partial r} + W_z \frac{\bar{\partial}}{\partial z}(r B \rho) + r B \rho \frac{\bar{\partial} W_z}{\partial z} = 0 .$$

Forming the special derivatives in the m-direction, and dividing by $rB\rho$,

$$\frac{W_m}{rB\rho}\frac{\bar{\partial}(rB\rho)}{\partial m} + \frac{\bar{\partial}W_r}{\partial r} + \frac{\bar{\partial}W_z}{\partial z} = 0.$$

$$\therefore \frac{W_m}{rB\rho}\left[rB\frac{\bar{\partial}\rho}{\partial m} + \rho\frac{\bar{\partial}(rB)}{\partial m}\right] + \frac{\bar{\partial}W_r}{\partial r} + \frac{\bar{\partial}W_z}{\partial z} = 0.$$

$$\therefore \frac{W_m}{\rho}\frac{\bar{\partial}\rho}{\partial m} = -\frac{W_m}{rB}\left[r\frac{\bar{\partial}B}{\partial m} + B\frac{\bar{\partial}r}{\partial m}\right] - \frac{\bar{\partial}W_r}{\partial r} - \frac{\bar{\partial}W_z}{\partial z}$$

$$= -\frac{W_m}{B}\frac{\bar{\partial}B}{\partial m} - \frac{W_m}{r}\sin\epsilon - \frac{\bar{\partial}W_r}{\partial r} - \frac{\bar{\partial}W_z}{\partial z}.$$

Now from the relationships between the special derivatives

$$\frac{\bar{\partial}W_z}{\partial z} = \frac{W_m}{W_z}\frac{\bar{\partial}W_z}{\partial m} - \frac{W_r}{W_z}\frac{\bar{\partial}W_z}{\partial r}$$

$$= \frac{\bar{\partial}W_m}{\partial m} + \frac{W_m}{\cos\epsilon}\frac{\bar{\partial}(\cos\epsilon)}{\partial m} - \tan\epsilon\frac{\bar{\partial}(W_m\cos\epsilon)}{\partial r}$$

$$= \frac{\bar{\partial}W_m}{\partial m} - W_m\tan\epsilon\frac{\bar{\partial}\epsilon}{\partial m} - \tan\epsilon\frac{\bar{\partial}(W_m\cos\epsilon)}{\partial r}$$

$$\therefore \frac{W_m}{\rho}\frac{\bar{\partial}\rho}{\partial m} = -\frac{W_m}{B}\frac{\bar{\partial}B}{\partial m} - \frac{W_m\sin\epsilon}{r} - \frac{\bar{\partial}(W_m\sin\epsilon)}{\partial r} - \frac{\bar{\partial}W_m}{\partial m}$$

$$+ W_m\tan\epsilon\frac{\bar{\partial}\epsilon}{\partial m} + \tan\epsilon\frac{\bar{\partial}(W_m\cos\epsilon)}{\partial r}.$$

$$= -\frac{W_m}{B}\frac{\bar{\partial}B}{\partial m} - \frac{\bar{\partial}W_m}{\partial m} - \frac{W_m\sin\epsilon}{r} - \frac{\bar{\partial}W_m}{\partial m}(\sin\epsilon - \cos\epsilon\tan\epsilon)$$

$$- W_m\cos\epsilon\frac{\bar{\partial}\epsilon}{\partial r} - \sin\epsilon\tan\epsilon W_m\frac{\bar{\partial}\epsilon}{\partial r} + \tan\epsilon W_m\frac{\bar{\partial}\epsilon}{\partial m}.$$

$$= -\frac{W_m}{B}\frac{\bar{\partial}B}{\partial m} - \frac{\bar{\partial}W_m}{\partial m} - \frac{W_mW_r}{W_zC} - \frac{W_m}{r}\left[\sin\epsilon + \frac{\bar{\partial}\epsilon}{\partial r}(r\cos\epsilon + \sin\epsilon\tan\epsilon)\right].$$

$$\therefore \frac{W_m}{\rho}\frac{\overline{\partial \rho}}{\partial m} = -\frac{W_m}{B}\frac{\overline{\partial B}}{\partial m} - \frac{\overline{\partial W_m}}{\partial m} - \frac{W_m W_r}{W_z C} - \frac{W_z}{r}\left[\tan\epsilon + r\sec^2\epsilon\frac{\overline{\partial \epsilon}}{\partial r}\right].$$

The equation of continuity may therefore be expressed:

$$\frac{W_m}{\rho}\frac{\overline{\partial \rho}}{\partial m} = -\frac{W_m}{B}\frac{\overline{\partial B}}{\partial m} - \frac{\overline{\partial W_m}}{\partial m} - \frac{W_m W_r}{W_z C} - \frac{W_z}{r}\frac{\overline{\partial (r\tan\epsilon)}}{\partial r}.$$

Turning now to the energy equation for steady, adiabatic, axisymmetric flow,

$$W_m \frac{\overline{\partial I}}{\partial m} = 0.$$

$$\therefore W_m \frac{\overline{\partial}}{\partial m}\left(h + \tfrac{1}{2}W^2 - \tfrac{1}{2}\omega^2 r^2\right) = 0.$$

$$\therefore W_m \frac{\overline{\partial h}}{\partial m} = \frac{W_m}{2}\left[-\frac{\overline{\partial W_m^2}}{\partial m} - \frac{\overline{\partial W_u^2}}{\partial m} + \frac{\overline{\partial (\omega r)^2}}{\partial m}\right]$$

$$= -W_m^2\frac{\overline{\partial W_m}}{\partial m} - W_m W_u\frac{\overline{\partial W_u}}{\partial m} + W_m \omega r\frac{\overline{\partial (\omega r)}}{\partial m}$$

$$= -W_m^2\frac{\overline{\partial W_m}}{\partial m} - W_m W_u\frac{\overline{\partial V_u}}{\partial m} + W_m W_u\frac{\overline{\partial (\omega r)}}{\partial m} + W_m \omega r\frac{\overline{\partial (\omega r)}}{\partial m}$$

$$= -W_m^2\frac{\overline{\partial W_m}}{\partial m} - W_m W_u\frac{\overline{\partial V_u}}{\partial m} + W_m V_u\frac{\overline{\partial (\omega r)}}{\partial m}.$$

Now $$\frac{\overline{\partial (\omega r)}}{\partial m} = r\frac{\overline{\partial \omega}}{\partial m} + \omega\frac{\overline{\partial r}}{\partial m}$$

$$= 0 + \omega\sin\epsilon$$

$$= \frac{(V_u - W_u)}{r}\frac{W_r}{W_m}.$$

$$\therefore W_m \frac{\overline{\partial h}}{\partial m} = -W_m^2\frac{\overline{\partial W_m}}{\partial m} - W_m W_u\frac{\overline{\partial V_u}}{\partial m} - \frac{W_r W_u V_u}{r} + \frac{W_r V_u^2}{r}$$

Also, $$W_m\frac{\overline{\partial V_u}}{\partial m} + \frac{W_r V_u}{r} = \frac{W_m}{r}\, r\frac{\overline{\partial V_u}}{\partial m} + V_u\sin\epsilon$$

$$= \frac{W_m}{r}\, r\frac{\overline{\partial V_u}}{\partial m} + V_u\frac{\overline{\partial r}}{\partial m}$$

$$= \frac{W_m}{r}\frac{\overline{\partial (r V_u)}}{\partial m}$$

$$= F_u + D_u \quad \text{from equation 3.3b}$$

The final form of the energy equation is then

$$W_m \frac{\partial h}{\partial m} = -W_m^2 \frac{\partial W_m}{\partial m} - W_u f + \frac{W_r V_u^2}{r}$$

where $f = F_u + D_u$.

If the fluid is a perfect gas, then

$$\frac{1}{\rho}\frac{\partial \rho}{\partial m} = \frac{1}{a^2}\frac{\partial h}{\partial m} - \frac{1}{R}\frac{\partial s}{\partial m}$$

and substituting from the equation of continuity and energy:

$$\frac{\partial W_m}{\partial m} = \left[\frac{1}{1-M_m^2}\right]\left[\frac{W_m}{R}\frac{\partial s}{\partial m} - \frac{W_z}{r}\frac{\partial (r\tan\epsilon)}{\partial r} - \frac{W_m W_r}{W_z C} - \frac{W_m}{B}\frac{\partial B}{\partial m} + \frac{W_u f}{a^2} - \frac{W_r W_u^2}{r a^2}\right].$$

This result is obtained by Marsh (1970, equation 27). In the usual streamline curvature analysis, $D_u = 0$ and then $f = F_u$. This completes the evaluation of $\partial W_m/\partial m$.

The left hand side of equation 3.11 now becomes

$$W^2\left[-\frac{W_m^2}{W_z}\frac{\cos\epsilon}{C} - \frac{W_m}{W_z}\frac{\partial W_m}{\partial r} + \frac{W_m}{W_z}\sin\epsilon\left\{\frac{1}{1-M_m^2}\right\}\left\{\frac{W_m}{R}\frac{\partial s}{\partial m} - \frac{W_z}{r}\frac{\partial (r\tan\epsilon)}{\partial r}\right.\right.$$

$$\left.\left. - \frac{W_m W_r}{W_z C} - \frac{W_m}{B}\frac{\partial B}{\partial m} + \frac{W_u f}{a^2} - \frac{W_r W_u^2}{r a^2}\right\}\right]. \qquad \ldots (3.13)$$

The terms in C combine to give

$$-\frac{W_m^2}{W_z}\frac{\cos\epsilon}{C} + \frac{W_m \sin\epsilon}{W_z(1-M_m^2)}\left[-\frac{W_m W_r}{W_z C}\right] = \frac{-W_m}{C}\left[1 + \frac{W_r^2}{W_z^2(1-M_m^2)}\right]$$

$$= \frac{-W_m^3}{W_z^2 C}\left[\frac{1-M_z^2}{1-M_m^2}\right]$$

within the square brackets of expression 3.13.

Hence equation 3.11 may be rewritten as

$$-\frac{W_m}{W_z}\frac{\partial W_m}{\partial r} - \left[\frac{1-M_z^2}{1-M_m^2}\right]\frac{W_m^3}{C W_z^2} + \frac{W_r}{W_z(1-M_m^2)}\left[\frac{W_m}{R}\frac{\partial s}{\partial m} - \frac{W_z}{r}\frac{\partial (r\tan\epsilon)}{\partial r}\right.$$

$$\left. - \frac{W_m}{B}\frac{\partial B}{\partial m}\right] + \frac{M_r M_u f}{(1-M_m^2) W_z} - \left[\frac{M_r^2}{1-M_m^2}\right]\frac{V_u^2}{r W_z} =$$

$$= \frac{1}{W^2}\left[-\rho B_r W^2 \frac{dI}{d\psi} - T W_u \left(\tan\mu \frac{\overline{\partial s}}{\partial r} - \tan\lambda \frac{\overline{\partial s}}{\partial z} \right) + T \left(V_z \frac{\overline{\partial s}}{\partial r} - V_r \frac{\overline{\partial s}}{\partial z} \right) \right.$$

$$\left. - \frac{W^2}{r} \left(\tan\mu \frac{\overline{\partial (rV_u)}}{\partial r} - \tan\lambda \frac{\overline{\partial (rV_u)}}{\partial z} \right) \right]$$

$$= -\rho B r \frac{dI}{d\psi} + \frac{T}{W^2} \left[\frac{\overline{\partial s}}{\partial r} \left(V_z - W_u \tan\mu \right) - \frac{\overline{\partial s}}{\partial z} \left(V_r - W_u \tan\lambda \right) \right]$$

$$- \frac{1}{r} \left[\tan\mu \frac{\overline{\partial (rV_u)}}{\partial r} - \tan\lambda \frac{\overline{\partial (rV_u)}}{\partial z} \right] .$$

Multiplying throughout by $(-W_z)$, the equilibrium equation in the N-direction is obtained in the form to be used:

$$W_m \frac{\overline{\partial W_m}}{\partial m} = -\left[\frac{1 - M_z^2}{1 - M_m^2} \right] \frac{W_m^2}{C \cos\epsilon} + W_r \left[\frac{W_m}{R} \frac{\overline{\partial s}}{\partial m} - \frac{W_z}{r} \frac{\overline{\partial (r \tan\epsilon)}}{\partial r} - \frac{W_m}{B} \frac{\overline{\partial B}}{\partial m} \right]$$

$$+ \left[\frac{M_r M_u}{1 - M_m^2} \right] f - \frac{M_r^2 V_u^2}{(1 - M_m^2) r} + W_z \rho B r \frac{dI}{d\psi}$$

$$- \frac{T W_z}{W^2} \left[\frac{\overline{\partial s}}{\partial r} \left(W_z - W_u \tan\mu \right) - \frac{\overline{\partial s}}{\partial z} \left(W_r - W_u \tan\lambda \right) \right]$$

$$+ \frac{W_z}{r} \left[\tan\mu \frac{\partial (rV_u)}{\partial r} - \tan\lambda \frac{\partial (rV_u)}{\partial z} \right] . \qquad \ldots (3.14)$$

The last two terms of equation 3.14 may be simplified, using the relationships between the special derivatives, to

$$- T \frac{\overline{\partial s}}{\partial r} + \frac{W_m}{W^2} \left(W_u \tan\lambda - W_r \right) \frac{\overline{\partial s}}{\partial m}$$

$$+ \frac{W_u}{r} \frac{\overline{\partial (rV_u)}}{\partial r} - \frac{W_m \tan\lambda}{r} \frac{\overline{\partial (rV_u)}}{\partial m} ,$$

which are preferable where the m-derivaties are readily calculable. Collecting all the $\overline{\partial s}/\partial m$ terms, the N-direction equilibrium equation appears in an alternative form discussed in Chapter 4:

$$W_m \frac{\partial W_m}{\partial r} = -\left[\frac{1-M_z^2}{1-M_m^2}\right]\frac{W_m^2}{C\cos\epsilon} + \frac{W_r}{(1-M_m^2)}\left[\frac{W_z}{r}\frac{\partial(r\tan\epsilon)}{\partial r} - \frac{W_m}{B}\frac{\partial B}{\partial m}\right]$$

$$+\left[\frac{M_r M_u}{1-M_m^2}\right] f - \frac{M_r^2 V_u^2}{(1-M_m^2)r} + W_z \rho B r \frac{dI}{d\Psi}$$

$$+ W_m \frac{\partial s}{\partial m}\left[\frac{T}{W^2}(W_r - W_u \tan\lambda) - \frac{W_r}{(1-M_m^2)R}\right] - T\frac{\partial s}{\partial r}$$

$$+ \frac{W_u}{r}\frac{\partial(rV_u)}{\partial r} - \frac{W_m \tan\lambda}{r}\frac{\partial(rV_u)}{\partial m} \qquad \ldots (3.15)$$

Comparisons of equations 3.14 and 3.15 with the commonly-used radial equilibrium equation are made in Section 3.5.

3.4 Axisymmetric Duct Flow Equations of Motion

For duct flow there is no prescribed stream surface, and so no geometrical condition relating the three velocity components. Therefore only one of the equations of motion can be replaced - by the loss model entropy equation.

As with the intrablade flow, the equation of motion to replace is that in the local flow direction, since it contains the dissipative force $\underline{D}$. The two remaining equations of motion both lie in the plane perpendicular to the velocity vector $\underline{V}$.

Taking $\underline{j}$ as the unit vector in the θ direction, it is convenient to choose the directions for the two equations of motion as $\underline{j} \times \underline{V}$ and $\underline{V} \times (\underline{j} \times \underline{V})$. In common with the intrablade flow, the direction of the vector $\underline{V}$ may be changed as calculations proceed so it is again helpful to form the $\underline{j} \times \underline{V}$ and $\underline{V} \times (\underline{j} \times \underline{V})$ equations of motion in terms of the r, θ, z co-ordinates.

For axisymmetric flow the equations of motion in the r, θ and z directions are respectively (Bosman and Marsh (1974)):

$$\frac{V_u}{r}\frac{\partial(rV_u)}{\partial r} - V_z\left[\frac{\partial V_r}{\partial z} - \frac{\partial V_z}{\partial r}\right] = \frac{\partial h_o}{\partial r} - T\frac{\partial s}{\partial r} - \mathcal{D}_r . \qquad \ldots (3.16a)$$

$$-\frac{V_r}{r}\frac{\partial(rV_u)}{\partial r} - \frac{V_z}{r}\frac{\partial(rV_u)}{\partial z} = -\mathcal{D}_u . \qquad \ldots (3.16b)$$

$$V_r\left[\frac{\partial V_r}{\partial z} - \frac{\partial V_z}{\partial r}\right] + \frac{V_u}{r}\frac{\partial(rV_u)}{\partial z} = \frac{\partial h_o}{\partial z} - T\frac{\partial s}{\partial z} - \mathcal{D}_z . \qquad \ldots (3.16c)$$

The equation of motion for the $\underline{j}$ x $\underline{V}$ direction is obtained by forming

(3.16a) V_z - (3.16c) V_r

which leads to an equation with no component of the dissipative force:

$$V_m^2\left[\frac{\partial V_r}{\partial z} - \frac{\partial V_z}{\partial r}\right] = \left[V_r\frac{\partial h_o}{\partial z} - V_z\frac{\partial h_o}{\partial r}\right] - T\left[V_r\frac{\partial s}{\partial z} - V_z\frac{\partial s}{\partial r}\right]$$

$$-\frac{V_u}{r}\left[V_r\frac{\partial(rV_u)}{\partial z} - V_z\frac{\partial(rV_u)}{\partial r}\right] .$$

Departing from the analysis of Bosman and Marsh (1974), the enthalpy terms may be collected in a manner similar to that in the intrablade analysis, using the energy equation

$$\frac{Dh_o}{Dt} = 0,$$

to obtain

$$V_m^2\left[\frac{\partial V_r}{\partial z} - \frac{\partial V_z}{\partial r}\right] = -\frac{dh_o}{d\psi}\rho r V_m^2 - T\left[V_r\frac{\partial s}{\partial z} - V_z\frac{\partial s}{\partial r}\right]$$

$$-\frac{V_u}{r}\left[V_r\frac{\partial(rV_u)}{\partial z} - V_z\frac{\partial(rV_u)}{\partial r}\right] \qquad \ldots (3.17)$$

The total enthalpy here is simply a special case of rothalpy, with the rotational speed zero.

Note that the factor B is unity in the free duct and has been omitted.

The task is now to reorganise equation 3.17 into the form

$$V_m \frac{\partial V_m}{\partial r} = V_m^2 \, K(r) + L(r).$$

Working on the left hand side of equation 3.17,

$$\frac{\partial V_r}{\partial z} = \frac{1}{V_z} V_m \left[\frac{\partial V_r}{\partial m} - V_r \frac{\partial V_r}{\partial r} \right].$$

Therefore the left hand side of equation 3.17 equals

$$V_m^2 \left[\frac{V_m}{V_z} \frac{\partial (V_m \sin\epsilon)}{\partial m} - \frac{V_r}{V_z} \frac{\partial V_r}{\partial r} - \frac{\partial V_z}{\partial r} \right]$$

$$= V_m^2 \left[-\frac{V_m^2}{V_z} \frac{\cos\epsilon}{C} + \sin\epsilon \frac{V_m}{V_z} \frac{\partial V_m}{\partial m} - \frac{V_m}{V_z} \frac{\partial V_m}{\partial r} \right].$$

Using Marsh (1970, equation 27),

$$(1-M_m^2) \frac{\partial V_m}{\partial m} = \frac{V_m}{R} \frac{\partial s}{\partial m} - \frac{V_z}{r} \frac{\partial (r \tan\epsilon)}{\partial r} - \frac{V_m V_r}{V_z C} + \frac{V_u f}{a^2} - \frac{V_r V_u^2}{r a^2},$$

where

$$f = \frac{W_r}{r} \frac{\partial (r V_u)}{\partial r} + \frac{W_z}{r} \frac{\partial (r V_u)}{\partial z}.$$

The left hand side of equation 3.17 with this substitution becomes

$$V_m^2 \left[-\frac{V_m^2}{V_z} \frac{\cos\epsilon}{C} - \frac{V_m}{V_z} \frac{\partial V_m}{\partial r} + \frac{V_m \sin\epsilon}{V_z} \left(\frac{1}{1-M_m^2} \right) \left(\frac{V_m}{R} \frac{\partial s}{\partial m} \right.\right.$$

$$\left.\left. - \frac{V_z}{r} \frac{\partial (r \tan\epsilon)}{\partial r} - \frac{V_m V_r}{V_z C} + \frac{V_u f}{a^2} - \frac{V_r V_u^2}{r a^2} \right) \right]$$

$$= V_m^2 \left[-\frac{V_m^3}{V_z^2 C} \left(\frac{1-M_z^2}{1-M_m^2} \right) - \frac{V_m}{V_z} \frac{\partial V_m}{\partial r} + \left(\frac{1}{1-M_m^2} \right) \frac{V_r}{V_z} \left(\frac{V_m}{R} \frac{\partial s}{\partial m} \right.\right.$$

$$\left.\left. - \frac{V_z}{r} \frac{\partial (r \tan\epsilon)}{\partial r} + \frac{V_u f}{a^2} - \frac{V_r V_u^2}{r a^2} \right) \right],$$

so that dividing by V_m^2, the entire equation 3.17 has now become:

$$-\frac{V_m}{V_z}\frac{\partial V_m}{\partial r} - \frac{V_m^3}{V_z^2 C}\left(\frac{1-M_z^2}{1-M_m^2}\right) + \frac{V_r}{V_z(1-M_m^2)}\left[\frac{V_m}{R}\frac{\partial s}{\partial m} - \frac{V_z}{r}\frac{\partial (r\tan\epsilon)}{\partial r}\right]$$

$$+\left(\frac{M_r M_u}{1-M_m^2}\right)\frac{f}{V_z} - \left(\frac{M_r^2}{1-M_m^2}\right)\frac{V_u^2}{r V_z}$$

$$= -\rho r \frac{dh_o}{d\psi} + \frac{T}{V_m^2}\left[V_z\frac{\partial s}{\partial r} - V_r\frac{\partial s}{\partial z}\right] - \frac{V_u}{V_m^2 r}\left[V_r\frac{\partial (rV_u)}{\partial z} - V_z\frac{\partial (rV_u)}{\partial r}\right].$$

Multiplying by V_z and rearranging,

$$V_m\frac{\partial V_m}{\partial r} = -\left[\frac{1-M_z^2}{1-M_m^2}\right]\frac{V_m^2}{C\cos\epsilon} + \left[\frac{V_r}{1-M_m^2}\right]\left[\frac{V_m}{R}\frac{\partial s}{\partial m} - \frac{V_z}{r}\frac{\partial (r\tan\epsilon)}{\partial r}\right]$$

$$+\left[\frac{M_r M_u}{1-M_m^2}\right]f - \left[\frac{M_r^2}{1-M_m^2}\right]\frac{V_u^2}{r} + V_z\rho r\frac{dh_o}{d\psi}$$

$$-\frac{T V_z}{V_m^2}\left[V_z\frac{\partial s}{\partial r} - V_r\frac{\partial s}{\partial z}\right] - \frac{V_u V_z}{V_m^2 r}\left[V_z\frac{\partial (rV_u)}{\partial r} - V_r\frac{\partial (rV_u)}{\partial z}\right]. \quad \ldots(3.18)$$

Equation 3.18 is the equation of motion in the $\underline{j}$ x $\underline{V}$ direction for duct flow, analogous to the equation of motion in the N direction for intrablade flow.

In a similar manner to that employed in the intrablade flow analysis, the last two terms of equation 3.18 may be expressed as:

$$-T\left[\frac{\partial s}{\partial r} - \sin\epsilon\frac{\partial s}{\partial m}\right] - \frac{V_u}{r}\left[\frac{\partial (rV_u)}{\partial r} - \sin\epsilon\frac{\partial (rV_u)}{\partial m}\right],$$

to give the alternative formulation of the equation of motion in the $\underline{j}$ x $\underline{V}$ direction:

$$V_m\frac{\partial V_m}{\partial r} = -\left[\frac{1-M_z^2}{1-M_m^2}\right]\frac{V_m^2}{C\cos\epsilon} + \left[\frac{V_r}{1-M_m^2}\right]\left[\frac{V_m}{R}\frac{\partial s}{\partial m} - \frac{V_z}{r}\frac{\partial (r\tan\epsilon)}{\partial r}\right]$$

$$+\left[\frac{M_r M_u}{1-M_m^2}\right]f - \left[\frac{M_r^2}{1-M_m^2}\right]\frac{V_u^2}{r} + V_z\rho r\frac{dh_o}{d\psi}$$

$$-T\left[\frac{\partial s}{\partial r} - \sin\epsilon\frac{\partial s}{\partial m}\right] - \frac{V_u}{r}\left[\frac{\partial (rV_u)}{\partial r} - \sin\epsilon\frac{\partial (rV_u)}{\partial m}\right]. \quad \ldots(3.19)$$

For duct flow the equation of motion in the $\underline{V} \times (\underline{j} \times \underline{V})$ direction is also required; this is a relatively straightforward matter. Following Bosman and Marsh (1974), the equation of motion for the $\underline{V} \times (\underline{j} \times \underline{V})$ direction is formed from

$$-(3.16a)\ V_r V_u + (3.16b)\ V_m^2 - (3.16c)\ V_z V_u,$$

which after substituting $h_o = h_o(\psi)$, leads to

$$\frac{V^2}{r}\left[V_r \frac{\partial(rV_u)}{\partial r} + V_z \frac{\partial(rV_u)}{\partial z}\right] = -T V_u \left[V_r \frac{\partial s}{\partial r} + V_z \frac{\partial s}{\partial z}\right],$$

or

$$\frac{D(rV_u)}{Dt} = -r V_u \frac{T}{V^2} \frac{Ds}{Dt} \quad . \qquad \ldots (3.20)$$

Equation 3.20, the equation of motion in the $\underline{V} \times (\underline{j} \times \underline{V})$ direction, shows that with losses corresponding to an entropy rise, the angular momentum decreases along a streamline.

3.5 Comparison of Equations With Those Commonly Used

Marsh (1970) gives the radial equation of motion as

$$W_m \frac{\overline{\partial} W_m}{\partial r} = -\left[\frac{1-M_z^2}{1-M_m^2}\right] \frac{W_m^2}{C\cos\epsilon} + \frac{\overline{\partial} I}{\partial r} - T\frac{\overline{\partial} s}{\partial r} - F_r$$

$$- \frac{W_u}{r} \frac{\overline{\partial}(rV_u)}{\partial r} - \left[\frac{M_r^2}{1-M_m^2}\right] \frac{V_u^2}{r} + \left[\frac{M_r M_u}{1-M_m^2}\right] F_u$$

$$+ \left[\frac{W_r}{1-M_m^2}\right]\left[\frac{W_m}{R} \frac{\overline{\partial} s}{\partial m} - \frac{W_z}{r} \frac{\overline{\partial}(r\tan\epsilon)}{\partial r} - \frac{W_m}{B} \frac{\overline{\partial} B}{\partial m}\right] \quad . \qquad \ldots (3.21)$$

For all applications the term F_u should be replaced by

$$\frac{W_r}{r} \frac{\overline{\partial}(rV_u)}{\partial r} + \frac{W_z}{r} \frac{\overline{\partial}(rV_u)}{\partial z} \qquad (= F_u + D_u)$$

This is a back-substitution to re-insert a term simplified in the derivation of equation 3.21. The term is denoted **f** in equations 3.14, 3.15, 3.18, and 3.19, since for the improved loss model there is a component D_u of the dissipative force in addition to the circumferential component of blade force F_u, so that $f \neq F_u$.

For the analysis of duct flow:

(i) the special derivatives may be replaced by regular partial derivatives;

(ii) B is unity everywhere, so $\frac{\bar{\partial} B}{\partial m} = 0$;

(iii) $\underline{W} = \underline{V}$, and all respective components are alike;

(iv) $I = h_o$.

3.5.1 Intrablade Flow

Equation 3.21 may be converted to the intrablade flow equation of motion in the N direction with the improved loss model by replacing:

(a) $\frac{\bar{\partial} I}{\partial r}$ by $V_z \rho B r \frac{dI}{d\psi}$;

(b) $\frac{\bar{\partial} s}{\partial r}$ by either $\frac{\bar{\partial} s}{\partial r} + \frac{W_m}{W^2}\left(W_u \tan\lambda - W_r\right)\frac{\bar{\partial} s}{\partial m}$

or $\frac{W_z}{W^2}\left[\frac{\bar{\partial} s}{\partial r}\left(V_z - W_u \tan\beta\right) - \frac{\bar{\partial} s}{\partial z}\left(V_r - W_u \tan\lambda\right)\right]$;

(c) $\frac{W_u}{r}\frac{\bar{\partial}(rV_u)}{\partial r}$ by either $\frac{W_u}{r}\frac{\bar{\partial}(rV_u)}{\partial r} - \frac{W_m \tan\lambda}{r}\frac{\bar{\partial}(rV_u)}{\partial m}$

or $-\frac{W_z}{r}\left[\tan\mu \frac{\bar{\partial}(rV_u)}{\partial r} - \tan\lambda \frac{\bar{\partial}(rV_u)}{\partial z}\right]$;

(d) F_r by zero.

For the case of simple radial equilibrium,

where $V_r = 0$ and $\lambda = 0$,

the equations 3.14 and 3.21 are in agreement.

3.5.2 Duct Flow

Equation 3.21 may be converted to the duct flow equation of motion in the $\underline{j} \times \underline{V}$ direction with the improved loss model by replacing:

(a) $\frac{\bar{\partial} I}{\partial r}$ by $V_z \rho r \frac{dh_o}{d\psi}$;

(b) $\frac{\bar{\partial} s}{\partial r}$ by either $\frac{\partial s}{\partial r} - \sin\epsilon \frac{\partial s}{\partial m}$

or $\frac{V_z}{V_m^2}\left[V_z \frac{\partial s}{\partial r} - V_r \frac{\partial s}{\partial z}\right]$;

(c) $\frac{W_u}{r}\frac{\partial}{\partial r}(rV_u)$ by either $\frac{V_u}{r}\left[\frac{\partial}{\partial r}(rV_u) - \sin\epsilon\frac{\partial}{\partial m}(rV_u)\right]$

or $\frac{V_u V_z}{V_m^2 r}\left[V_z\frac{\partial}{\partial r}(rV_u) - V_r\frac{\partial}{\partial z}(rV_u)\right]$;

(d) F_r by zero.

3.6 Discussion of New Terms in Equations

3.6.1 Rothalpy Terms - substitution (a)

For steady adiabatic flow, the energy equation

$$\frac{DI}{Dt} = 0$$

shows that the rothalpy remains constant along any streamline, and is therefore a function of ψ alone, so that as shown by Bosman and Marsh (1974),

$$\frac{\partial I}{\partial r} = \frac{dI}{d\psi}\frac{\partial \psi}{\partial r} .$$

By definition of the stream function,

$$\frac{\partial \psi}{\partial r} = \rho\, Br V_z ,$$

so that

$$\frac{\partial I}{\partial r} = V_z\, \rho\, Br\, \frac{dI}{d\psi}$$

is simply a re-expression of the original term. The units of stream function here are those of mass flowrate, so that numerically if it is zero on one annulus wall then it is equal to the specified mass flow rate on the other. In adiabatic flow, $dI/d\psi$ remains constant along a streamline until entry to or exit from a rotor row. It is constant through stator rows, where $I = h_o$.

In a duct region, B is unity and $I = h_o$.

3.6.2 Entropy Terms - substitution (b)

The N direction equation of motion for blade rows was formed by adding the r, θ and z direction equations of motion, equations 3.3, in such proportions that the result contained no component of forces $\underline{D}$ or $\underline{F}$:

$$(3.3a)(W_z F_u - W_u F_z) + (3.3b)(W_r F_z - W_z F_r) + (3.3c)(W_u F_r - W_r F_u).$$

Equations 3.3a and 3.3c contain respectively the radial and axial derivatives of entropy, so that from the above formulation, four entropy terms appear, two each in the radial and axial derivatives. These may be re-grouped as

$$T \frac{\bar{\partial} s}{\partial r} (V_z - W_u \tan \mu) - T \frac{\bar{\partial} s}{\partial z} (V_r - W_u \tan \lambda).$$

The multiplier W_z/W^2 was introduced to give the magnitude of the main unknown as $W_m \frac{\bar{\partial} W_m}{\partial m}$.

In duct flow the equation of motion in the $\underline{j} \times \underline{V}$ direction has a simpler formulation involving only two of the equations 3.16:

$$(3.16a)\ V_z - (3.16c)\ V_r.$$

Of the r, θ, z set of equations of motion, 3.16a and 3.16c are the two to contain entropy terms, but the factors V_z and $(-V_r)$ here give only one pair of entropy derivatives:

$$V_z \frac{\bar{\partial} s}{\partial r} - V_r \frac{\bar{\partial} s}{\partial z}.$$

The intrablade equation of motion in the N-direction was produced by combining all three of the equations in the r, θ and z directions, equations 3.3, but the equivalent equation of motion for duct flow, in the $\underline{j} \times \underline{V}$ direction, contains no component of the circumferential equation 3.16b. This difference may be traced through to explain the contrasting denominators in the prefixes on the substituted entropy terms: $\frac{V_z}{V_m^2}$ for duct flow, but $\frac{W_z}{W^2}$ for intrablade flow.

The first version of the substitution, for both duct and intrablade cases, consists of the original $\frac{\overline{\partial s}}{\partial r}$ term, plus a new term in $\frac{\overline{\partial s}}{\partial m}$. It follows that in lossless flow, where $\frac{\overline{\partial s}}{\partial m}$ vanishes although $\frac{\overline{\partial s}}{\partial r}$ may remain, the entropy term is in agreement with that in the radial equilibrium equation.

Losses in blades being higher than those in duct regions, the entropy gradient $\frac{\overline{\partial s}}{\partial m}$ will in general change near blades. The effect of such sudden changes is discussed in Chapter 4.

3.6.3 Angular Momentum Terms - substitution (c)

These arise for similar reasons to the entropy terms - the combination of the r, θ and z direction equations of motion in varying proportions cause the more complicated algebra.

As with the new entropy terms, the first versions of the replacement angular momentum terms for both duct and intrablade flow are expressed as the original r-derivative with a new meridional derivative. The duct flow equation term shows that for lossless flow, where $\frac{\overline{\partial}}{\partial m}(rV_u) = 0$ the angular momentum term remains the same as in the radial equilibrium equation.

The purpose of a blade row is to change angular momentum, so that $\frac{\overline{\partial}}{\partial m}(rV_u)$ is generally non-zero in a blade row, even if the flow is lossless. Thus within a blade row the angular momentum term for the consistent-loss analysis will differ from that in the radial equilibrium analysis, unless the blade geometry is such that $\tan \lambda = 0$ or $\frac{\overline{\partial}}{\partial m}(rV_u) = 0$. The significant behaviour of derivatives of angular momentum is discussed in Chapter 4.

3.6.4 Radial Force Term - substitution (d)

The N direction equation of motion within blades was derived to contain no component of the forces $\underline{F}$ or $\underline{D}$, and so no force terms appear within it and the term F_r is eliminated from the equation.

The force $\underline{F}$ does not act outside a blade row, so that no duct flow equations contain any component of $\underline{F}$. The dissipative loss force $\underline{D}$ is present, but the $\underline{j} \times \underline{V}$ direction equation of motion was derived to contain no component of $\underline{D}$.

3.7 Reported Errors in the Literature

The criticism by Hong (1980) of the loss model used by Horlock (1971), Bosman and Marsh (1974) and in the present work has been noted in Section 3.2. Hong also scrutinizes the analyses of other papers, including those by Silvester and Hetherington (1966), Smith (1966), Novak (1967), Frost (1972), and an unpublished work of Hetherington (1974). The last two of these are reported by Hong (1980) to contain errors in principal equations. The paper by Hetherington (1974) was unobtainable, but the analysis of Frost (1972) was examined.

Hong (1980) sets down the radial equation of motion in the following form, using the notation of the present work:

$$\frac{1}{\rho}\frac{\bar{\partial} p}{\partial r} = \frac{W_z^2}{(1-M_z^2\sec^2\epsilon)}\left[\frac{\tan^2\epsilon}{r} + \frac{1}{2}\frac{\bar{\partial}(\tan^2\epsilon)}{\partial r} + \frac{\tan\epsilon}{B}\frac{dB}{dz}\right.$$
$$+\left(1-M_z^2\right)\left(\frac{\tan^2\alpha}{r} - \frac{d^2 r}{dz^2}\right)$$
$$\left.+\left\{\left(1-M_z^2\right)\tan\lambda + M_z^2\tan\epsilon\tan\mu\right\}\frac{1}{rW_z}\frac{d(rV_u)}{dz}\right] ,$$

where

$$\frac{d}{dz} = \frac{W_m}{W_z}\frac{\bar{\partial}}{\partial m} .$$

He then notes a difference between this and Frost's (1972) similarly-presented principal equation, numbered (1). The present author has determined that the error is indeed in Frost's paper, and can be traced to the formation of his equation (A.15).

It is wise to follow through the analysis presented in published works, both to gain an understanding of the principles and assumptions involved, and also because errors occasionally appear, whether mathematical or merely typographical.

CHAPTER 4

Flow Effects At Blade Entry And Exit

4.1 Introduction

Fluid moving in a section of duct experiences low losses, no enforced turning (as occurs within blade rows) and no blockage effects. Consequently the rate of change of entropy in the streamwise direction, $\frac{\partial s}{\partial m}$, is low and is matched by a correspondingly small streamwise derivative of angular momentum, according to equation 3.20. The streamwise rate of change of the blockage term, $\frac{\partial B}{\partial m}$, is zero.

In the vicinity of a blade row, losses are usually rather higher, and so higher values of $\frac{\partial s}{\partial m}$, occur there. Quite how the loss is distributed through the blade row depends on the application, but in any case is open to some debate: the loss may be regarded as all appearing at, or even downstream of, the trailing edge, in the wake; a blade operating near stall at inlet will incur losses near the leading edge; and there is generally a boundary layer loss over the entire blade surface. In the computer program the empirical data for the ratios of total pressure across a blade row are translated into entropy changes. For the sake of argument, the entropy is assumed to vary linearly with axial position between the leading and trailing edges. This gives rise to sharp changes in the value of $\frac{\partial s}{\partial m}$ over the distances from leading or trailing edges to the adjacent calculation stations in the duct region, and so considering equation 3.15 there is at blade entry or exit an abrupt change in the term

$$W_m \frac{\partial \bar{s}}{\partial m} \left[\frac{T}{W^2} (W_r - W_u \tan \lambda) - \frac{W_r}{(1 - M_m^2) R} \right]$$

unless the contents of the square bracket equal zero.

Such changes indicate changed values of $\frac{\partial \bar{W}_m}{\partial r}$ on the left hand side of the equation 3.15, leading to redistribution of the meridional

velocity and repositioned streamline paths, but in practice such streamline shifts could be accommodated over the distance to the adjacent calculation stations. The most important entropy effect in a multistage machine is always the accumulation of the radial entropy gradient over several stages.

Similarly the streamwise gradient of the blockage factor $\frac{\overline{\partial B}}{\partial m}$ presented no problems in practice, since in the N direction equation of motion its factor is $\frac{-W_r \quad W_m}{(1-M_m^2)B}$, and W_r is often small compared to other velocity components.

Discontinuity problems were encountered, however, because of the numerically larger changes in the terms involving the streamwise derivative of angular momentum, $\frac{\overline{\partial}}{\partial m}(rV_u)$, and it is in the light of these that this chapter is formulated.

4.2 An Example Involving A Free Vortex Blade Row

Consider uniform, lossless fluid flow in a cylindrical annular duct with streamlines straight and parallel to the axis (z direction). Let there be no swirl in the flow, which is a special case of the 'free vortex' circumferential velocity distribution wherein the product rV_u is a constant at all radii. The value of the constant may be varied from place to place axially, but the significance of free vortex flow is that there is no consequent radial redistribution of the streamlines with changing swirl component of velocity. Thus the radial velocity for this example is zero everywhere, and many terms in equation 3.18, the main equation for duct flow, are zero. All the other terms on the right hand side vanish because: the radius of curvature of the streamlines is infinite; entropy and total enthalpy are uniform everywhere; and $\frac{\overline{\partial}}{\partial r}(rV_u) = 0$.

Inspection shows that uniform-flow is a solution of equation 3.18 since the left hand side of the equation also becomes zero.

Now let the flow in the duct encounter a row of stator blades with uniform axial length, whose entry angle is zero at all radii, to match the arriving flow. Through the blades, the flow is redirected so that the fluid exit angle varies radially as:

$$\tan \alpha_2 = \text{constant}/r,$$

which is the flow angle distribution for free vortex flow.

With α_2 varying radially, blade cross-sections at different radii will be of different shapes. The circumferential length of the blade will be greater for sections of greater camber angle, causing varying lean angle λ on the camber surface, as shown in Figure 4.1.

Depending on the relative circumferential positions of the different cross-sections (the section 'stacking'), the lean angle λ may be varied by the designer. Taking the mean stream surface to follow closely the blade camber surface, tan λ is obtained in the N-direction intrablade equation of motion. However, it is shown below that even for the flow in this example with little or no radial velocity, the circumferential positions of neighbouring cross-sections have an important effect on the flow which is not revealed by the radial equilibrium analysis.

4.3 Consideration of the N-Direction Equation of Motion

At entry to the blade row, the meridional velocity is uniform radially, with no radial velocity component, and as with equation 3.18 for duct flow, many terms in equation 3.14 become zero. Once inside the blade, V_u starts to change, following the parabolic camber line, such that

$$\frac{\partial V_u}{\partial z} = \text{constant},$$

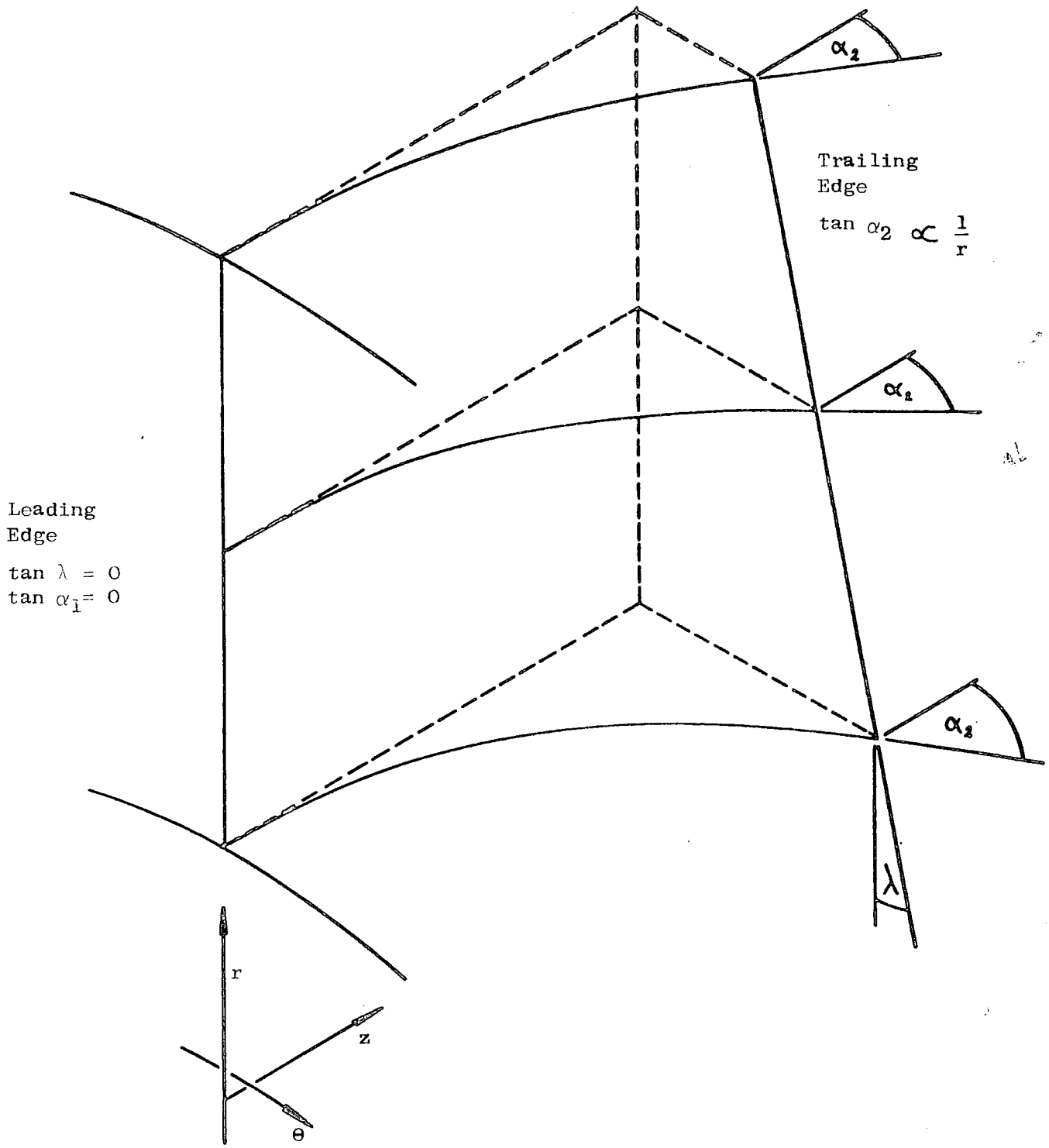

FIGURE 4.1: DISTRIBUTION OF LEAN ANGLE λ

or assuming a camber line which follows the quasi-streamline as described in Chapter 5,

$$\frac{\bar{\partial}(rV_u)}{\partial m} = \text{constant}$$

This is shown in Figures 4.2(a) and 4.2(b). Thus the term $-\frac{W_m}{r} \tan\lambda \frac{\bar{\partial}}{\partial m}(rV_u)$ in equation 3.15 is non-zero unless $\tan\lambda = 0$ or $\frac{\bar{\partial}}{\partial m}(rV_u) = 0$.

It is possible to construct a blade shape, and hence create a mean stream surface, with $\tan\lambda = 0$ over all or part of the leading edge or at any other chosen location, but for $\tan\lambda \neq 0$ at the leading edge, as is generally the real case, the step-change in the value of $\frac{\bar{\partial}(rV_u)}{\partial m}$ on blade entry indicates a sudden change in $\frac{\bar{\partial}W_m}{\partial m}$, which leads to redistribution of the fluid flow and a streamline shift.

At the blade trailing edge, the flow paths once again change from following the curve

$$\frac{\bar{\partial}(rV_u)}{\partial m} = \text{constant},$$

to the lossless free duct flow

$$\frac{\partial(rV_u)}{\partial m} = 0 .$$

The analysis indicates another redistribution here, unless $\tan\lambda = 0$; see Figure 7(c).

The radial gradient $\frac{\bar{\partial}}{\partial r}(rV_u)$ in equation 3.15 does not undergo these abrupt changes on passing a blade row edge, so does not raise the same problem, even if $\tan\mu \neq 0$.

4.4 Deviation

Although fluid close to the blade surfaces must follow their shapes, fluid distant from the surfaces does not turn fully onto the blade angle at exit, and so the mean flow direction downstream may differ considerably from the exit angle of the blade geometry. This difference is

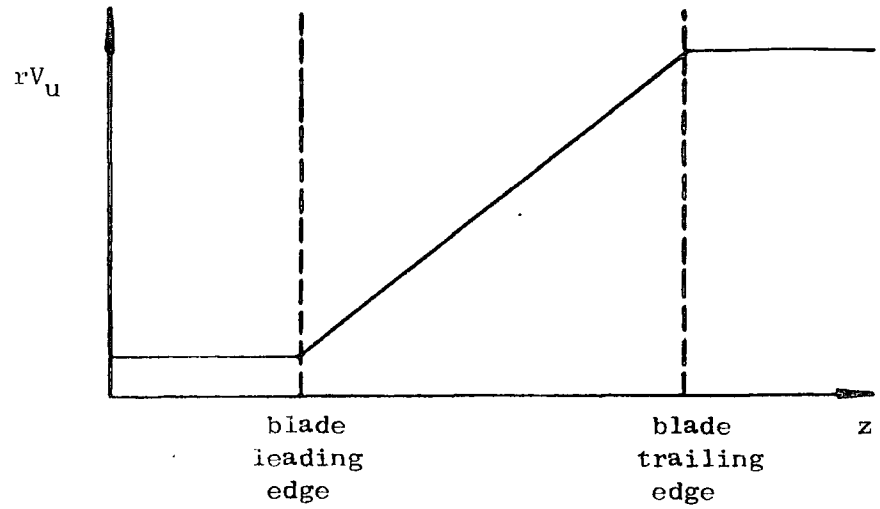

4.2(a)

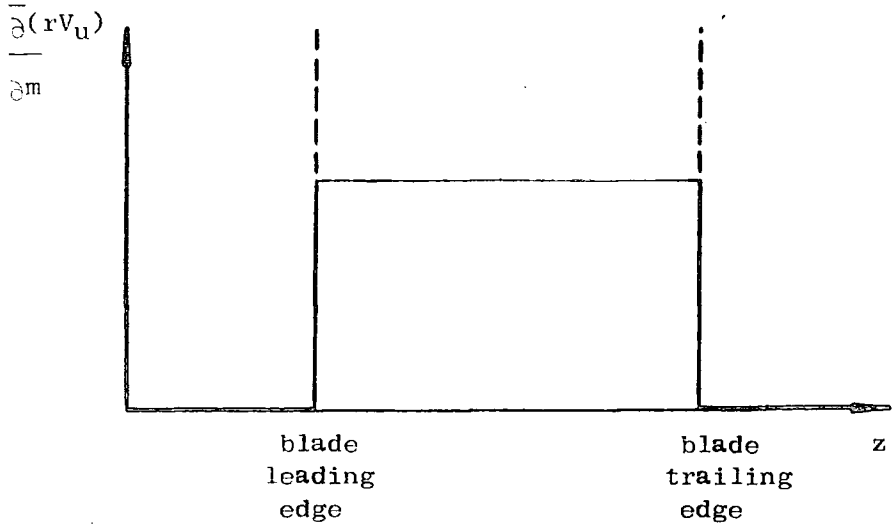

4.2(b)

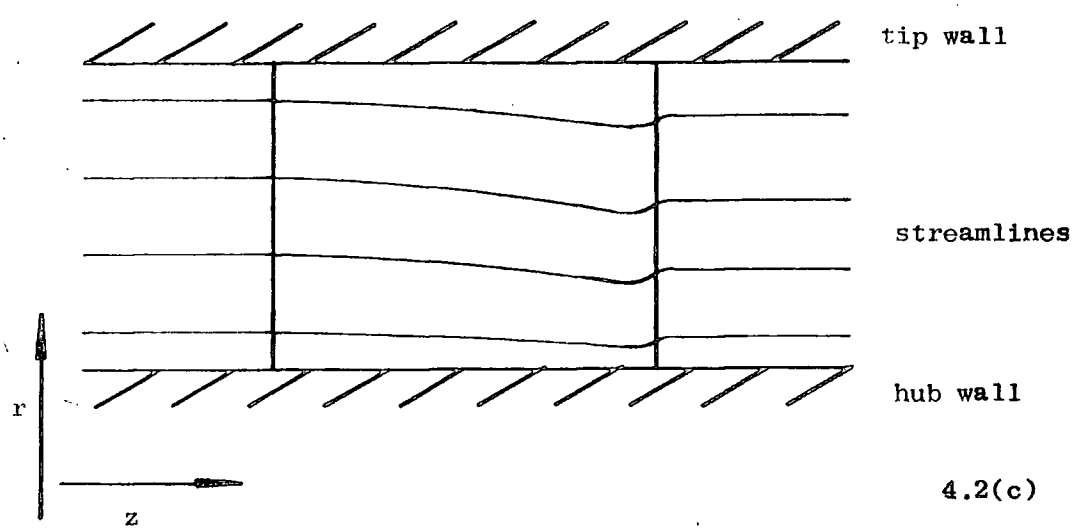

4.2(c)

Tan λ = 0 at leading edge only.

FIGURE 4.2: FREE VORTEX BLADE ROW WITH PARABOLIC CAMBER LINE

called the deviation, δ, and is a well-known effect (Horlock (1958); Cohen, Rogers and Saravanamuttoo (1972)). A widely-used empirical rule to estimate deviation is that included in Howell's blade design method, described by Horlock (1958), Cohen, Rogers and Saravanamuttoo (1972) and Dixon (1975). Howell's deviation rule is included in Appendix D.

It is reasonable to assume that fluid entering, at zero incidence, a row of blades with parabolic camber lines may follow a path which is parabolic, though reaching a different angle at exit from the blade angle, as shown graphically in Figure 4.3.

4.5 Non-Parabolic Flow Paths

The discussion of Section 4.2 emphasised that real fluid flow can not undergo discontinuities in its path, or sudden velocity changes. Thus where $\tan \lambda \neq 0$ on the mean stream surface, there cannot occur abrupt changes in $\frac{\overline{\partial}}{\partial m}(rV_u)$, but the fluid path must depart from the parabolic to one whereby circumferential curvature is acquired over a finite length after blade entry, and lost progressively before blade exit. The effect on the axial distribution of rV_u and of its meridional derivative, for $\tan \lambda \neq 0$ at both leading and trailing edges, are shown diagrammatically in Figure 4.4. The mean flow is assumed to leave the blade row at the angle predicted from deviation considerations; its progress to that flow angle is the matter in question.

From the principal equations 3.14 and 3.18, it is seen that

$$F_u + D_u = \frac{W_m}{r} \frac{\overline{\partial}}{\partial m}(rV_u).$$

In lossless flow, $D_u = 0$; in a duct region $F_u = 0$. By setting $\frac{\overline{\partial}}{\partial m}(rV_u)$ to zero at blade entry and exit, there is no circumferential load on the blade there: the value of $\frac{\overline{\partial}}{\partial m}(rV_u)$ may be used as a measure of the

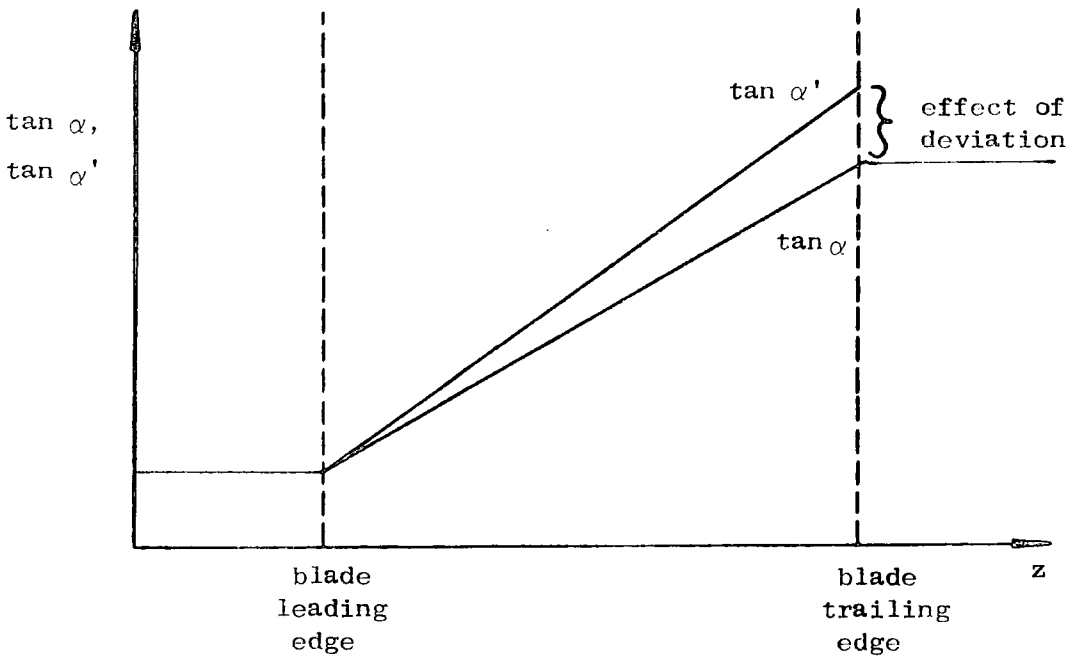

FIGURE 4.3: FLOW ANGLE DEVIATION

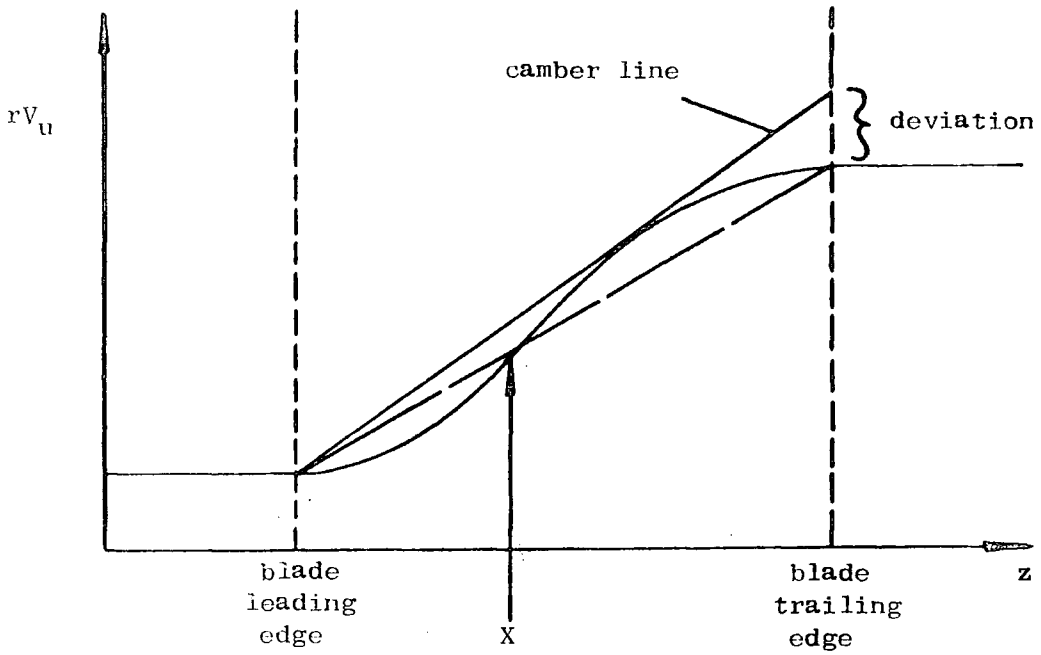

4.4(a)

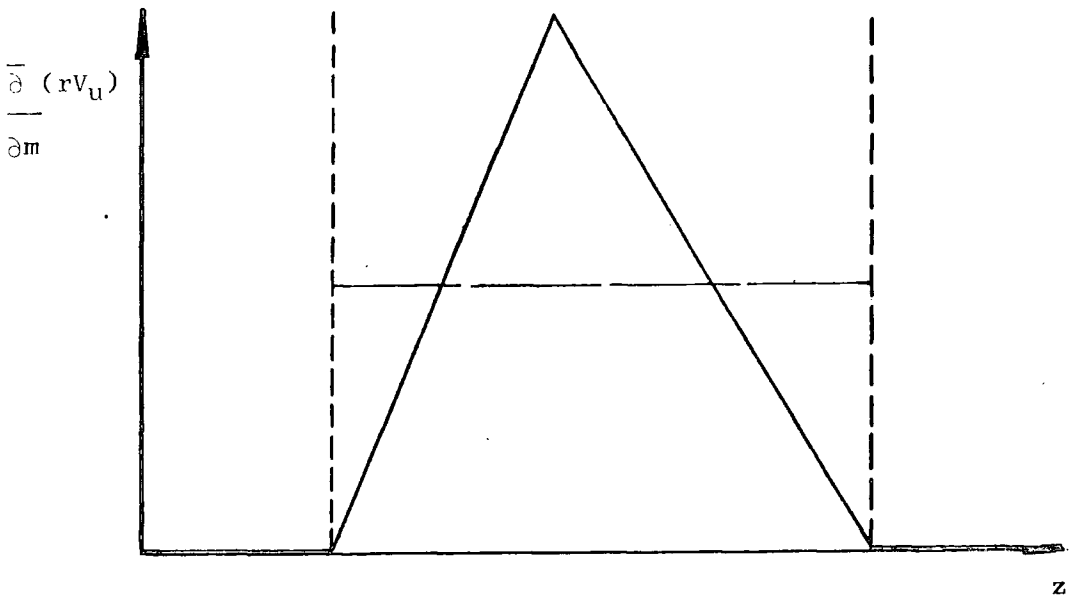

4.4(b)

———— parabolic fluid path

———————— realistic streamline

FIGURE 4.4: BLENDING OF CIRCUMFERENTIAL CURVATURE - ZERO INCIDENCE

local blade loading, and it is seen that the proposed modification to the assumed flow path implies that at other points within the blade, loadings are higher than originally reckoned.

The assumed form of the blending of circumferential curvature does not appear to be critical when using a mean S2 stream surface, and a workable rule was adopted which appears intiutively realistic.

The point X in Figure 4.4(a), at which the fluid is assumed to have turned fully onto the angle of the equivalent parabolic path, is thought to be about 0.2 to 0.4 of the distance through the blade row. Downstream of X, the fluid is over-turning relative to the parabola, though as drawn in Figure 4.4(a) its flow angle nowhere exceeds that of the blade camber line.

4.6 Non-Zero Incidence At Blade Inlet

Fluid entering a blade row at an angle different from the blade inlet angle will be turned rapidly to align closely with the direction followed if the fluid were entering at zero incidence. This is illustrated in Figure 4.5, assuming that downstream of X there is no difference between the two paths just described.

The curved rV_u profile upstream of X, shown by the solid line on the graph of Figure 4.5(a), must satisfy conditions of value and slope at the leading edge, and at point X, and is thus a curve of cubic or higher order.

As drawn in Figure 4.5, for case 'A' the circumferential velocity of the incident flow is first reduced and then increased again, on entering the blade. This indicates that the front portion of the blade will suffer reversed loading. The incident angle of flow 'B' is such that extra turning is applied to it immediately after blade entry, and so the loading just behind the leading edge is higher than for flow arriving with no incidence.

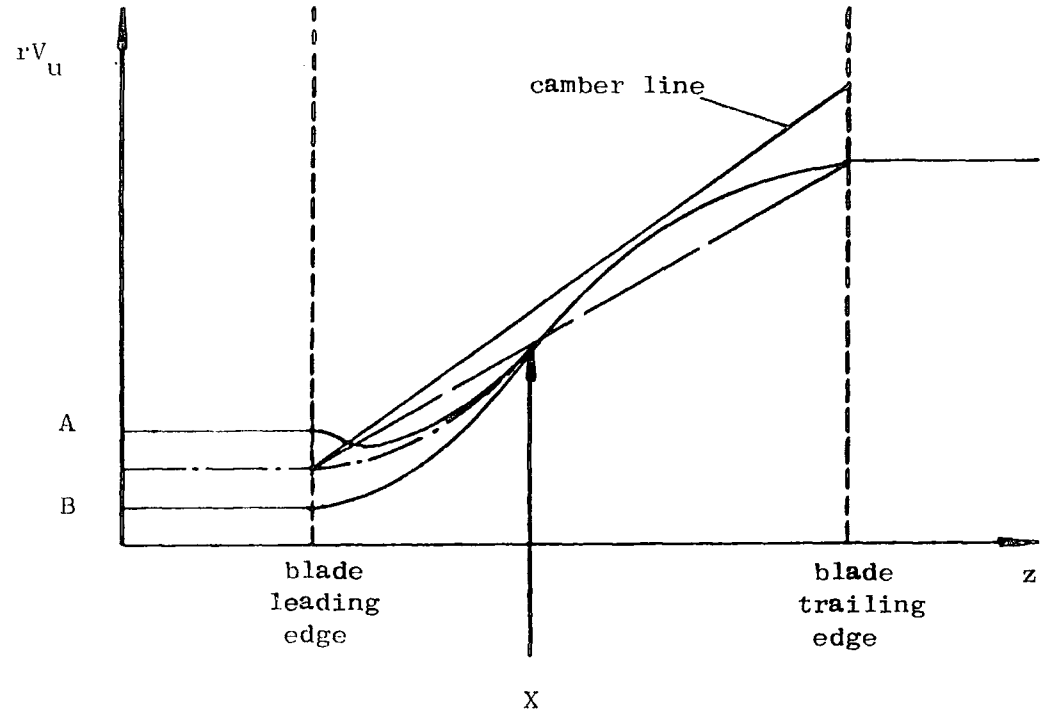

4.5(a)

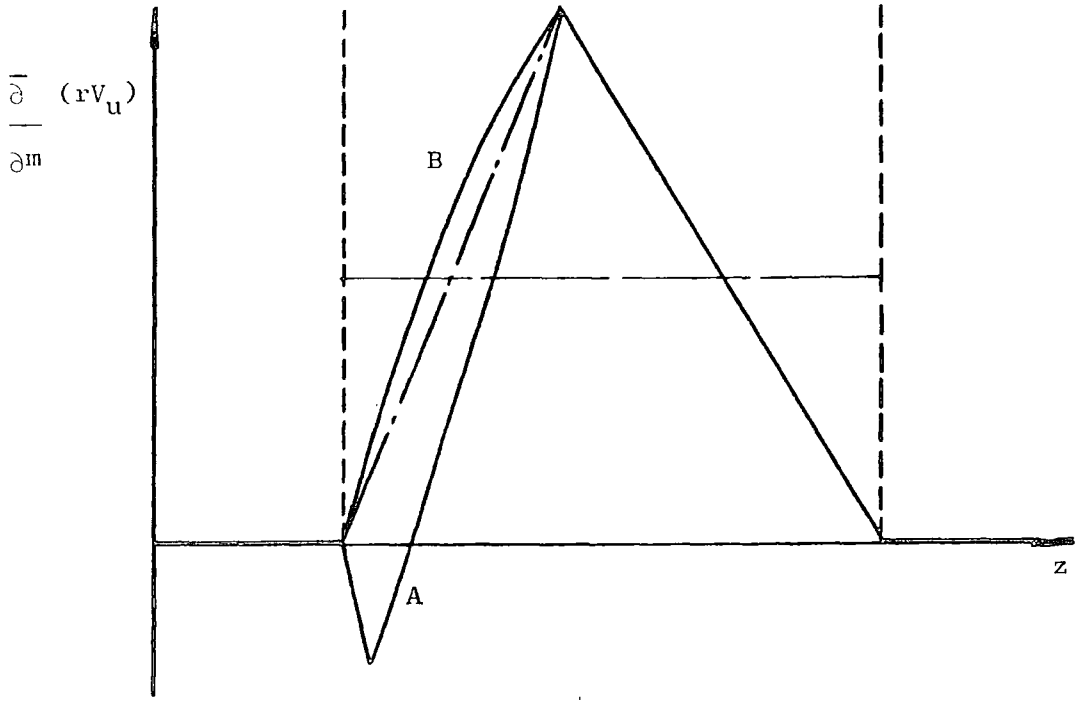

4.5(b)

——— ——— ——— parabolic path through blade

——— - ——— - ——— flow with zero incidence at entry

——————————— flow with non-zero incidence at entry

FIGURE 4.5: BLENDING OF CIRCUMFERENTIAL CURVATURE - NON-ZERO INCIDENCE

CHAPTER 5

BLADE DESIGN

5.1 Introduction

The purpose of the rows of blades in a turbomachine is to change the angular momentum of the fluid passing through, as by this means work may be transferred into or extracted from the fluid. The rate of change of angular momentum is matched by a circumferential force on the blade row, giving rise to a torque on the annulus. The rate of work transfer, or power, at a blade row is given by the relationship:

Power = Torque x Angular Velocity.

For a non-rotating stator row, no work is transferred, and for adiabatic flow the stagnation enthalpy of the working fluid remains unchanged. The fluid velocity, and thus its kinetic energy, is changed and there are compensatory changes in, for example, the pressure, temperature and density. In a compressor stator the desired end-product is a high pressure and so blades are used to decelerate the flow. A turbine stator is usually used to provide a high circumferential velocity for entry to the following rotor.

In a rotor row power is transferred from a rotating shaft to the working fluid, or vice versa, and the stagnation enthalpy changes between rotor entry and exit. There is consequently a change in the fluid stagnation temperature and generally also in the static values of properties.

The boundary layers on the blades and the annulus walls encounter favourable pressure gradients in turbines, but face adverse pressure gradients in compressors, and the difficulty of achieving flows free from separation over the blade surfaces resulted in axial-flow compressor development lagging behind that of turbines, and means that compressor design is much the more delicate task.

The cross-sectional shapes of axial-flow compressor blades are usually those of aerofoils known to give good performance. The profile is defined by a central camber line with a given distribution of material thickness along it, as illustrated in Appendix D. The chord line length is the straight line distance between the centres of curvature of the rounded leading and trailing edges. The camber line shape is usually composed of one or more circular arcs, or of a parabola; the leading and trailing edge angles are defined, and the curve constructed between them. For any curve other than a single circular arc, the proportion of the chord length is required at which the camber reaches a maximum. For the single circular arc this proportion is always 0.5; for the parabola it may be between 0.25 and 0.75, but is normally around 0.4.

Experimental tests on such aerofoils are often performed under conditions and in configurations very different from those actually occurring within the turbomachine; the aerofoil base profiles often originate from those used in isolation for the wings of aeroplanes, rather than in the proximity of several other aerofoils to each side, forming a cascade. Recorded data are generally available for linear cascades of identical aerofoils set in wind tunnels with uniform approaching flow. In the annular cascades in turbomachines, the pitch varies from the hub to the tip radius, the blades are often of twisted shape, and the approaching flow may be considerably non-uniform.

Radial shifting of streamlines may be minimised across turbomachine blade rows by adopting the free-vortex radial distribution of circumferential velocity, as discussed in Chapter 4, where it was shown that it is impossible to satisfy the free-vortex condition at all points within a blade row, and so there is some radial deviation from the most direct flow paths. Blades for free-vortex flow are considerably twisted, creating mechanical strength problems in such designs.

Another factor affecting streamline positioning is the partial blockage caused by the thickness of real blades, which varies in proportion both radially and axially through a blade row.

5.2 Sign Conventions for Blade Angles

The nomenclature for a cascade of blades is shown in Appendix D. For annular rows of blades the symbol usage holds over small displacements of the θ co-ordinate. For rotors, the absolute gas angles are still denoted by α, but the rotor-relative gas and blade angles are denoted by β and β' respectively, so that as shown in Figure 5.1,

$$\tan \alpha = \frac{V_u}{V_z} ; \qquad \tan \beta = \frac{W_u}{W_z} .$$

The angle θ and the velocities V_u, W_u, are taken as positive in the direction of rotor rotation ω. The sign convention for angles α, β follows from the definitions given for their tangents.

Further defining positive streamline slope such that

$$\tan \epsilon = \frac{V_r}{V_z}$$

equation 3.8 shows that

$$\tan \mu = - \tan \beta - \tan \epsilon \tan \lambda .$$

5.3 Stream Surfaces for Blade Design

In flow normal to a long untwisted aerofoil of uniform section, stream surfaces are plane, and the flow paths coincide with the cross-section for which data are tabulated.

Figure 5.2 shows flow with a spanwise component approaching the aerofoil which will clearly be presented with a longer path over the surface and, to an observer travelling with the flow, the aerofoil will appear longer and give a different camber angle from that for

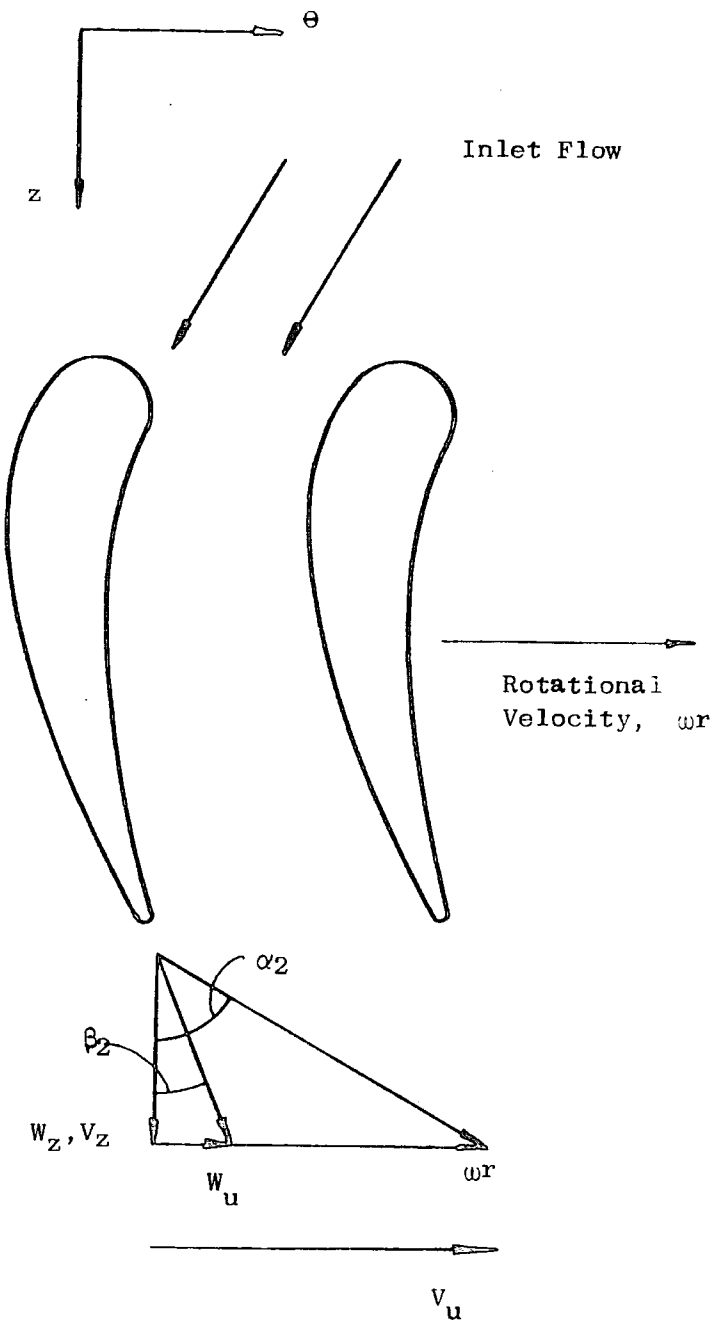

FIGURE 5.1: BLADE VELOCITY TRIANGLES

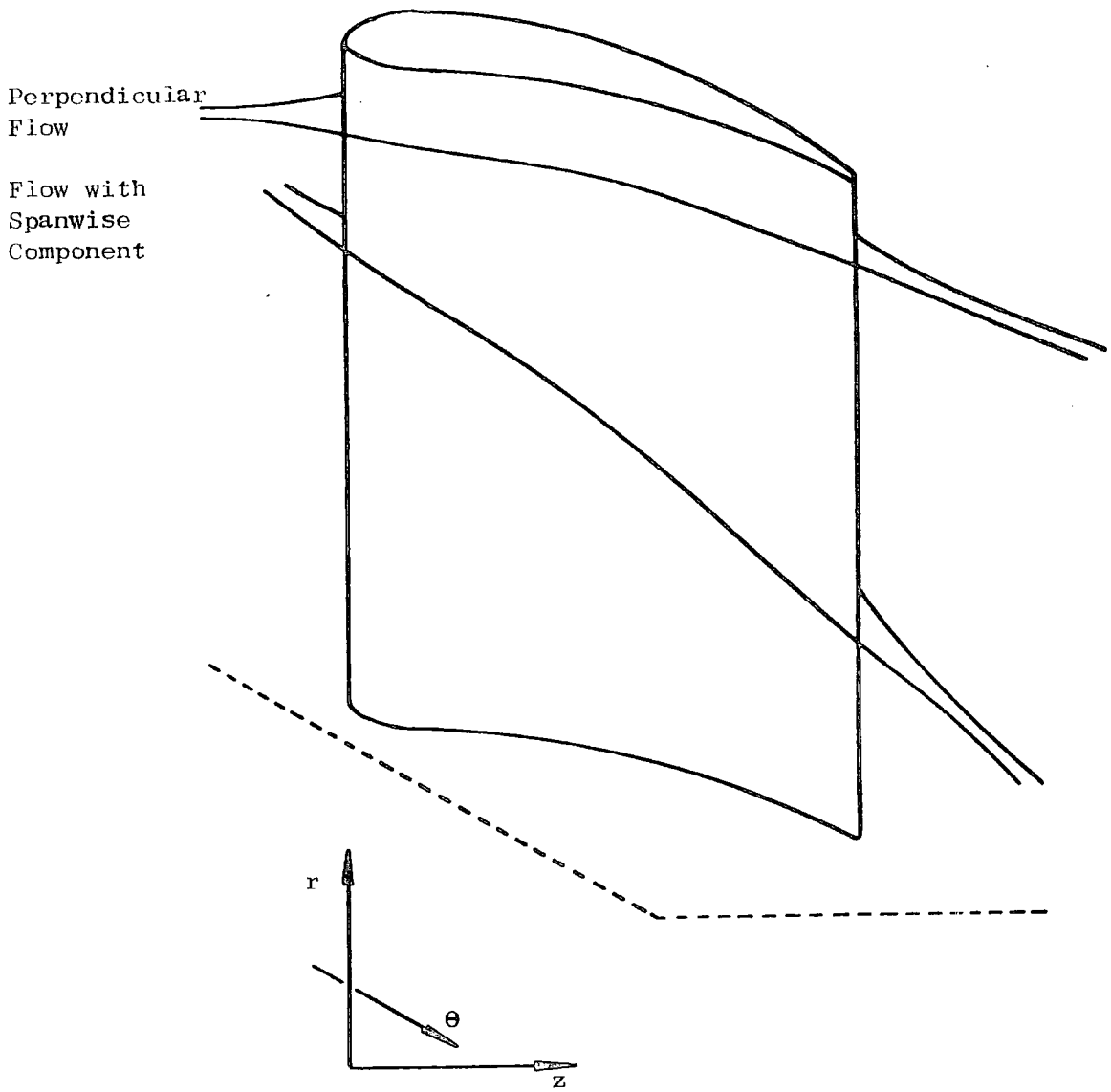

FIGURE 5.2: FLOW PATHS OVER AEROFOIL

perpendicular flow. Furthermore, if the aerofoil were twisted in shape the camber line would appear to the observer to depart from the design parabola or circular arc. Thus to make sensible use of aerofoil performance data, the standard aerofoil shape must be constructed on the true stream surface, and not on a surface merely of geometric convenience. Such a design procedure will be iterative, since the introduction of a row of blades will alter the streamline paths from those adopted if no blades were present; and the final stream surface shapes are not known until flow calculations are complete.

In the computer program, conical surfaces as shown in Figure 5.3 are used as approximations to the truesurfaces, eliminating the iterative nature of the design procedure.

At both the casing walls, the cone angle ϵ is matched to the slope of the casing at its intersection with the design line. Other conical surfaces are defined, based at 10% radial intervals along the design line, with tan ϵ varying linearly from hub to tip.

Clearly, in a duct with walls curved in the (r, z) plane, conical surfaces at the hub and tip will not match the wall profiles at points other than the design line. Therefore after the design of the aerofoil has been completed on the conical surfaces, the radii of the grid points set up are modified so that the hub and tip sections follow the walls, and intermediate blade sections are altered proportionately. The θ co-ordinate and the blockage factor need to be trimmed accordingly, but the blade angle α' is unchanged.

5.4 The Stacking of Blade Sections

The 'stacking' of the aerofoil sections making up the blade as a whole was introduced in Chapter 4. Radially-varying flow conditions require a set of differing aerofoil cross-sections, and a certain

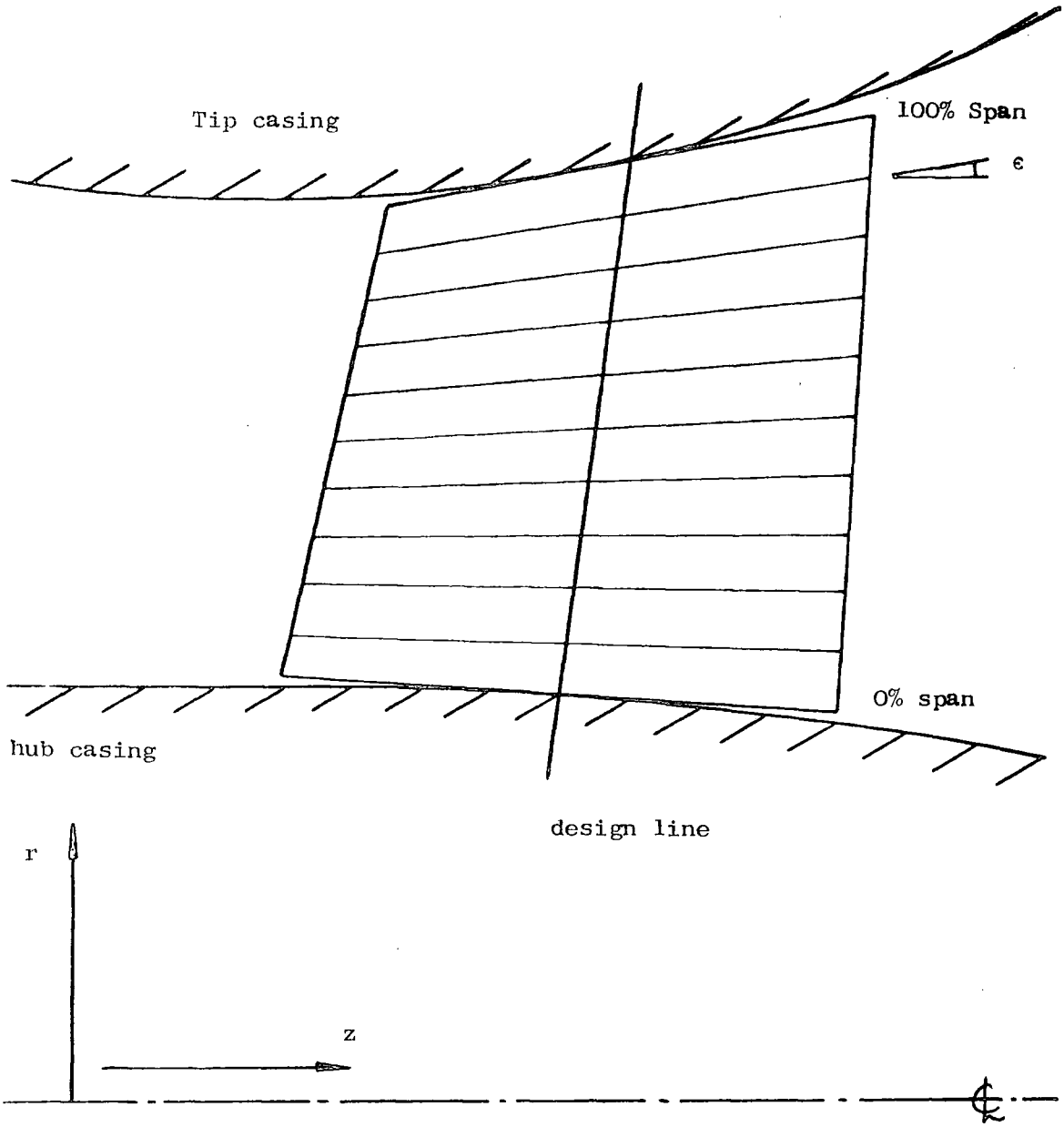

FIGURE 5.3: BLADE DESIGN GRID GEOMETRY

freedom is available to the designer in arranging them, axially and circumferentially, relative to their neighbours. The aerodynamic implications of the stacking have been discussed in terms of the angles λ and μ, which vary as the stacking is altered. Other constraints on the designer's freedom arise from mechanical stress limitations, and manufacturing feasibility.

The computer program requires as input data the geometry of the annulus walls, together with a 'design line' on which the blade section chords are centred axially. By setting an inclined design line it is possible to generate blade shapes with sweepback, as is seen in Figure 5.3.

As viewed axially, the blade sections are stacked radially on their centres of mass, found by considering not only the blade thickness distribution but also the changing radial depth between the non-parallel neighbouring cones.

Input data for the chord lengths at hub, mid-span and tip may be specified as being either the true chord lengths, or only the meridional component (the view in Figure 5.3), of the chords. Values at locations other than the three entered are found by interpolation. Radial variations in chord, together with varying stagger angle τ, mean that the blade leading and trailing edge profiles in the meridional (r, z) plane will generally be curved. Intermediate points, at 10% intervals axially along each cross-section, are found as reference grid points, and thus the whole blade mesh is in general curved in the meridional plane, except that the grid line connecting all the mid-chords is the original straight design line.

5.5 Conical-to-Planar Conformal Mapping

Cascades of uniform aerofoils possess camber lines lying in plane cross-sections, and chords which are straight lines. Applied to the

conical design surface of the turbomachine, the equivalent geometry lies on a curved surface and it is necessary to construct an aerofoil shape as seen by an observer moving with the fluid in the turbomachine, to provide equivalence between the behaviour of the turbomachine blades and the known behaviour of the linear cascade.

Considering Figure 5.4, let q be a co-ordinate on a conical surface, following constant θ, and originating at the apex of the cone. The conical surface may be mapped onto a plane with rectangular co-ordinates by the transformation

$$\eta = \theta \quad ; \qquad \zeta_2 - \zeta_1 = \frac{1}{\sin\epsilon} \ln\left(\frac{q_2}{q_1}\right). \qquad (\epsilon \neq 0)$$

The transformation may be manipulated for use in the reverse direction:

$$\theta = \eta \quad ; \qquad \frac{q_2}{q_1} = \exp\left[(\zeta_2 - \zeta_1)\sin\epsilon\right].$$

The mapping is used in designing conical blade sections, the cones being approximations to the true stream surfaces. A linear cascade of aerofoils is constructed on the (ζ, η) plane, following Appendix E, with straight chord lines AB, and parabolic camber lines, with the thickness distribution of a desired standard aerofoil. The geometry constructed is then mapped onto the cone, and while angles are preserved (e.g. the stagger angle τ), the blade shape is altered.

The data required are the true length of A'B' on the turbomachine conical design surface, and the entry and exit blade angles on the conical surface, σ_1 and σ_2 respectively, which are related to α_1' and α_2' by

$$\tan\sigma = \tan\alpha' \cos\epsilon .$$

The entry and exit angles appear unchanged in the construction on the (ζ, η) plane, and so the stagger angle of the blade, τ, or the slope of the straight line AB may be found for a blade with a parabolic camber line by:

$$\tan\tau = \tan\sigma_1 + \tfrac{1}{2}(\tan\sigma_2 - \tan\sigma_1).$$

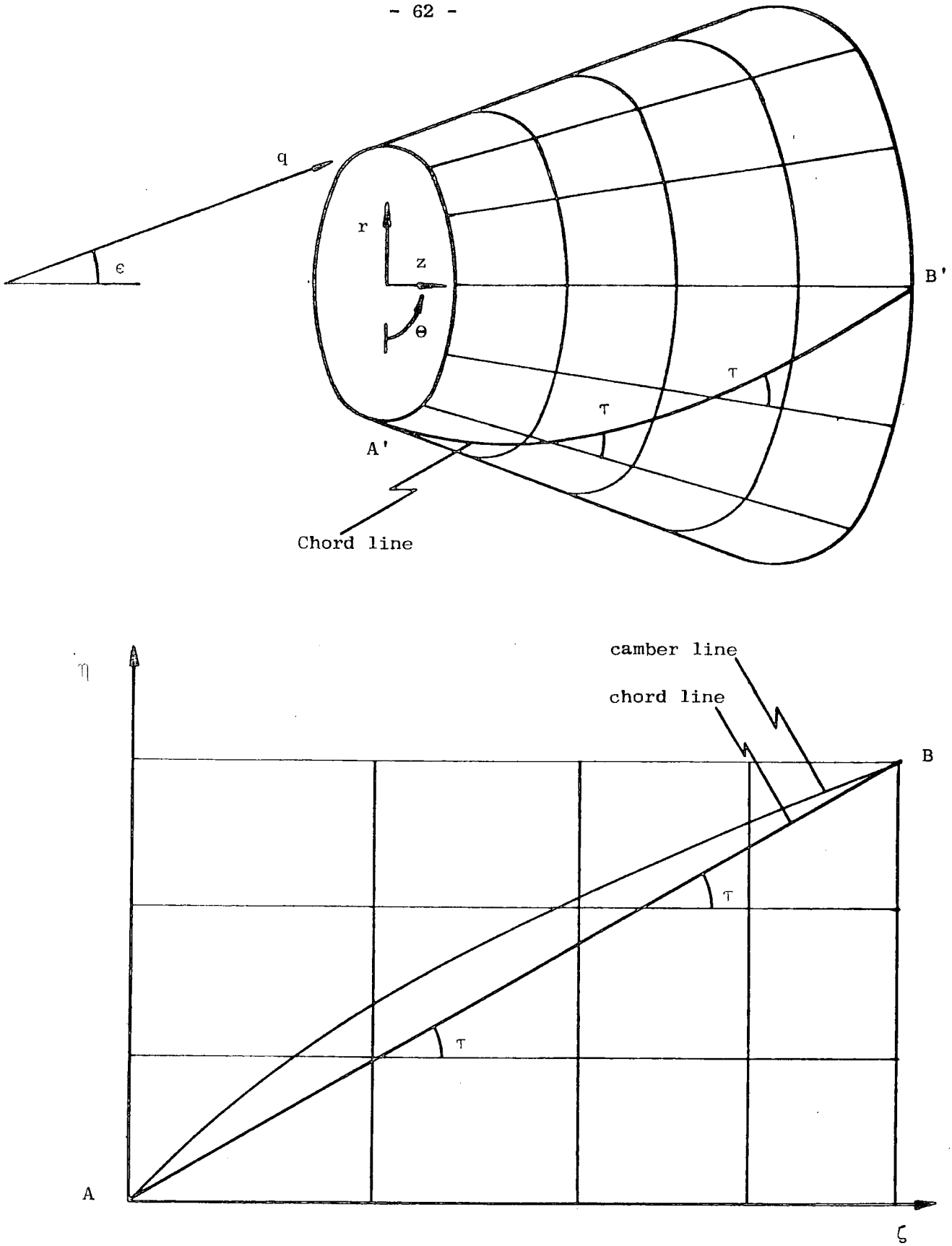

FIGURE 5.4: CONICAL TO PLANAR TRANSFORMATION

This is for the case of the parabola axis being parallel to the η-axis. The ratio a/c may then be calculated.

If a/c is specified as design data, then the construction comprising the parabola, its axis and the chord line may need to be rotated to satisfy both the angle change $(\sigma_2 - \sigma_1)$ and the ratio a/c. The stagger angle then changes also, and the camber line shape is constructed according to the procedure in Appendix E.

The length of any straight chord line, whether on a 'rotated' construction or not, may be determined as follows, for use in scaling the blade thickness distribution on the (ζ, η) plane. The ratio (q_2/q_1) is needed, and is found by considering the conical surface to be unrolled into a plane section of an annulus, as depicted in Figure 5.5. The chord line A'B' crosses all the radiating constant-q lines at the same angle τ. Such a line is a logarithmic spiral of form

$$q = q_o e^{k\varphi}$$

where q_o is a constant, the value of q at $\varphi = 0$;

$$k = 1/\tan \tau;$$

$$\varphi = \theta \sin \epsilon.$$

The length of the logarithmic spiral between points A' and B' is

$$A'B' = (q_2 - q_1) \frac{\sqrt{1 + k^2}}{k}$$

so that

$$(q_2 - q_1) = A'B' \frac{k}{\sqrt{1 + k^2}}$$

Hence if q is fixed at one end of the chord, or at its centre, then q_1, q_2 and the ratio (q_2/q_1) are found, and thus the length AB from the mapping.

A symmetrical aerofoil with its camber line coincident with its chord line generates no lift if the angle of attack $(\alpha_1 - \alpha_1')$ is

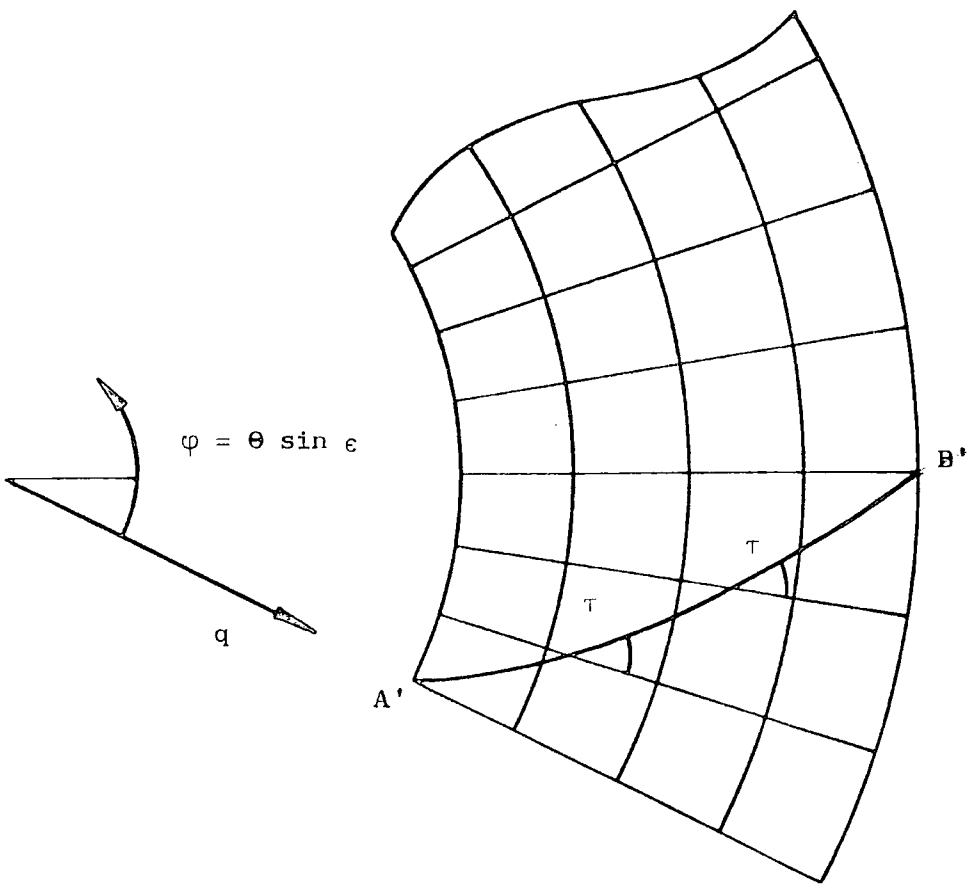

FIGURE 5.5: CHORD LINE AS LOGARITHMIC SPIRAL

zero. Note that such a zero-lift aerofoil on a conical stream surface nevertheless has a three-dimensionally-curved camber line.

The calculation technique for applying blade thickness data to the transformed aerofoil is detailed in Appendix E.

CHAPTER 6

NUMERICAL TECHNIQUES

6.1 Introduction

Closed solutions to the equations of motion, equations 3.14 or 3.18, derived in Chapter 3, are available for only a few special cases of flow fields; three are described in Chapter 7 by which the behaviour of the computer program was checked. Expressing the main equation in the form:

$$\frac{\partial W_m}{\partial r} = K(r)\, W_m + \frac{L(r)}{W_m} \qquad \ldots (6.1)$$

these cases are those in which many terms in the functions K(r) and L(r) vanish.

More generally, the values of K(r) and L(r) at any point depend upon the local values and rates of change of various properties and velocities, so that the solution of equation 6.1 is found iteratively.

An initial estimate of the flow pattern gives first guesses for K(r) and L(r) at every calculation point on an arbitrary set of calculation stations, such as is shown in Figure 6.1. At some position, such as mid-span, on one of the calculation stations, the radial gradient of W_m is found from equation 6.1, and a new value is established for W_m at the adjacent position on the station (but see Section 6.3). Calculations proceed towards the hub and tip walls, to produce a new profile of meridional (and hence axial) velocity. The mass flowrate across the calculation annulus may be found by numerical integration, and compared with the flowrate at the machine inlet, where conditions will have been defined by input data. If necessary, a new choice is made for the central velocity, and the calculations repeated until the required mass flowrate is obtained.

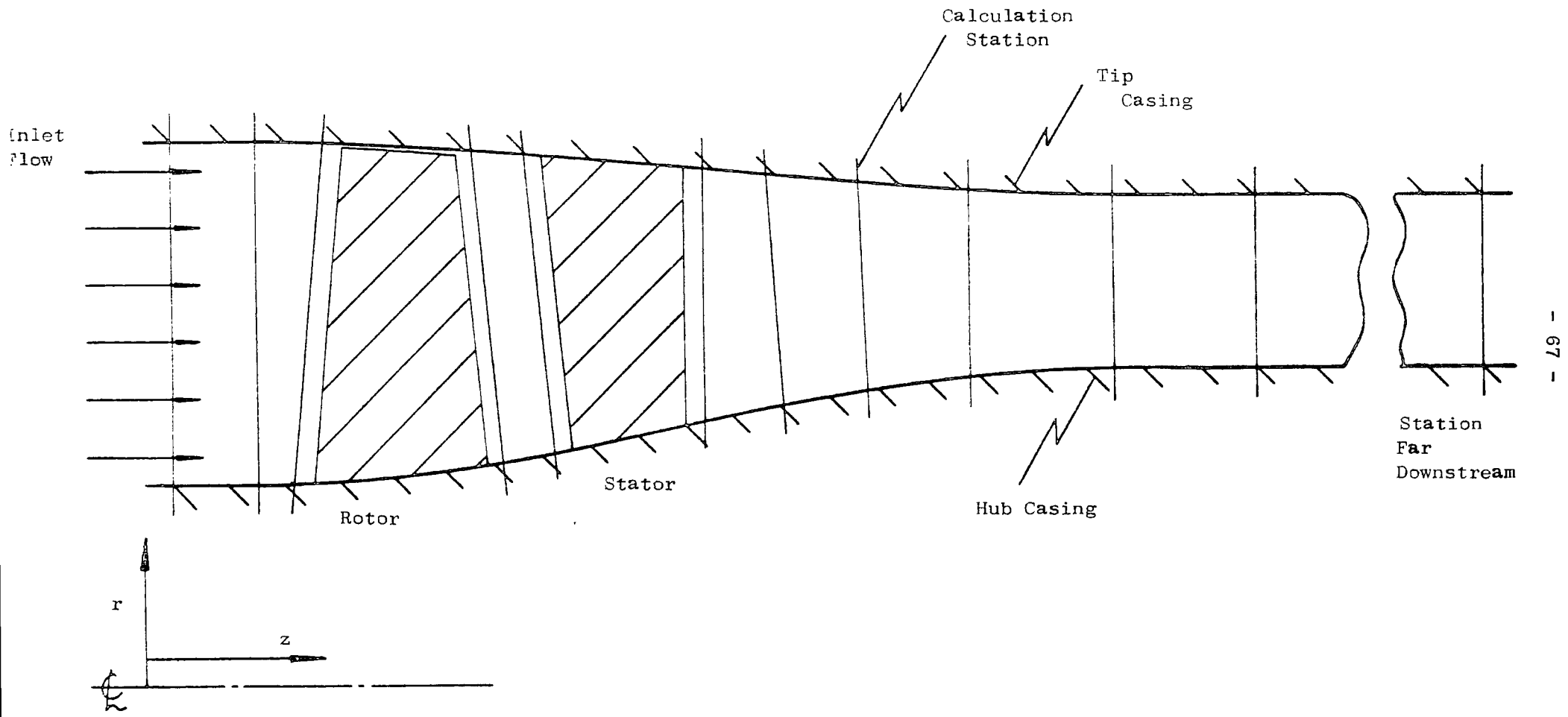

FIGURE 6.1: CALCULATION GRID

The velocity profiles are found at all calculation stations through the machine, usually working in a downstream direction, and then a new streamline pattern can be calculated, with new values for K(r) and L(r). The process of working on successive calculation stations is known as 'marching' down the machine. The complete cycle is repeated until one or more convergence criteria are satisfied. The numerical procedure can become unstable, and it is usually necessary to allow only small changes in the flow pattern from one iteration to the next, by the use of 'relaxation factors'.

6.2 Geometry of the Calculation Grid

It is necessary to define the geometry of the annular walls of the duct through which the fluid flows, and which contains the various rotor and stator blade rows. This is achieved by supplying the (r, z) co-ordinates of pairs of points, one of each pair lying on the inner (hub) wall, the other on the outer (tip) wall. Such points serve not only to define the shape of the duct, but also to provide quasi-orthogonal calculation stations, each pair of inner and outer wall co-ordinates being used as the extremities of a series of locations on the straight line joining them. A grid of calculation points is thus produced; enough points must be generated in the space between the two walls to give sufficient definition of the fluid flow.

Stations may be inclined from the radial direction, which is useful in ducts which are either severely-flared, or of the 'swan-neck' type, and for stations near to swept-back blade row edges.

The fluid flow at any calculation station is heavily dependent on that at adjacent stations both upstream and downstream, and so the flow pattern at the inlet station must be defined, there being no upstream station. The flow at exit from the machine is assumed to reach conditions of straight flow parallel to the machine axis far downstream of the exit.

In the computer program, this has to be modelled at a finite position, and so a dummy calculation station is formed, following the method of Silvester and Hetherington (1966), with inner and outer radii the same as those at the last real station in the machine. It is arbitrarily positioned downstream of the last station by a distance equal to the axial length of the defined duct.

The formation of the calculation grid within rows of blades has been described in Chapter 5. The small clearance between real rotor blade tips and the outer casing is not modelled; it is assumed there is no flow leakage over the blade tips.

6.3 Inclined Stations and Non-Axial Flow

Figure 6.2 shows a flared portion of duct carrying a flow which is not parallel to the axis of rotation. Sited on the duct are non-radial calculation stations PQ, RS and TU.

A and B represent two adjacent calculation points on the station RS. In finding the profile of W_m along the line RS, let equation 6.1 supply a value of the radial gradient of W_m at A. Applying this gradient over the radial distance δr gives the velocity W_m at point C, not at point B. The axial gradient of W_m at B is applied over the length δz to obtain finally the new estimate for the meridional velocity at B. The latest figures from which to find the axial gradient are those produced by the previous march through the duct, so the axial gradients lag, by one iteration, behind the radial gradients of W_m. Tracking along the station RS using real r - and z-derivatives gives for ready handling of curved calculation stations, such as are formed within blade rows.

It is difficult to find the axial gradient of any property directly near the duct edges, say at R or S, because neighbouring stations PQ and TU do not extend between the same radii as RS, so no data are available

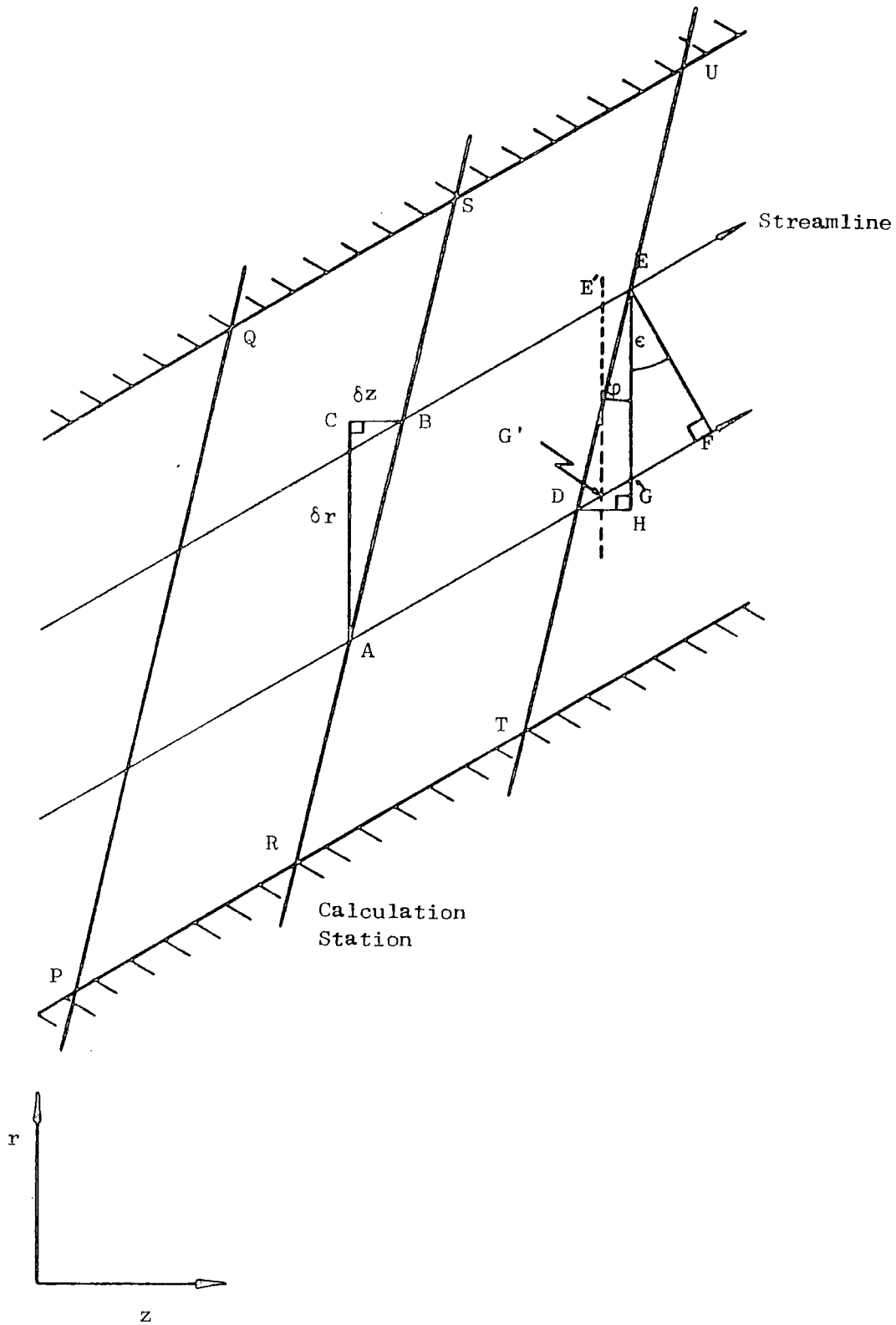

FIGURE 6.2: INCLINED STATIONS AND NON-AXIAL FLOW

downstream of R or upstream of S. It is easier to calculate first the meridional gradient by following streamlines QSU or PRT, and then to find the axial gradient using the relationships between the radial, meridional and axial gradients set out in Appendix B.

The summation of the mass flowrate across a calculation station is now considered, referring to station TU on Figure 6.2. BE and AF represent streamlines, across which no flow passes. EF is perpendicular to the local meridional direction, and so the increment of mass flow-rate

$$\delta\dot{m} = 2\pi r \rho V_m (EF) .$$

The radius r used here will be taken as the mean over the geometry line used. Line EGH is radial, and the calculation station is inclined locally at angle φ to the radial. The streamline slope is the angle ϵ, and

$$\cos \epsilon = \frac{V_Z}{V_m} = \frac{EF}{EG} .$$

$$\therefore \delta\dot{m} = 2\pi r \rho V_Z (EG) .$$

It is significant to note that DGF is a streamline, with no flow crossing it, so that the mass flow rate increment in terms of axial velocity and radial length involves EG, and not EH, the difference in radius between D and E.

E'G' represents the line EG repositioned so that the mean values of V_Z and r on it are also those for station increment DE. Then

$$\delta\dot{m} = 2\pi r \rho V_Z (E'G') .$$

It is r_D and r_E which do not vary as the flow field is recalculated, and it is convenient to calculate $\delta\dot{m}$ from the readily-available parameters V_m and $(r_E - r_D)$. The relationships

$$\cos \varphi = \frac{EH}{ED} ; \qquad \cos (\varphi + \epsilon) = \frac{EF}{ED}$$

yield

$$\frac{EF}{EH} = \frac{\text{Cos } (\varphi + \epsilon)}{\text{Cos } \varphi} = \text{Cos } \epsilon - \text{Sin } \epsilon \tan \varphi.$$

Hence

$$V_z \text{ (EG)} = V_m \text{ (EF)} = V_m \text{ (EH)} \text{ (Cos } \epsilon - \text{Sin } \epsilon \tan \varphi).$$

Following the nomenclature on streamline RS,

$$EH \equiv \delta r$$

$$\therefore \delta \dot{m} = 2\pi r \rho V_m \delta r \text{ (Cos } \epsilon - \sin \epsilon \tan \varphi).$$

The mass flowrate increments between all adjacent pairs of streamlines are found, using as property values the means of the values on the two streamlines. The sum of all the small increments provides the overall flowrate at the station.

6.4 Calculation of Velocity Profiles

K(r), L(r) and their components, the various properties, velocities and Mach numbers, are revalued only once per march through the machine, and so the production of an updated velocity profile for W_m is performed with distributions of K(r) and L(r) which are not changing as different mid-span W_m values are tried, despite the appearance of W_m in terms within L(r).

With fixed distributions of K(r) and L(r), a chosen central velocity, $W_{m \text{ mid-span}}$, yields a particular velocity profile from hub to tip, and correspondingly a single value for mass flowrate. A typical variation of mass flowrate with choice of central meridional velocity is shown in Figure 6.3, following Frost (1972). It will be seen from this Figure that though the mass flowrate may be determined uniquely from a given velocity value, the reverse is not true, in that a prescribed mass flowrate may be produced by two different flow solutions, one subsonic and the other supersonic. This point is discussed by Marsh (1971).

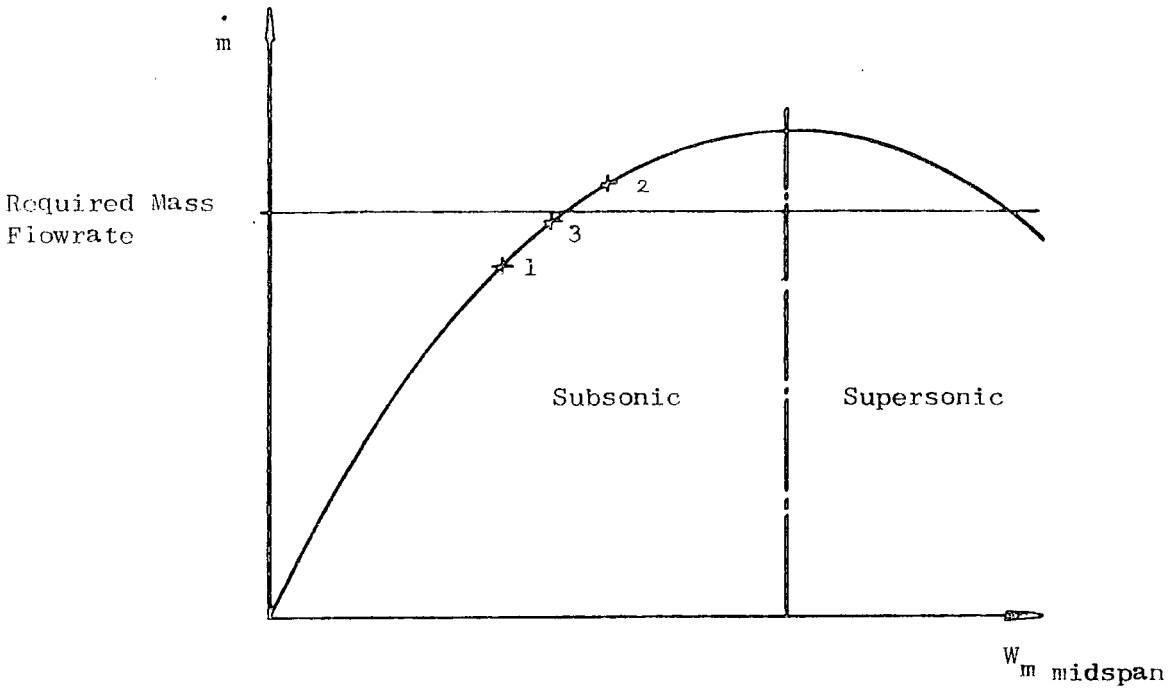

FIGURE 6.3: MASS FLOWRATE VARIATION

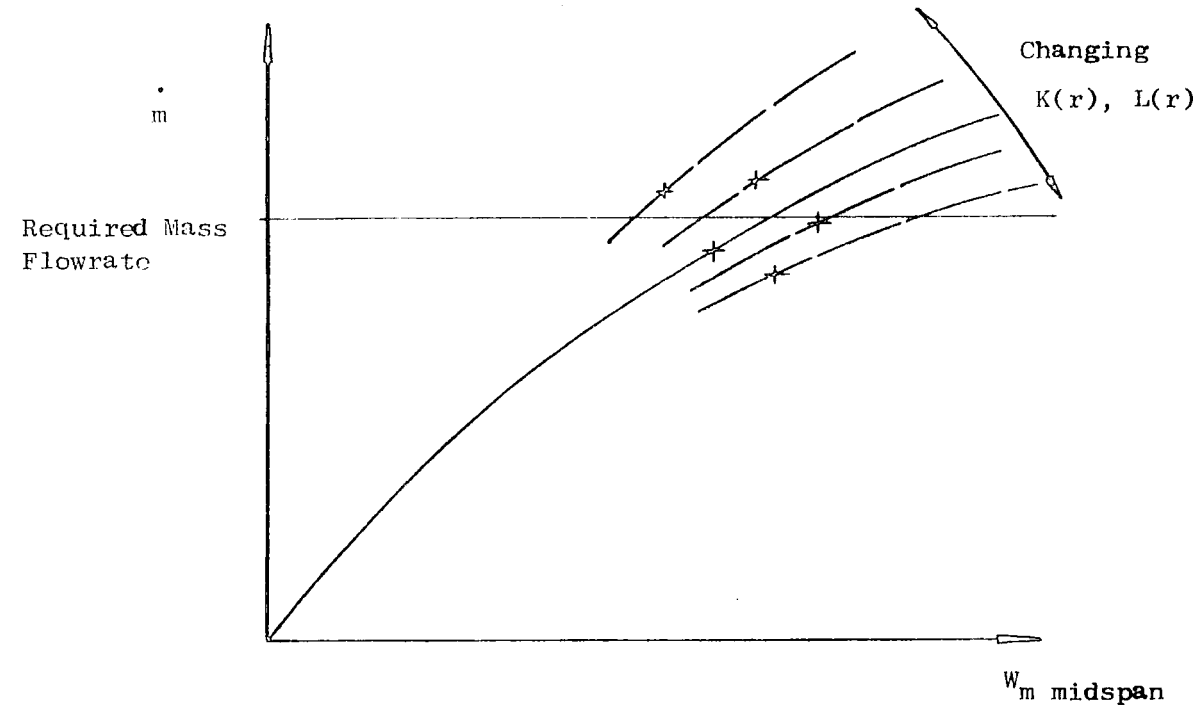

FIGURE 6.4: EFFECT OF CHANGING K(r) AND L(r)

The boundary between the subsonic and supersonic régimes is not distinct. Although there is a definite peak in the mass flowrate of Figure 6.3, any flow field with non-uniform velocity must exhibit a combination of subsonic and supersonic areas when operating around the maximum flowrate and the definition of 'choked' flow is then open to some debate.

It may be considered as simply the flow for which mass flowrate is a maximum - the peak of the curve in Figure 6.3. Alternatively, choking may be defined as the condition where no flow effects can propagate upstream, but unless the flow is sufficiently fast that a supersonic region extends across the entire blade passage, information about the downstream flow is transmitted upstream through the subsonic regions. Following this definition, the transition point may appear on Figure 6.3 to the right of the peak in the curve, indicating a flowrate which is less than the maximum.

In equations 3.14 and 3.18, the denominator $(1 - M_m^2)$, which appears several times, vanishes at $M_m = 1$, and so a singularity occurs there, preventing the analysis of transonic flows by this streamline curvature method. As mentioned above, there is a supersonic as well as a subsonic solution giving the required mass flowrate. For these reasons the overall solution method is envisaged as being applied to subsonic flow problems only.

In finding the distribution of W_m consistent with the mass flowrate, the initial guess used for mid-span velocity is that from the solution of the previous march through the flow field. With the revalued K(r) and L(r) terms, the velocity may now be in error, and produce a plot on Figure 6.3 such as point 1. The relationship between mass flowrate and $W_{m\ \text{mid-span}}$ is not linear, as Figure 6.3 shows, because the density changes with the fluid velocity, and so point 2 is taken as the next guess, with an over-large change in W_z, so that point 2 can be expected to lie

on the opposite side to point 1 of the required flow value. The small portion of the graph between points 1 and 2 is rather better to use for linear interpolation, and as more accurate estimates are obtained, the upper or lower limits, originally points 1 and 2, may be brought closer together. Convergence to very small errors in flowrate, point 3, is rapid.

It has already been mentioned that the factors K(r) and L(r) in equation 6.1 are held constant at each grid location, for the duration of the calculations to find a new velocity distribution. If they were changed during these calculations, to incorporate the very latest velocity values, for example, then the graph of Figure 6.3 would contain not one but many curves, each relating to a set of K(r) and L(r) values, but with only one point known on each curve. It is seen from Figure 6.4 that no conclusions as to a correct answer could be drawn from the resulting scattered solutions.

A widely-used condition in initialising the flow pattern, before any solution to the main equation is performed, is to assume an infinite radius of curvature, C, for all streamlines at all calculation points. This results in all K(r) terms becoming zero for the first march through the flow field, and equation 6.1 simplifies to:

$$\frac{\partial W_m}{\partial r} = \frac{L(r)}{W_m}$$

In examples where additionally the radial velocity may be initialised as zero, the equation simplifies further to that of Simple Radial Equilibrium.

It is quite usual for the velocity profiles at calculation stations to be changed dramatically on the first machine march, and this is enhanced over parts of the span where W_m is reduced, because with fixed L(r), $\frac{\partial W_m}{\partial r}$ increases in magnitude as W_m falls. The effect is shown in

Figure 6.5, accumulating as the integration of equation 6.1 proceeds towards the duct wall. The gradient $\frac{\partial W_m}{\partial r}$ becomes infinite if W_m falls to zero. To restrain such behaviour, limits are placed on the allowable profile change, being progressively tightened after the first few marches, to avoid instability and negative axial velocities: the latter would lead to double-valued stream functions.

It proved helpful to maintain the K(r) terms at zero for both the first and second flow field marches, so that the first is effectively used only to provide better estimates of L(r), and not to initialise K(r).

6.5 The Calculation of Streamline Slope and Curvature

The stream function ψ is constant along each of the walls of the flow duct and also, in axisymmetric flow, over any surface generated by revolving a streamline about the duct axis. The stream function values at one wall, say the hub, may usefully be set to zero, when the value on the other wall will correspond to the fluid mass flowrate passing through the duct.

The distribution of the stream function along each calculation station may be determined easily from the mass flowrate distribution, found during the calculation of the velocity profile. A series of streamline loci is thus available at the calculation stations, spread axially along the duct, including through the rows of blades.

Constructing the streamline as a curve through points of the same value of stream function, the streamline slope and curvature may be determined at the calculation points. The slope ($\tan \epsilon$) and curvature (C) both appear in the main equations 3.14 and 3.18, and the slope allows the determination of W_r and W_z from W_m. The curvature, with units of $(\text{length})^{-1}$, is defined as

$$C = -\frac{\partial \epsilon}{\partial m} \quad .$$

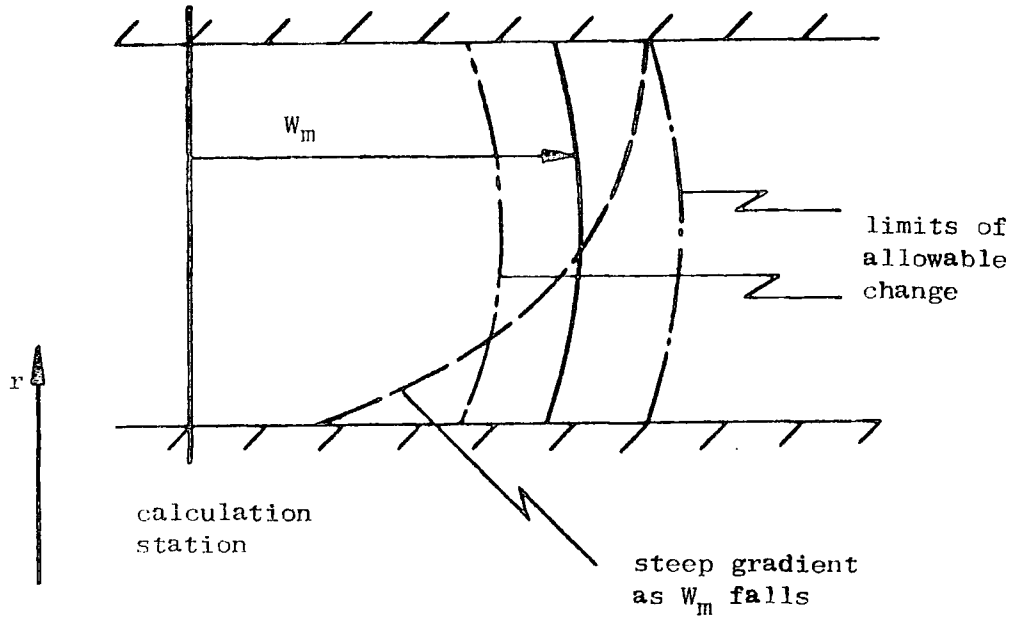

W_m profiles:

——— original estimate

— — — — first machine march

FIGURE 6.5: LIMITED VELOCITY PROFILE CHANGE

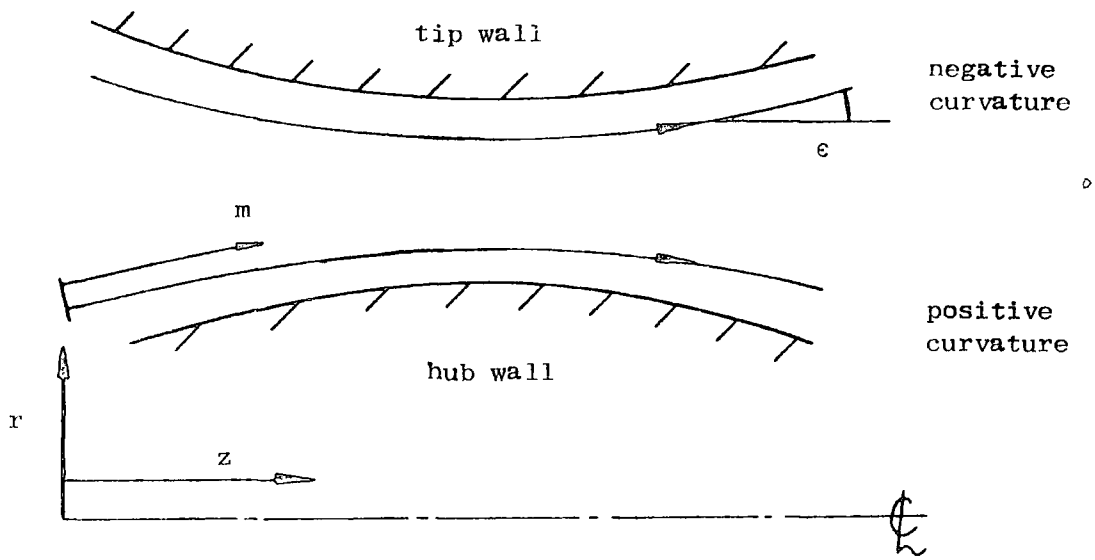

FIGURE 6.6: STREAMLINE CURVATURE

If the streamline is some function f(r, z), with z-derivatives

$$f' = \frac{\partial f}{\partial z} \quad ; \quad f'' = \frac{\partial^2 f}{\partial z^2} \quad ,$$

then

$$C = \frac{f''}{(1 + f'^2)^{1.5}} \quad .$$

Streamlines of positive and negative curvature appear as shown in Figure 6.6.

The method of fitting the curve through the streamline loci has been a matter of debate (Wilkinson (1970), Shaalan and Daneshyar (1969, 1972), Denton (1978)) and is a problem not encountered in the Matrix Throughflow solution technique (Marsh (1968)). It is, however, characteristic of the type of analysis presented here, which has thus become known as the Streamline Curvature method.

Shaalan and Daneshyar (1969, 1972) examine various polynomial and spline curve-fits to obtain slope and curvature. Their test cases are regular geometrical shapes - the circular arc and the sine curve. They propose that a piece-wise cubic spline be constructed through a set of data points and the streamline slope determined from the first derivative. Rather than differentiate this curve twice to produce the curvature, they recommend creating a new spline curve using the streamline slopes as data, and finding the curvature via the first derivative of this curve: the double-spline fit.

Wilkinson (1970) applies a wider variety of curve fits to the sine wave, and suggests an empirical combination of two different fitting methods as being best. Both he and Shaalan and Daneshyar find that curvature can be determined with good accuracy if there are many data points (> 20) per wavelength, but that the accuracy decreases as the point spacing is increased, reducing the number of data points per

wavelength. The 'best' curve fit is the one which remains accurate to the lowest wavelength/point spacing ratio. Wilkinson (1970) and Shaalan and Daneshyar (1972) present similar graphs of the accuracy obtained in predicting the curvature at a point on a sine wave using various curve fits and various spacings of the data points. However, the two papers show some anomalous results.

For spline curve fits they agree that as wavelength/point spacing ratio is reduced from 20 to 5, the ratio of predicted curvature/true curvature becomes progressively greater than unity. A second example common to both papers, a piece-wise parabola through five points, with a least-squares fit, is shown by Shaalan and Daneshyar (1972) to behave similarly to the spline curve, though with greater error, but Wilkinson (1970) shows the predicted/true curvature ratio as progressively falling below unity as wavelength/point spacing is reduced.

Wilkinson (1970) and Shaalan and Daneshyar (1969, 1972) refer to the data-smoothing technique of Wood and Marlow (1967) to damp high order harmonics. This technique was developed empirically as a means of obtaining convergence in streamline curvature calculations, performed apparently with no form of relaxation (Section 6.7). However Cornock, in the Communications on Wood and Marlow's paper, presents a mathematical basis for the technique and reports stability and rapid converegence using it on iterative problems.

Denton (1978) has found overall computing accuracy in programs to be more dependent on the empirical data input than on the numerical scheme, and has used at C.E.G.B. a three-point parabolic curve fit to obtain slope and curvature. Stow (1971) at Rolls-Royce also uses the parabolic fit. Denton (1978) sets the axis of the parabola perpendicular to the line joining its two outer points, so that greatly-sloped streamlines may be constructed realistically. Wilkinson (1970) shows the three-point parabola to be a more accurate method of determining curvature than many more complicated curve fits.

The calculation method used in the present work employs the three-point parabolic curve fit, following Denton (1978) to find the slope, but inspired by the methods of Shaalan and Daneshyar (1969, 1972) the curvature is determined from the slope of a second parabola, constructed using the streamline slopes as data. Curvature is thus affected by more data points than just those adjacent to the calculation point, reducing the expected error.

6.6 Convergence Criteria

A converging iterative procedure is terminated when changes in some selected parameter become sufficiently small. There are several usable terms in the streamline curvature analysis. Stow (1971) measures proportional change in static pressure at each calculation point, and terminates calculations when sufficient of the points in the flow field have experienced sufficiently small pressure changes between successive marches through the flow field. Novak (1966) inspects for the greatest shift of streamline position, as a proportion of duct height. Wilkinson (1970) comments that at Mach numbers approaching unity, streamline shifts are small even for large velocity changes, and that the maximum velocity change is a better convergence criterion; in the present work the proportional change in meridional velocity is used.

The formation of the meridional velocity profiles at the individual calculation stations is also an iterative process, requiring a matching on mass flowrate. The mass flowrate tolerance here is set rather tighter (at least 100 times smaller) than the tolerance on the meridional velocity change for the whole machine being analysed, to ensure that the error introduced into W_m by an inexact flowrate value is insignificant, compared to the changes in W_m caused by streamline redistribution.

Section 6.8 deals with the optimum size of relaxation factors to use. The resulting values for closely-spaced calculation stations can be very small, and without careful inspection the small flow field changes they allow can be mistaken for arrival at the converged solution. At the stage in the calculation cycle where the relaxation factors are applied, e.g. in the calculation of slopes from stream function distributions, a discrepancy is generated between the stored values (of slope) and the values produced if no relaxation were applied. This discrepancy only becomes negligible when the true convergence is achieved, which is worth verifying if closely-spaced calculation grids are involved, as in the present application with several stations within each blade row. Such a check was built into the program as described in Section 6.9 and used after the velocity change criterion had been finally met.

6.7 The Location of Relaxation Factors

Wood and Marlow's (1967) data-smoothing technique for streamline loci has already been mentioned (Section 6.5) as an aid to convergence in Streamline Curvature calculations. Silvester and Hetherington (1966) describe the application of an empirical relaxation factor to the changes in mass flowrate distribution predicted after each march through the flow field. If superscript n denotes the number of the iteration, $\bar{m}$ the mass flowrate predicted at a particular grid point, and m the value stored there, then the relaxation factor μ is used thus:

$$m^{(n+1)} = \mu \bar{m}^{n} + (1 - \mu)m^{n}.$$

Silvester and Hetherington (1966) cite an example wherein $\mu = 0.2$ realised a converged solution, but $\mu = 0.3$ caused divergent oscillation of the velocity profile as calculations proceeded.

Having applied the relaxation factor to mass flowrate changes, the subsequent parameters, namely stream function distribution, streamline slope and finally streamline curvature are calculated with no further

damping. Silvester and Hetherington's (1966) method leaves a discrepancy between velocity profiles and mass flowrate profiles though, clearly, when a converged solution has been obtained the matching will be close.

It is possible to apply the relaxation factor later in the calculations, to changes in the stream function distribution, or to the streamline slope calculation. This moves the discrepancy in property values to appear between mass flowrate and stream function, or between stream function and slope, and so alters some of the data to be used in the next march through the flow field.

The relaxation factor is usually applied to changes in the stream function distribution, i.e. streamline shifts, as done by Novak (1966) and Bosman and El-Shaarawi (1977), and also in the Matrix Throughflow method by Marsh (1968). Formulae to optimise relaxation factors for fastest convergence in such applications have been derived by Wilkinson (1970) and Stow (1971), and are discussed in Section 6.8.

Denton (1978) proposes an unorthodox use of damping factors, splitting his version of the main equation into 'streamline curvature' terms and 'radial equilibrium' terms, and relaxing on the streamline curvature terms rather than on changes of stream surface position. He also makes use of the same main equation for both duct and intrablade analysis, but finds that the radial equilibrium terms need to be damped in the latter case by the factor $\cos^2 \beta$, to maintain stability.

Instability had been encountered with the computer program of the present work when performing calculations in regions of significant swirl. It was found that such problems could be circumvented by applying a $\cos^2 \beta$ relaxation factor to changes in the function L(r) of equation 6.1, in both duct and intrablade applications. The separation of the terms in equations 3.14 or 3.18 into the groups K(r) and L(r) is similar to Denton's (1978) distinction between streamline curvature terms and radial equilibrium terms.

A further empirical trial, to perform the main relaxation in the streamline curvature calculations, involved the transfer of Stow's (1971) relaxation factors from the stream function calculation to the streamline slope calculation. For the example tried, this ad hoc system did indeed produce faster convergence, as detailed in Section 8.4, and was maintained in the program.

6.8 Optimum Values of Relaxation Factors

Wilkinson (1970) and Stow (1971) have derived similar expressions for optimum relaxation factors, f', used in streamline curvature procedures with approximately orthogonal calculation grids. The value of f' may change from location to location, and also to a lesser extent from iteration to iteration, since a Mach number effect is included in the formulae. The relaxation factors are intended for application to the repositioning of streamlines after successive marches through the flow field, though the advisability of using velocity, and not streamline position, for the convergence criterion has been mentioned in Section 6.6, and the experimental re-application of f' to the streamline slope calculation discussed in Section 6.7.

The formula of Stow (1971) is similar to that of Wilkinson (1970), which is given as

$$f' = \frac{1}{1 - \frac{5}{96} k_{min} (1-M_m^2) A^2}$$

k_{min} depends on the curve fit used; for the parabola through three points, $k_{min} = -4$. Note that k_{min} is negative, so $0 < f' < 1$ for subsonic flow. Wilkinson (1970) also gives an estimate of the number of iterations, n required to reduce an initial streamline positional error to some small proportion, ϵ, of it:

$$n = \frac{\ln \epsilon}{\ln(1-f')}$$

For closely-spaced calculation stations, the aspect ratio, A, is nigh, so that then f' is approximately proportional to $\frac{1}{A^2}$, and f' reduces rapidly as stations are brought close together. This is significant in inserting stations within blade rows, as the close spacing implies the need for very many iterations before an accurate solution is obtained. The necessity to distinguish between small flow field changes caused by low f' values, and those due to convergence of the solution, was emphasized in Section 6.6.

6.9 Treatment of Closely-Spaced Intrablade Grids

Figure 6.7 depicts an isolated blade row in a cylindrical annular duct, with intrablade and duct calculation stations as shown. In determining the relaxation factor f' at any station, the grid aspect ratio used is the higher of the two obtainable with respect to the upstream and downstream stations. Thus low relaxation factors are set at the blade edge stations, owing to the close intrablade grid spacing. Applying the relaxation factors to the slope calculation rather than to the calculation of the stream function distribution, leads rapidly to the establishment of the overall streamline shift caused by the blade row (dash-dotted line in Figure 6.7), but the slope values lag considerably behind, and the result after only a few iterations, e.g. the second, which contains no curvature consideration, is very like that from Simple Radial Equilibrium calculations, which assume that the entire streamline shift occurs through the blade row. The process of slope incrementation, iteration by iteration, is very sluggish, though one would like to think it is running at the optimum rate. Correspondingly slow is the spread of the blade effects upstream and downstream, to produce a streamline like the dashed line in Figure 6.7, of the type given by the Actuator Disc Theory.

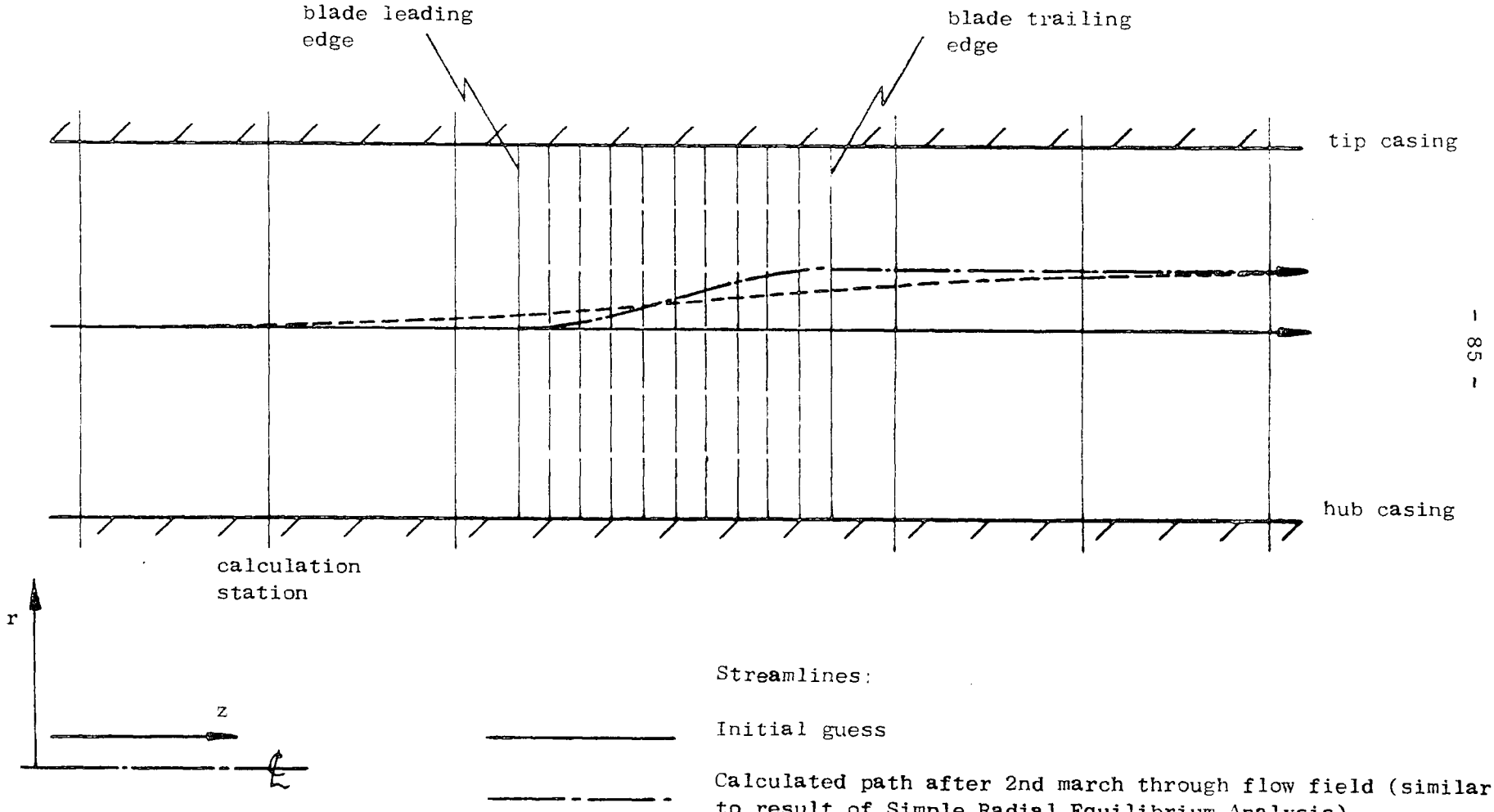

FIGURE 6.7: DEVELOPING FLOW THROUGH BLADE ROW

To accelerate the dissemination of the streamline shifts, the following scheme was devised:

(i) Consider initially all main grid stations, but only those intrablade stations at leading edge, mid-chord and trailing edge. This gives relaxation factors within the blade row 25 times as great as those obtained when using all eleven intrablade stations (set at intervals of 10% axial chord). Perform the calculations on the system until the solution is converged.

(ii) Obtain estimates, by interpolation, of the flow properties at the four intrablade stations at 20%, 40%, 60% and 80% chord length, and using these and the blade edges to form a finer grid, continue calculations until convergence is again obtained.

(iii) From the results of (ii), interpolate to estimate the properties at the other intrablade stations, and thus continue again to find the flow pattern using every station.

In part (i) there is little definition of intrablade flow, and the process of redistributing the axial variation of (rV_u) (Chapter 4) was limited to a matching of flow direction at blade entry, to that of the arriving flow.

The results of part (ii) may be used in a computer program, developed by Gregory-Smith (1977) using the analysis of Glynn and Marsh (1980), to find the change in mean stream surface flow angle at blade exit caused by secondary flow. Such modified flow angles are first used in a repetition of part (ii) (which often converges on its first iteration after being restarted), before entering part (iii). An extra convergence criterion was available for part (iii) as reasoned in Section 6.6: a check on the compatibility of the streamline slopes stored, with the unrelaxed slope values (i.e. plots through neighbouring points of equal stream function).

CHAPTER 7

Flow Fields With Analytical Solutions

7.1 Introduction

Far downstream of blade rows in an unflared annular duct, the fluid streamlines may be taken as straight and parallel, with no curvature or slope, and no radial component of velocity. The equation of motion in the $\underline{j} \times \underline{V}$ direction, equation 3.18, then reduces to that for simple radial equilibrium:

$$\frac{\partial h_o}{\partial r} - T \frac{\partial s}{\partial r} = V_z \frac{\partial V_z}{\partial r} + \frac{V_z \tan \alpha}{r} \frac{\partial}{\partial r} (r V_z \tan \alpha)$$

Assuming the flow to be axisymmetric, the partial derivatives may be replaced by ordinary ones. If the flow is homentropic at duct entry, and lossless in passing along the duct and through any blade rows, then $\frac{ds}{dr} = 0$ everywhere. If the total enthalpy is uniform at inlet, the flow adiabatic, and the blade rows are stators, not rotors, then $\frac{dh_o}{dr} = 0$ everywhere. Under these conditions the simple radial equilibrium equation becomes

$$\frac{dV_z}{dr} = - \frac{\tan \alpha}{r} \frac{d}{dr} (r V_z \tan \alpha) \qquad \ldots (7.1)$$

The tangent of the flow angle appears here; certain choices for the radial distribution of $\tan \alpha$, applied to equation 7.1 for the far downstream flow, allow the radial variation of axial velocity to be predicted there without recourse to iterative methods.

By creating suitable numerical examples to be solved by the computer program, aspects of its behaviour may be checked, since its solutions should be the same as the analytical answers.

For all cases, uniform non-swirling flow was modelled entering an annular duct, as shown in Figure 7.1, and the swirl was changed by a single stator row. The different types of stator flow exit angle distribution caused flow patterns far downstream which matched the predictions closely.

In using the program the flow angle variation for the far downstream location was applied at blade exit, but because a streamline shift does not occur entirely within the blade row (as is assumed in Simple Radial Equilibrium analysis - Chapter 2), some radial redistribution of the angle profile, and hence also of the axial velocity profile, took place between the stator and the calculation station far downstream. This introduced small differences between the solution obtained from the program, and that from Simple Radial Equilibrium analysis. It would be possible to trim manually the flow angle at blade exit, to arrive more nearly at the analytical angle distribution downstream, and to approach the predicted velocity profile more exactly. However, by specifying angle distributions which would produce modest velocity gradients and streamline shifts, close agreement was shown between the program results and the mathematical analysis.

The next three sections in this chapter describe three examples of flow types amenable to such treatment. Where the radius r appears in the function for tan α, it must be made non-dimensional by referral to some datum radius, r_d, such as the mid-span value. In each example, k is a constant of selected value for a particular design; clearly kr_d and k/r_d are themselves constant.

7.2 Angle Distribution tan $\alpha = k/(r/r_d)$

Inserting this type of angle variation into equation 7.1 gives

$$\frac{dV_z}{dr} = -\frac{kr_d}{r^2}\,\frac{d}{dr}\,(kr_d\,V_z)$$

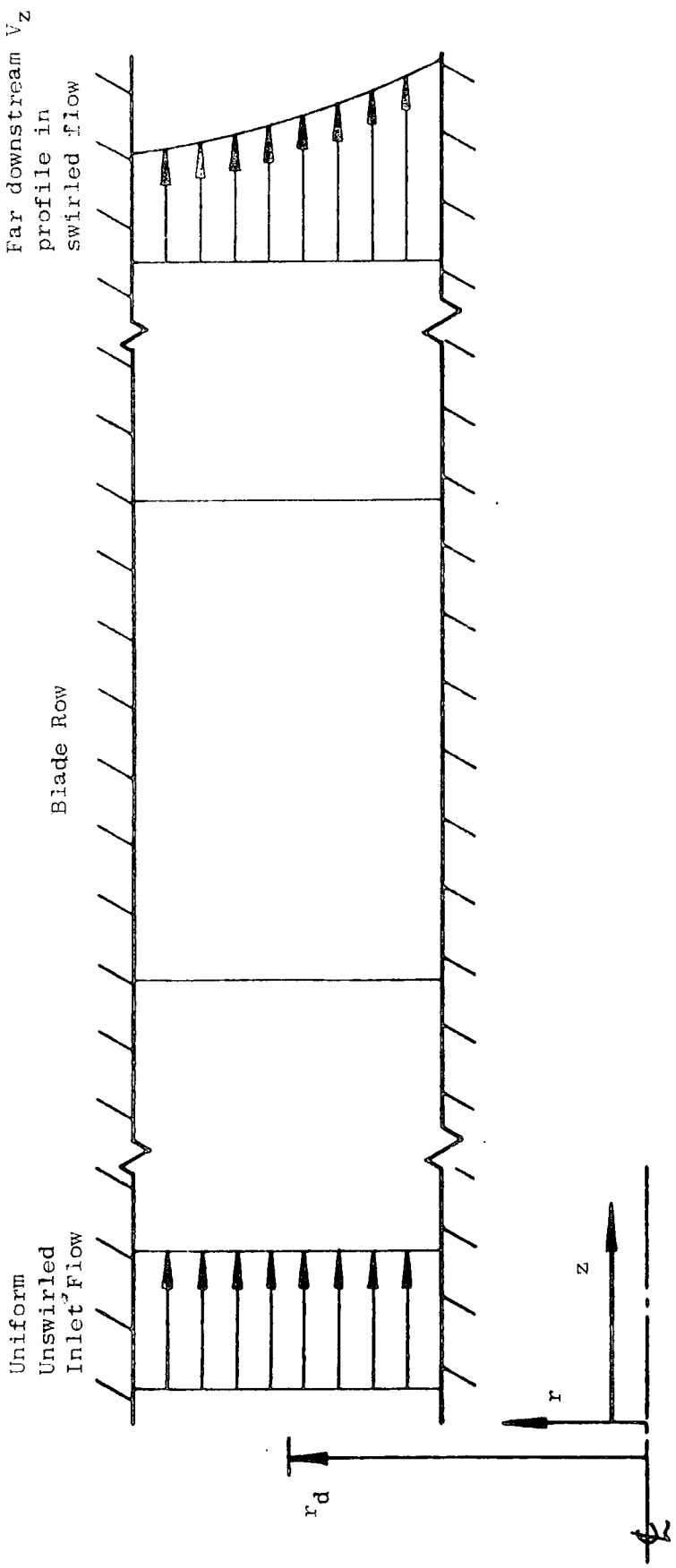

FIGURE 7.1: BLADE ROW PRODUCING SWIRL Tan α = f(r)

$$= - \frac{(kr_d)^2}{r^2} \frac{dV_z}{dr} .$$

$$\therefore \quad \frac{dV_z}{dr} \left(1 + \frac{(kr_d)^2}{r^2} \right) = 0,$$

which has the solution, for real $\frac{kr_d}{r}$,

$$\frac{dV_z}{dr} = 0 \qquad \ldots (7.2)$$

This is the free vortex flow field described in Chapter 4, since

$$\tan \alpha = \frac{V_u}{V_z} = \frac{kr_d}{r}$$

yields

$$rV_u = r_d k V_z = \text{constant}$$

if both kr_d and V_z are unchanging with radius. The uniform velocity profile from equation 7.2 is plotted in Figure 7.2.

7.3 Angle Distribution $\tan \alpha = k$

Setting the tangent of the flow angle constant with radius means that the angle itself also does not vary. Equation 7.1 may be re-written as follows:

$$\frac{dV_z}{dr} = - \frac{\tan \alpha}{r} \left[rV_z \frac{d}{dr}(\tan \alpha) + r \tan \alpha \frac{dV_z}{dr} + V_z \tan \alpha \right]$$

Inserting $\frac{d}{dr}(\tan \alpha) = 0$ and rearranging gives

$$\frac{dV_z}{dr} \left[1 + \tan^2 \alpha \right] = - \frac{V_z}{r} \tan^2 \alpha$$

$$\therefore \quad \frac{dV_z}{dr} = - \frac{V_z}{r} \sin^2 \alpha .$$

Dividing by V_z:

$$\frac{d}{dr} (\ell n \, V_z) = - \frac{\sin^2 \alpha}{r} .$$

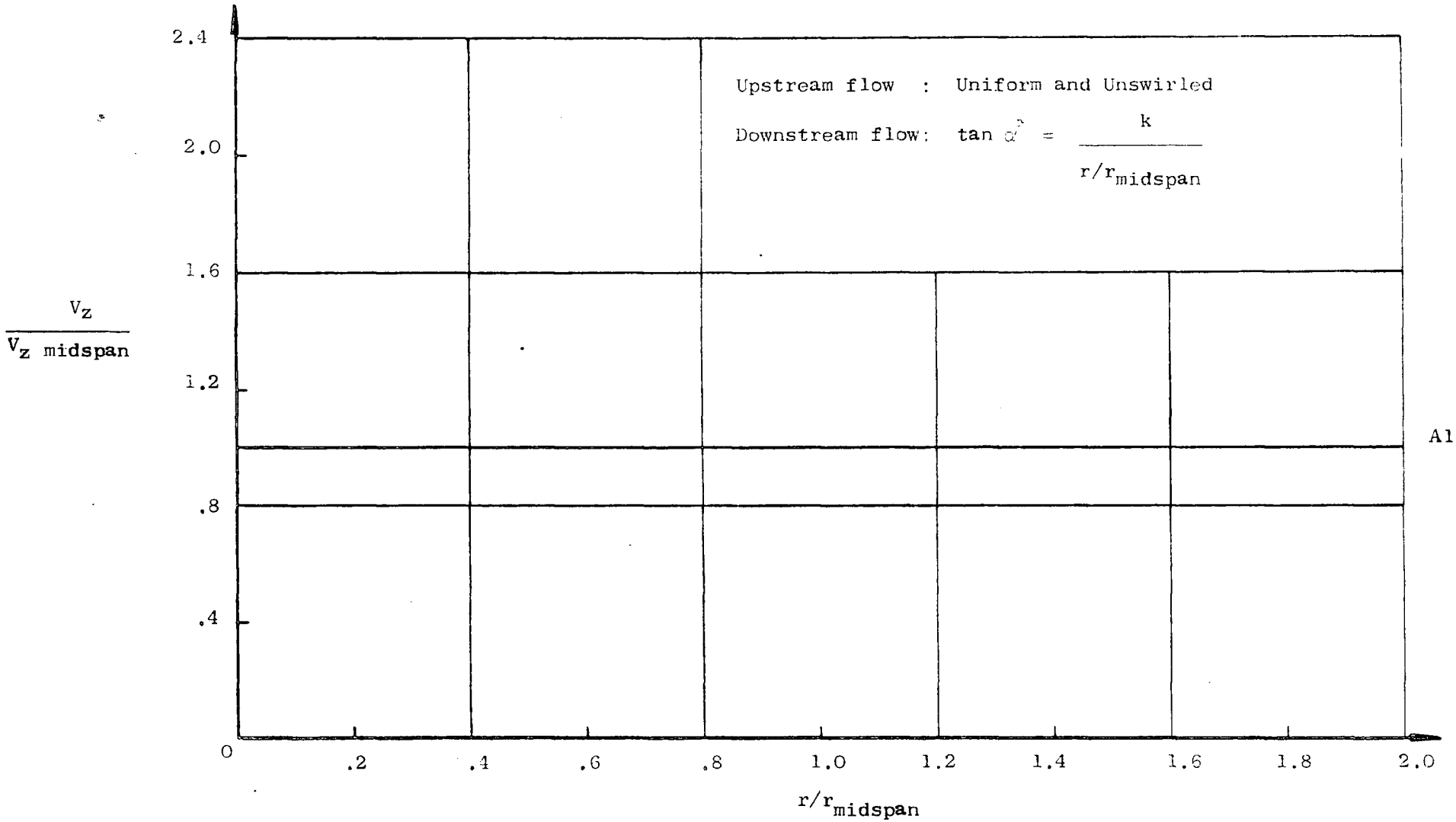

FIGURE 7.2: DOWNSTREAM AXIAL VELOCITY PROFILE FOR Tan $\alpha = \frac{k}{r/r_{midspan}}$

Integrating from $r = r_a$ to $r = r_b$, noting that $\sin \alpha$ is constant with radius:

$$\ell n \; V_{zb} - \ell n \; V_{za} = - \sin^2 \alpha \; (\ell n \; r_b - \ell n \; r_a)$$

$$\therefore \quad V_{zb} = V_{za} \left(\frac{r_a}{r_b} \right)^{\sin^2 \alpha} \qquad \ldots (7.3)$$

A dimensionless plot of equation 7.3 is given in Figure 7.3, where for different values of k the variation of axial velocity ratio with radius ratio is shown. The datum value for velocity is taken at the same place as that for radius; the mid-span is used.

7.4 Angle Distribution $\tan \alpha = kr/r_d$

For this case equation 7.1 becomes

$$\frac{dV_z}{dr} = - \frac{k}{r_d} \frac{d}{dr} \left[\frac{kr^2}{r_d} V_z \right]$$

$$= - \left[\frac{k}{r_d} \right]^2 r^2 \frac{dV_z}{dr} - \left[\frac{k}{r_d} \right]^2 V_z \frac{d(r^2)}{dr}$$

$$\therefore \quad \frac{dV_z}{dr} \left[1 + \left(\frac{k}{r_d} \right)^2 r^2 \right] = - 2 \left[\frac{k}{rd} \right]^2 r V_z$$

$$\therefore \quad \frac{1}{V_z} \frac{dV_z}{dr} = \left[\frac{-2 \left(\frac{k}{r_d} \right)^2 r}{1 + \left(\frac{k}{r_d} \right)^2 r^2} \right]$$

$$\therefore \quad \frac{d}{dr} (\ell n \; V_z) = - 2 \left[\frac{k}{r_d} \right]^2 \left[\frac{r}{1 + \left(\frac{k}{r_d} \right)^2 r^2} \right]$$

To integrate from $r = r_a$ to $r = r_b$, a result given by Petit Bois (1961) may be used:

$$\int \frac{r}{1 + \left(\frac{k}{r_d} \right)^2 r^2} \, dr = \frac{1}{2 \left(\frac{k}{r_d} \right)^2} \ell n \left[1 + \left(\frac{k}{r_d} \right)^2 r^2 \right] + \text{constant.}$$

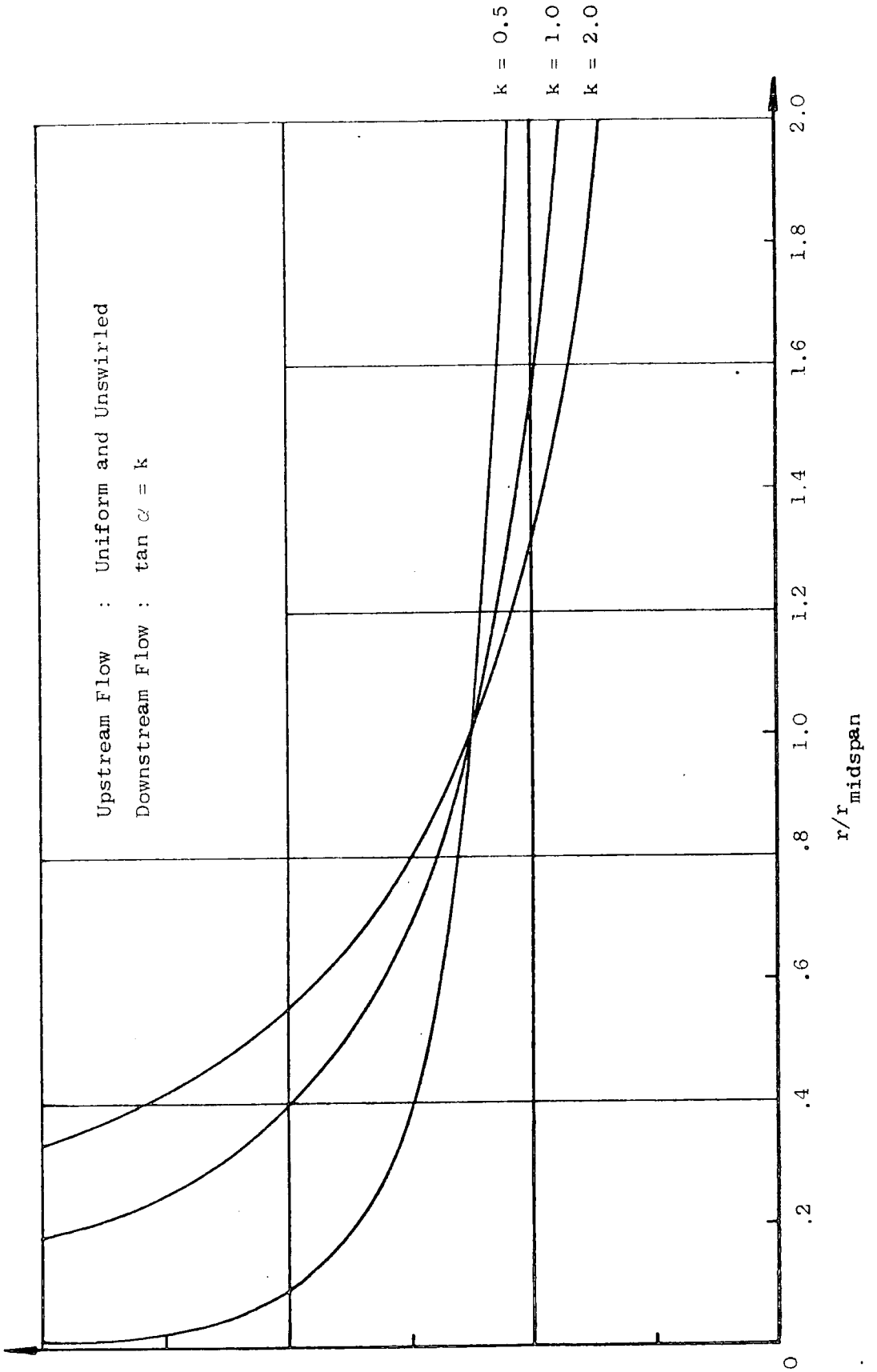

FIGURE 7.3: DOWNSTREAM AXIAL VELOCITY PROFILES FOR Tan α = k

Thus $$\ell n\, V_{zb} - \ell n\, V_{za} = \ell n \left[1 + \left(\frac{k}{r_d} \right)^2 r_a^2 \right] - \ell n \left[1 + \left(\frac{k}{r_d} \right)^2 r_b^2 \right]$$

$$\therefore \quad V_{zb} = V_{za} \left[\frac{1 + \left(\frac{k}{r_d} \right)^2 r_a^2}{1 + \left(\frac{k}{r_d} \right)^2 r_b^2} \right] \qquad \ldots (7.4)$$

A graph of equation 7.4 is presented in Figure 7.4 in a similar manner to Figure 7.3, for comparison.

7.5 Numerical Trials

An annular duct of the type shown in Figure 7.1 was designed, with the hub and tip radii similar to those on the test rig of Oxford (1965) and Gregory-Smith (1970). For ease of analysis the test rig radii of 1 ft and 2.5 ft were rounded to S.I. equivalents of 0.3 m and 0.75 m, these maintaining the same hub:tip ratio of 0.4. Chapter 8 describes the computer simulation of Gregory-Smith's (1970) experimental results, when the apparatus was modelled accurately.

In the presently-considered test cases, the distance between the duct inlet and the calculation station 'far' downstream was set at 10 m, with the mid-chord of the stator blade row positioned 2.5 m from the duct inlet. The point of interest in the blade row design was the fluid exit angle distribution, which was varied from test to test to produce the various types of swirl described in Sections 7.2 to 7.4. Several parameters were held constant for all blade designs, viz:

Sweepback:	None
Inlet Blade Angle:	0° at all radii
Axial Chord Length:	0.7 m at all radii
Aerofoil type:	C4 on parabolic camber line; $t_{max}/c = 0.1$; $a/c = 0.4$.
Number of Blades:	Notionally zero (see below)

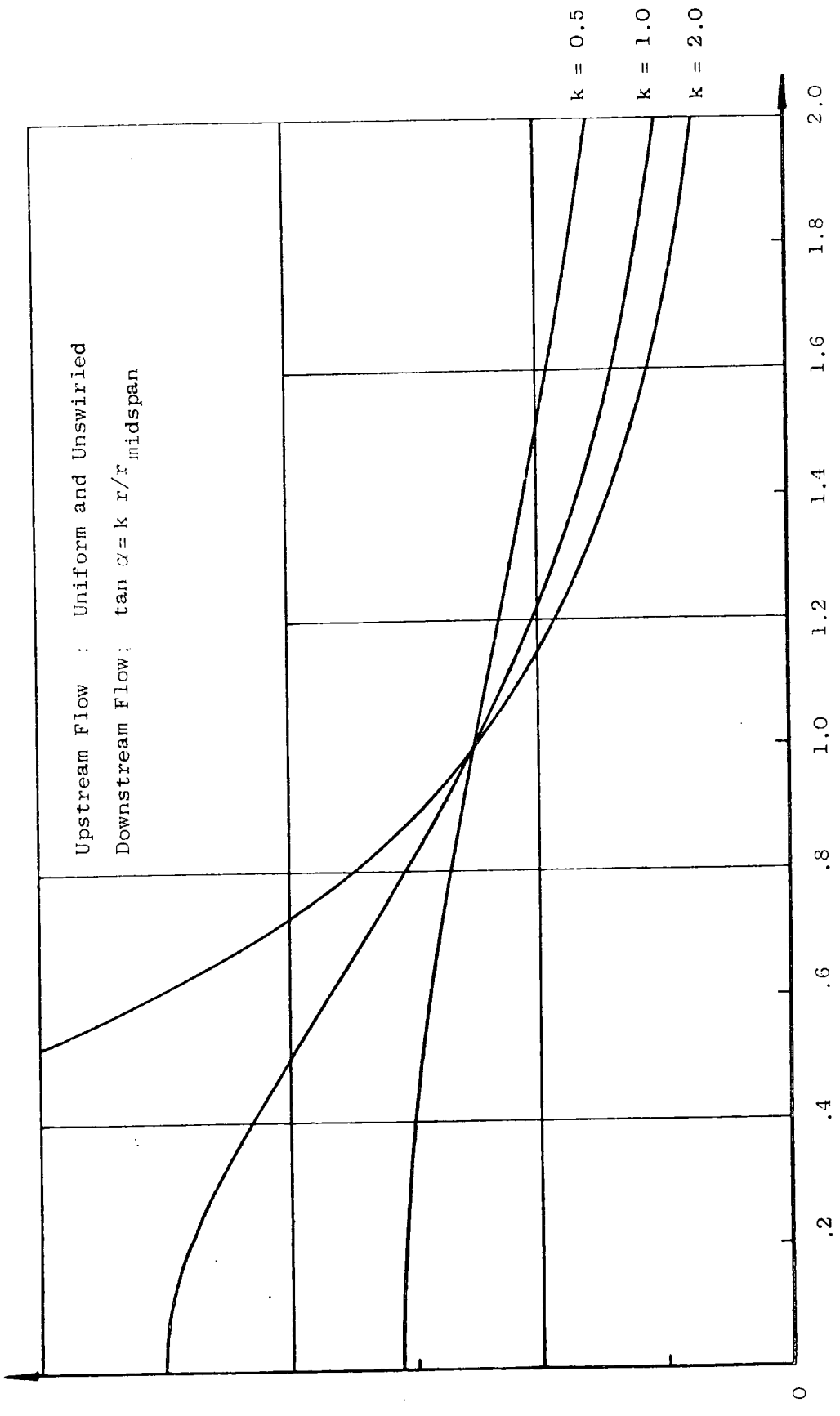

FIGURE 7.4: DOWNSTREAM AXIAL VELOCITY PROFILES FOR Tan $\alpha = k\, r/r_{midspan}$

The long axial chord length allowed for rapid convergence of calculations (Section 6.7) and also for more gentle streamline slopes than would appear within shorter blades. Setting the number of blades to zero was a programming 'fix' to eliminate varying blade blockage as a cause of intrablade streamline shifting. For this case, with blade pitch undefined, the pitch : chord ratio was taken as unity in using Howell's deviation correlation (Appendix D).

An example of each type of flow angle variation described in Sections 7.2 to 7.4 was applied at exit from the stator row, viz:

$$\tan \alpha = 0.5 \frac{r_{midspan}}{r} \quad \ldots(7.5)$$

$$\tan \alpha = 0.5 \quad \ldots(7.6)$$

$$\tan \alpha = 0.5 \frac{r}{r_{midspan}} \quad \ldots(7.7)$$

For the designed duct, $r/r_{midspan}$ varied from 0.57 at the hub to 1.43 at the tip casing, and over this radius range the choice k = 0.5 in equations 7.6 and 7.7 gives the modest radial gradients of velocity mentioned in Section 7.1 as desirable for these tests. This may be seen from Figures 7.3 and 7.4. Equation 7.5 corresponds to equation 7.2 which indicates flow with uniform axial velocity for all values of k, though k = 0.5 was selected for consistency with equations 7.6 and 7.7.

A further example was modelled with increased k,

$$\tan \alpha = 1 \quad \ldots(7.8)$$

to observe the increasing departure from the velocity profile predicted in Section 7.3.

Two specifications for the fluid passing through the duct were used. One modelled compressible air, with C_p = 1005 J/kg/K and γ = 1.4; the other assumed an incompressible fluid, again with C_p = 1005 J/kg/K, but an effective value of infinity for γ. (The

computer program was written to treat as incompressible any fluid with a supplied value of γ exceeding 10). For all cases, the flow entered the duct at a temperature of 300 K and a velocity of 100 m/s, with no swirl.

7.6 Results of Trials

Figure 7.5 shows the result far downstream of applying at blade exit the flow angle variation defined by equation 7.5. The graph contains plots of the analytical solution (V_z = constant) and of the dimensionless velocity profiles produced by the program for the compressible and incompressible flow cases. All three curves are non-dimensionalized with respect to the mid-span velocity. The vertical axis scale is 100 times as large as that of the horizontal axis to show the errors incurred, which are small; they are tabulated in Figure 7.9. These errors arise because within the blade row the flow is not held to the free vortex pattern, and so streamlines leaving the stator are slightly inclined, changing the effective flow angle μ, and they undergo some redistribution downstream as their meridional curvature disappears.

The axial velocity upstream of the blade row being 100 m/s, incompressible flow may be expected to travel at the same axial velocity in the downstream end of the duct. As Figure 7.5 shows, the velocity profile generated by the program was not perfectly uniform, and the resulting mid-span axial velocity, given in Figure 7.9 was 99.9965 m/s.

The effect of performing the calculations for the compressible fluid was that the axial velocity profile produced remained nearly uniform, but the central axial velocity was raised to 101.28 m/s. The introduction of swirl into the flow increased the magnitude of the velocity vector $\underline{V}$, and thus the static density was reduced. This in turn caused a further increase in $\underline{V}$, in its axial component, to maintain the mass flowrate in the downstream part of the duct.

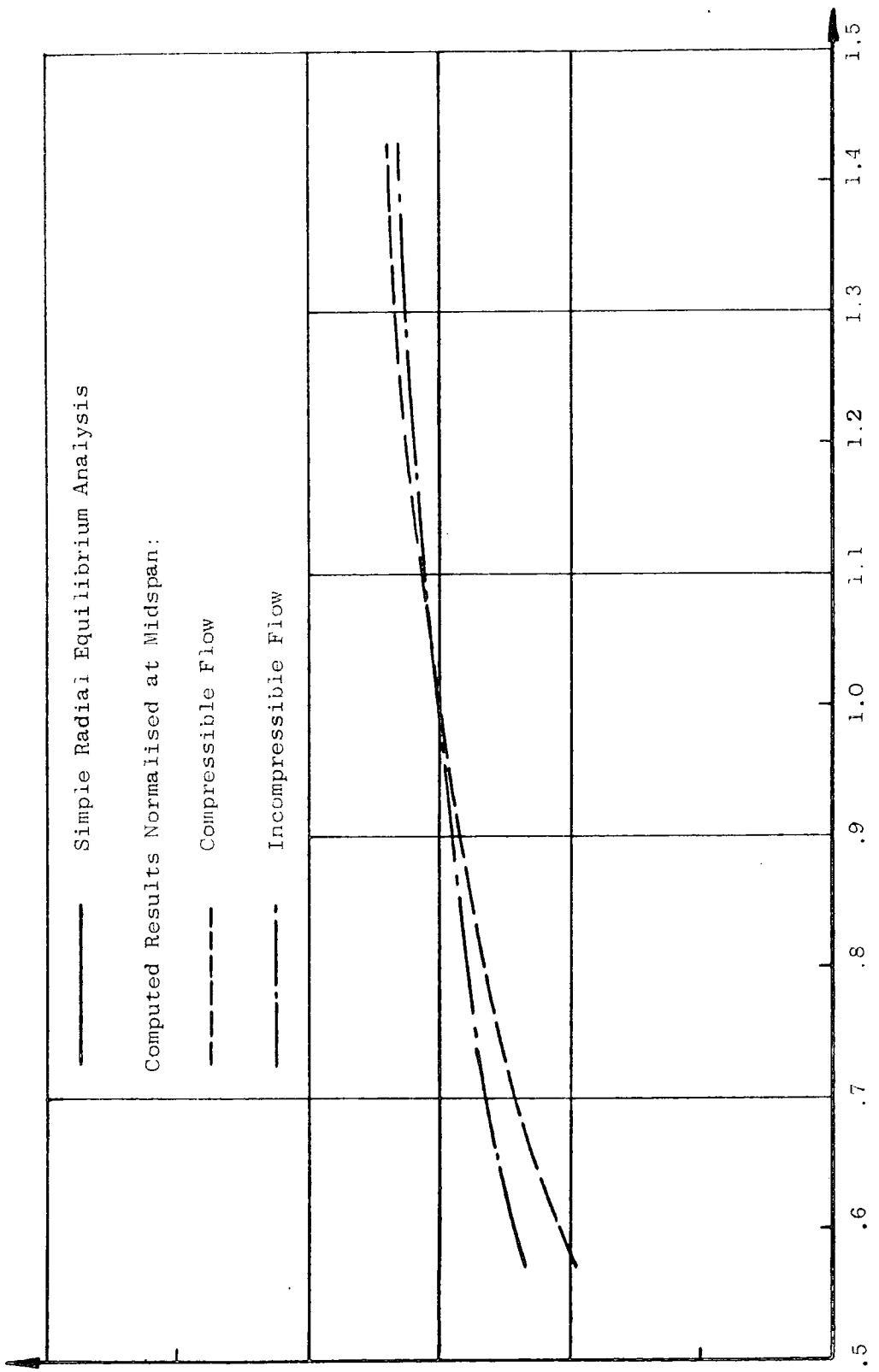

FIGURE 7.5: COMPUTED RESULTS FOR DOWNSTREAM FLOW ANGLE Tan α = 0.5 $\frac{r_{midspan}}{r}$

Figures 7.6 to 7.8 show results of trials using the blade exit flow angle distributions from equations 7.6 to 7.8 respectively. Differences from the layout of Figure 7.5 are that the velocity ratio axes cover a much larger range than that of Figure 7.5, and that the analytical velocity ratio is assumed to be held accurately at the hub, not at the mid-span of the duct. The reasoning for this is that the discrepancy between the computed and the analytical velocity profiles is least at the duct edges, because only there does no radial shift of streamlines occur, as described in Section 7.1, to alter the circumferential component of the velocity as the flow passes downstream of the blades. The conditions at the outer, tip, casing could equally well be used as the basis for comparison. In tests with compressible flow, changes in density, as described above, additionally cause axial velocity changes which are not readily determined and so away from the duct walls both the axial and circumferential velocity components may be altered. With the velocity profiles normalised on the hub value, $V_z/V_{z_{midspan}}$ does not appear as exactly unity at the duct centre.

Referring to Figures 7.6, 7.7 and 7.8, the departure of the dimensionless velocity profiles from the analytical Simple Radial Equilibrium solutions is not excessive and the difference between the respective curves for compressible and incompressible flow are nearly everywhere so small that they do not show on the graphs; the differences are presented in tabular form in Figure 7.9.

Figures 7.6 and 7.8, for flow angle constant with radius, appear to justify the use of the hub velocity as the base for comparison of the program results, since although the discrepancy between the analytical and the modelled flow rises from hub to mid-span, it decreases considerably between the mid-span and the tip. The errors at the duct centre for $k = 1$ are approximately double those for $k = 0.5$.

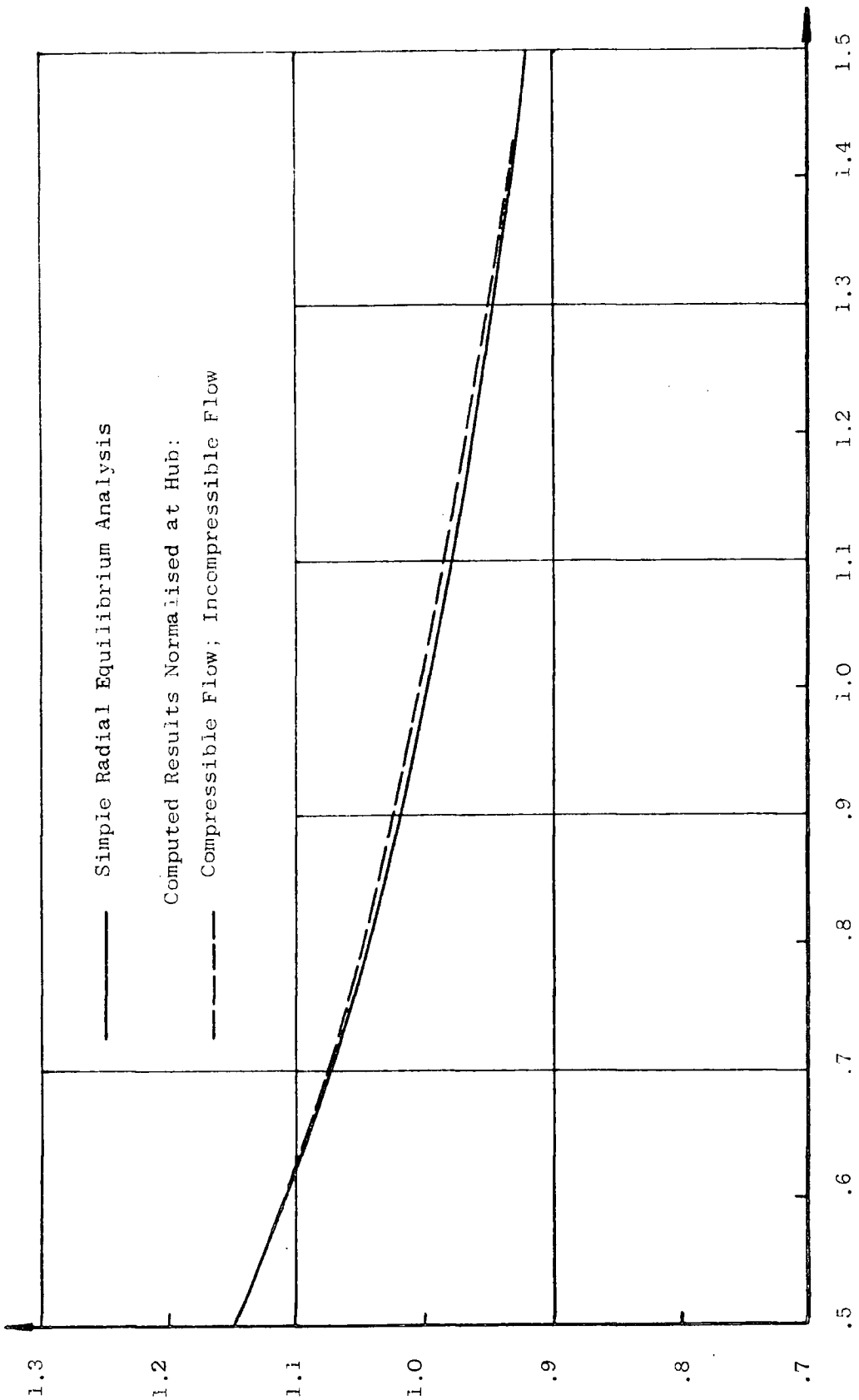

FIGURE 7.6: COMPUTED RESULTS FOR DOWNSTREAM FLOW ANGLE Tan α = 0.5

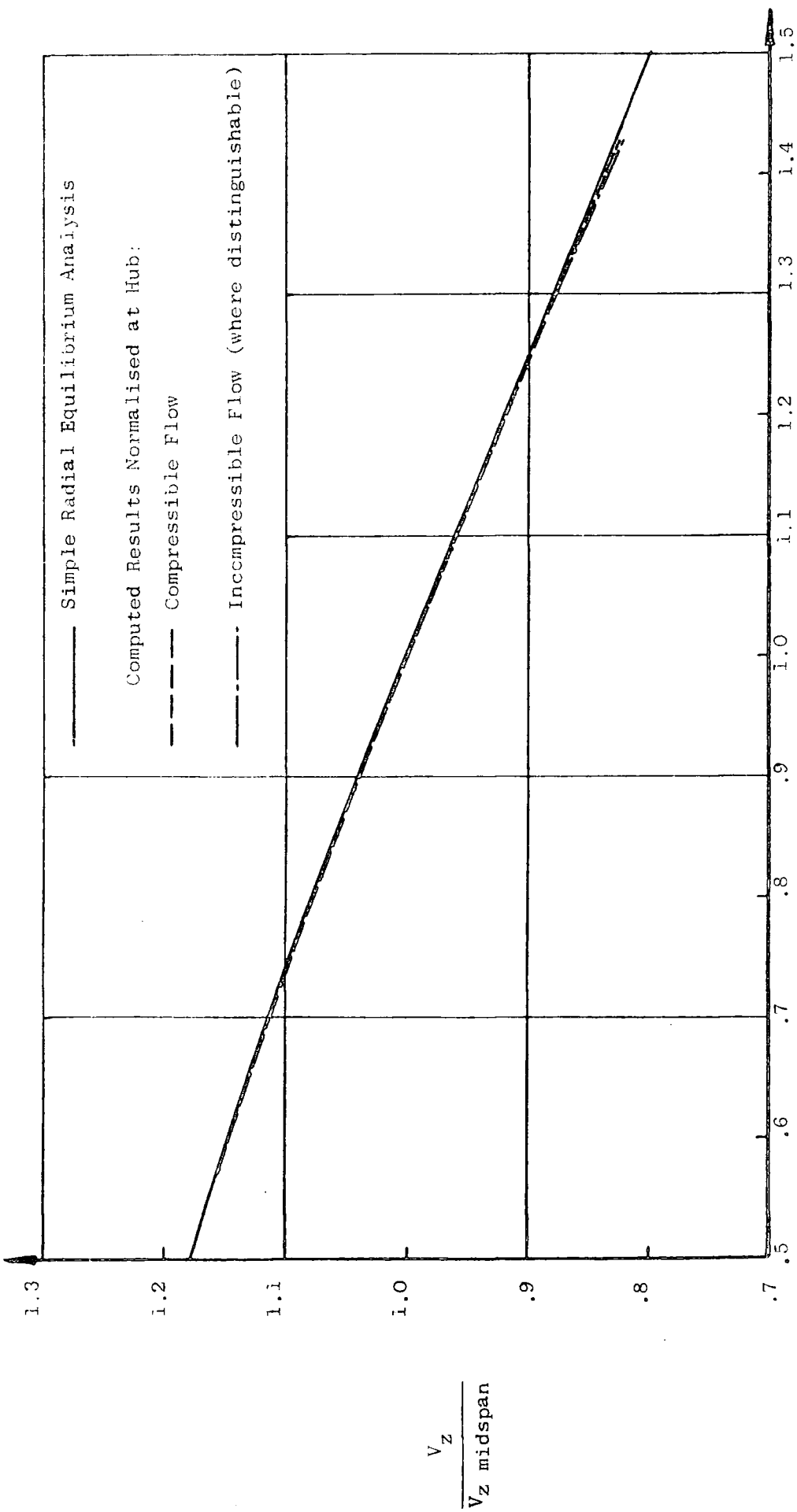

FIGURE 7.7: COMPUTED RESULTS FOR DOWNSTREAM FLOW ANGLE Tan α = 0.5 $\frac{r}{r_{midspan}}$

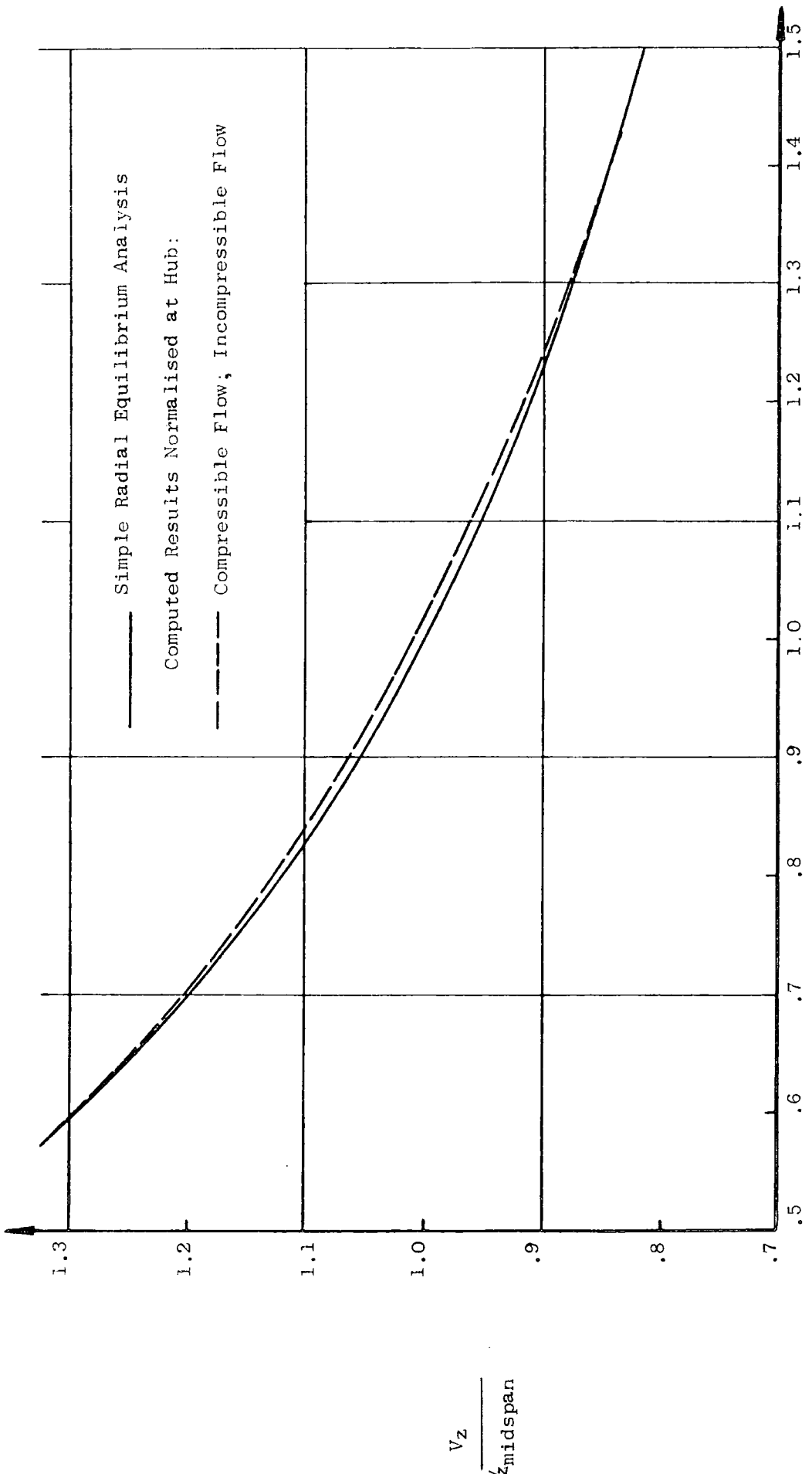

FIGURE 7.8: COMPUTED RESULTS FOR DOWNSTREAM FLOW ANGLE Tan α = 1.0

FIGURE 7.9

DEPARTURE FROM ANALYTICAL SOLUTIONS OF VELOCITY PROFILES GENERATED THROUGH PROGRAM TESTING

Desired Flow Angle Distribution	Figure No.	Differences Zeroed at:	Fluid Incompressible or Compressible	$V_{Z_{midspan}}$ m/s	% Discrepancy in V_Z Profile at:		
					Hub	Mid-Span	Tip
$\tan \alpha = .5\frac{r_{mid}}{r}$	7.5	mid-span	Incomp. Comp.	99.99(65) 101.28	-.067 -.106	0 0	.033 .042
$\tan \alpha = .5$	7.6	hub	Incomp. Comp.	100.68 101.92	0 0	.57 .59	.30 .33
$\tan \alpha = .5\frac{r}{r_{mid}}$	7.7	hub	Incomp. Comp.	102.73 104.12	0 0	-.10 -.15	-.48 -.22
$\tan \alpha = 1$	7.8	hub	Incomp. Comp.	101.39 107.35	0 0	1.2 1.05	-.27 -.16

Figure 7.7 shows close matching of results over almost the whole radius range, except at the tip.

7.7 Streamline Paths

In the foregoing parts of this Chapter the radial repositioning of the streamlines within the blade row and outside it proved to be a hindrance in establishing in the downstream flow a pre-determined angle distribution. The computer program includes within its output the stream function values stored at each grid point in the calculation mesh, and from these it is possible to plot streamline loci to quantify the radial movement involved and observe the propagation of effects from the blade row into flow upstream and downstream.

Figure 7.10 shows the meridional projection of the stream line for $\psi = 0.5\,\dot{m}$ ($\dot{m}$ being the entire mass flowrate) drawn from the test of equation 7.8 for incompressible flow, the test which produced the greatest axial shear in the downstream flow. The radial position expressed as a proportion of the duct span forms the vertical axis; its scale is large to make visible the streamline shift. The overall radial shift is nearly 5% of the span.

The results depicted in Figure 7.8 were obtained using a convergence criterion of 1% on the greatest meridional velocity change between successive marches (Section 6.6). The three-stage program application described in Section 6.9 was used, with the check on slope compatibility in the third part set sufficiently slack that no more iterations were required once the velocity adjustment criterion had been satisfied. The slopes within the blade row for the plotted streamline are given in Figure 7.11, together with the greatest tan ϵ incompatibility in the flow field. This was found at the trailing edge of the blade, and is seen to translate to an angular error there of the same order of magnitude as the calculated slope.

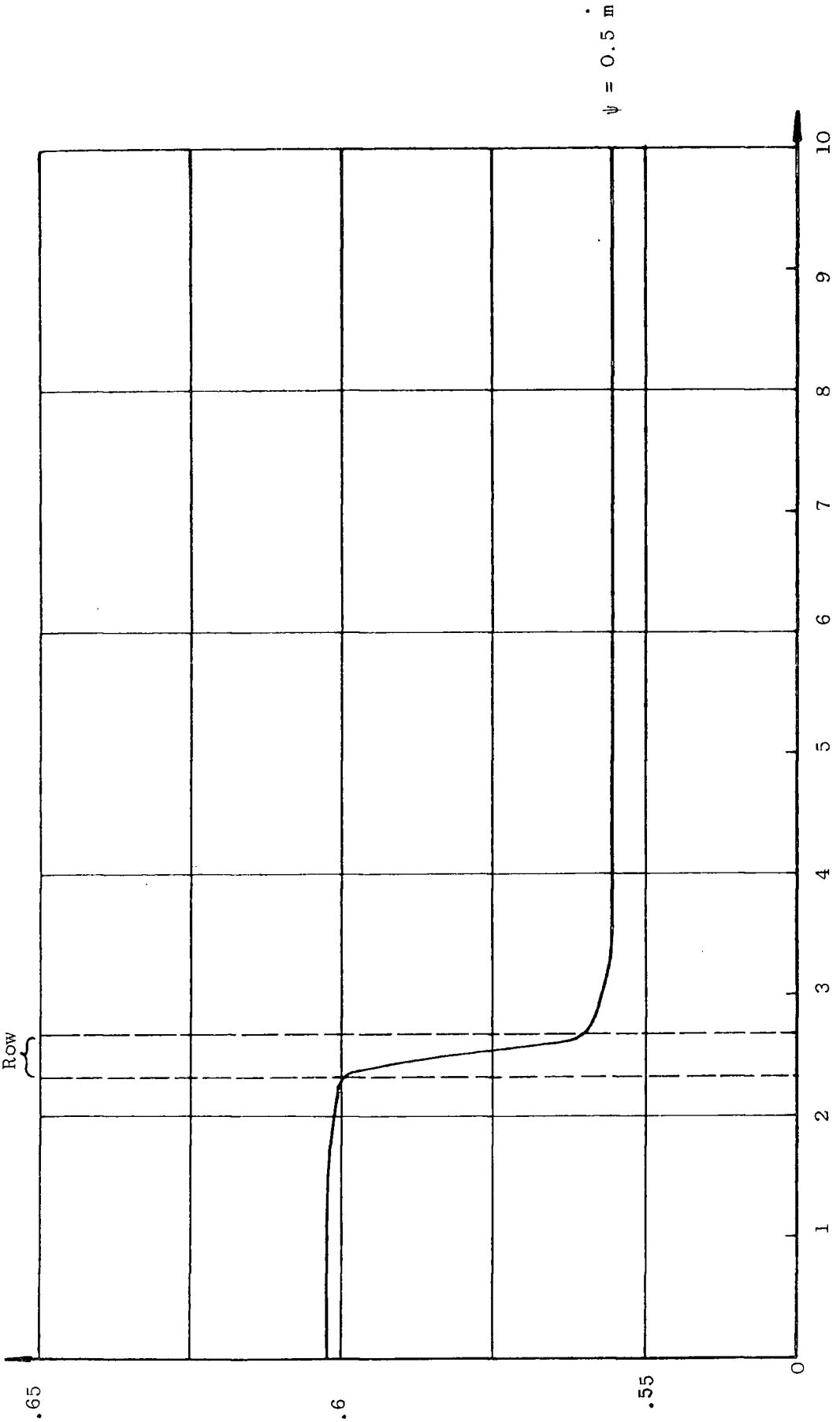

FIGURE 7.10: $\psi = 0.5\ \dot{m}$ STREAMLINE LOCUS FROM INCOMPRESSIBLE FLUID CALCULATIONS FOR FIGURE 7.8

FIGURE 7.11

EFFECT OF SLOPE COMPATIBILITY CRITERION ON

STREAMLINE SLOPES AND DURATION OF CALCULATIONS

	Number of Iterations	Convergence on:		Streamlines slope given at:			Angular error at t.e. (from $\Delta \tan \varepsilon$)
		V_m change	$\Delta (\tan \varepsilon)$	Blade l.e.	Blade mid-chord	Blade t.e.	
Calculations for Figure 7.8 (Incompressible)	13	1% demanded .703% obtained (station following blade t.e.)	.05 demanded .0111 obtained (blade t.e.)	$-.47^\circ$	-2.42°	$-.86^\circ$	$\pm .64^\circ$
Extended Calculations	19	1% demanded .103% obtained (station following blade t.e.)	.001 demanded .00099 obtained (blade t.e.)	$-.50^\circ$	-2.44°	$-.70^\circ$	$\pm .057^\circ$

For comparison the calculations were re-run demanding convergence to a much smaller incompatibility on tan ε. The ψ = 0.5 m streamline from these extended calculations was negligibly different from the plot on Figure 7.10, but the slope values through the blade row were altered and are listed in Figure 11. Far downstream the mid-span axial velocity was reduced by 0.4%.

At the blade trailing edge, where the greatest errors in streamline slope compatibility were detected, the change in the slope effected by performing the extra iterations was only one quarter of the slope error indicated at the end of the calculations for Figure 7.8, yet the error now diagnosed was smaller than the former estimated by a factor of more than ten. It would appear that the slope incompatibility test may give pessimistic results, and that as calculations are continued, streamline slope convergence may occur sooner than the test would indicate, since both the stream function field and the slope distributions approach each other.

Inspection of Figure 7.10 reveals that the flow effects of the blade row extend about two chord-lengths upstream and two downstream, which is of the order of magnitude found in practice.

7.8 Flared Ducts and Non-Radial Calculation Stations

The examples considered in Sections 7.2 to 7.7 have all involved cylindrical annular ducts, and were modelled on the computer with all calculation stations set radial. Hirsch (1976) presents an example, with results, in which incompressible fluid passes with no losses along an axisymmetric duct comprising two cylindrical annuli of different radii, connected by a curving transition piece - a 'swan-necked' duct.

At inlet the hub radius is 0.25 m and the tip radius 0.35 m. At exit the respective radii are 0.1 m and 0.2 m. The exit flow pattern

appears to be independent of the shape of the transition length, but a design similar to that depicted by Hirsch (1976) was used.

The inlet flow has uniform axial velocity; by integrating Hirsch's (1976) result for the exit axial velocity profile, the uniform inlet axial velocity to pass the same mass flow was found to be 44.24 m/s. Hirsch does not specify the fluid, but assuming it to be air at ambient conditions - a temperature of 300 K and a pressure of about 1 atmosphere (105 kPa) - gives close agreement with the mass flowrate figure of 10 kg/s given by Hirsch.

The circumferential velocity at inlet is in the form of a solid body rotation. Denoting the fluid rotational speed by Ω, the circumferential velocity at any radius is given by

$$V_u = \Omega r \quad (\Omega = 100\ s^{-1}).$$

This type of swirling flow, entering along straight parallel streamlines, may be shown by Simple Radial Equilibrium considerations to exhibit a radial pressure gradient at inlet, as follows:

$$\frac{1}{\rho}\frac{\partial p}{\partial r} = \frac{V_u^2}{r} = \Omega^2 r$$

Integrating radially:

$$p = \tfrac{1}{2}\rho\Omega^2 r^2 + k$$

where k is a constant.

For incompressible flow,

$$p_o = p + \tfrac{1}{2}\rho(V_z^2 + V_u^2)$$

$$\therefore \quad p = p_o - \tfrac{1}{2}\rho V_z^2 - \tfrac{1}{2}\rho\Omega^2 r^2$$

$$= k + \tfrac{1}{2}\rho\Omega^2 r^2$$

$$\therefore \quad p_o = k + \tfrac{1}{2}\rho V_z^2 + \rho\Omega^2 r^2.$$

V_z, ρ, Ω and k are all constant with radius.

Then for the data given in this example, the inlet total pressure is 731 Pa higher at the tip than at the hub, a small variation of 0.7%

on the atmospheric pressure. Further implications are discussed in Section 7.9, where it is shown that total temperature does not vary radially.

The duct geometry was supplied to the computer program with radially inclined calculation stations along the curved part. The results obtained at exit for the axial and circumferential velocity distributions matched the graphical results presented by Hirsch (1976) to the accuracy to which his graphs could be read; the printing of the graphs was such that the axes were not perpendicular, so that interpretation errors were expected.

Convergence to less than 1% change in meridional velocity anywhere was achieved in 9 flow field marches, and a requirement that the slope incompatibility ($\Delta \tan \epsilon$) be less than 0.001 was satisfied after 2 more marches. The greatest streamline slopes in the transition duct were about 45°.

7.9 Enthalpy and Entropy in Flow With Solid-Body Rotation

The analysis presented in Section 7.8 was required to determine the radial variation of total pressure in flow with solid-body rotation. The test rig of Oxford (1965), discussed in Chapter 8, was built to produce flow of this type. Air is drawn into the annular wind tunnel with uniform total pressure, but is then passed through several annular wire gauzes, all extending radially outwards from the hub wall, but terminating at different radii, so that flow losses are incurred, varying with radius, to produce the total pressure profile required. Downstream of the gauzes the axial velocity is also non-uniform, but with subsequent turning through a blade row, flow results with solid-body rotation and with uniform axial velocity.

The flow through the gauzes may be considered adiabatic, and the total enthalpy is unchanged (and hence total temperature), but since the flow is irreversible, it is not isentropic, and so radial entropy gradients are created in accordance with the equation:

$$T_o \frac{\partial s}{\partial r} = \frac{\partial h_o}{\partial r} - \frac{1}{\rho_o} \frac{\partial p_o}{\partial r} .$$

For adiabatic flow from a plenum of uniform enthalpy, $\frac{\partial h_o}{\partial r} = 0$.

Substituting for ρ_o and p_o from the result in Section 7.8,

$$\frac{\partial s}{\partial r} = \frac{- R \ (2 \ \rho \ \Omega^2 r)}{p_o}$$

$$\therefore \quad \frac{\partial s}{\partial r} = \frac{-2R \ \rho \ \Omega^2 \ r}{k + \frac{1}{2} \rho V_z^2 + \rho \ \Omega^2 r^2}$$

Thus for the example of Section 7.8, the computer program must set up a radial entropy gradient at inlet, to be consistent with the specified data there.

7.10 Conclusions

Several predictable flow patterns have been closely realised by the computer program. Small deviations from the calculated velocity profiles are due to radial redistribution of the flow angle between the plane at which the flow angle was defined, and the measuring plane, where all streamlines were constrained to be straight and parallel. Compressible flow is altered in density as the swirl component of its velocity changes, and so produces downstream flow with axial velocity different from that for the comparative test with an incompressible flow model. However, the non-dimensionalised axial velocity profiles produced for these two flow types were found to be remarkably similar to each other.

A study of meridional streamline paths for the most severely sheared example revealed that the radial positions of the streamlines

downstream may be different from the upstream positions by up to 5% of the duct span. Flow effects caused by the blade row are propagated to realistic distances into the free duct.

Despite the application of relaxation factors in the program such that discrepancies appear between the flow field stream function values and the indicated streamline slopes, checks on the incompatibility may give pessimistic results, and convergence to finer criteria causes only minimal redefinition of streamlines.

Calculations performed on grids with non-rectuangular geometry were shown to give reliable results.

CHAPTER 8

Comparisons With Two Experimental Examples

Sections 8.1 to 8.3 describe the computer modelling of an annular row of Inlet Guide Vanes, designed by Oxford (1965), but as used by Gregory-Smith (1970). In Sections 8.4 to 8.6, results are presented from the computer simulation of the flow through the guide vanes, modelling Gregory-Smith's experiments.

A three-row axial compressor tested by Fanmi (1968) is discussed in Sections 8.7 to 8.10, as a test example of a multi-row machine. Computed profiles of axial velocity at exit from each blade row are compared with the experimental data.

8.1 The Test Rig of Oxford and of Gregory-Smith

A large annular wind tunnel was constructed in the Department of Engineering at Cambridge University in the 1960's to study flow with 'solid-body' rotation. Such flow travels with radially-uniform axial velocity, but with swirl velocity varying so that all the flow revolves around the annulus axis at uniform angular velocity. There is thus neither axial nor circumferential shear.

A set of inlet guide vanes and gauzes was designed by Oxford (1965) to produce such flow from an approaching unswirled flow. To provide a uniform axial velocity profile downstream of the blade row, the upstream axial velocity had to be constrained to enter the guide vanes with a particular axial shear, which Oxford achieved by placing in the upstream flow a set of annular gauzes. These gauzes extended from the wind tunnel hub across to various radii, giving a radial variation of flow resistance, and so creating the required profile of upstream annular velocity.

Oxford also designed an experimental rotor which could be installed in the tunnel. Jones (1969) performed experiments on the flow through

the inlet guide vanes without the gauzes or the rotor being present. Gregory-Smith (1970) used the apparatus to study boundary layers on the annulus walls, using the guide vanes and the rotor separately. He too operated the rig with the gauzes removed, and the guide vane tests were conducted with the vanes rotated to give 6^{o} of inlet incidence, a configuration tested by Jones (1969).

The present work does not include modelling of boundary layers, except insofar as suitable pressure loss values may be specified near duct walls, but Gregory-Smith (1970) produced plots of axial velocity across the entire duct span which are useful as test data for the presently-developed computer program.

The blade design procedure may also be tested in attempting to replicate Oxford's (1965) inlet guide vane design, as used in the application of Jones (1969) and Gregory-Smith (1970).

8.2 Design of Inlet Guide Vanes

Oxford (1965) designed the inlet guide vanes to the following specification:

Inner radius	:	1 ft (.3048 m)
Outer radius	:	2.5 ft (.7620 m)
Axial chord	:	5.351 inch at all radii
True chord-hub	:	5.675 inch
midspan	:	6.183 inch
tip	:	6.734 inch
Inlet blade angle	:	0^{o} at all radii
Outlet flow angle (deduced)	:	follows $\tan \alpha$ = .5022 r (r in feet) = 1.6476 r (r in metres)
Camber line shape	:	parabolic
a/c		0.4
t_{max}/c		0.1

Thickness profile	:	type C4
Number of blades	:	31
Deviation rule used in design	:	Carter (1950)

The axial chord length listed above is drawn from Oxford's (1965) Appendix XI; in the main text he briefly mentions a 6 inch total chord length, though from the table above it is seen that only at one radius is the chord exactly 6 inches, and this radial position appears to be of no significance. Gregory-Smith (1970) lists the axial chord as 6 inches, and the camber line shape as being a circular arc, two details which are true of Oxford's (1965) rotor blade design, and so perhaps misapplied here to the inlet guide vanes.

Although the axial chord length (5.357 inch was assumed to be the correct figure) is constant at all radii in the design position, rotation of the blades through 6^{o}, as in Gregory-Smith's (1970) experiments alters the axial projection of the chord by an amount dependent at any radius upon the local stagger angle. Consequently it was more straightforward, in compiling data for the computer program design procedure, to supply the differing true chord lengths at the hub, midspan and tip; the program contains options whereby either the true chord length or the meridional projection (in this case the same as the axial component) may be entered.

The blade design performed by the computer program was for the blades in their rotated position, using the exit flow angle distribution for this arrangement given by Gregory-Smith (1970) as shown on Figure 8.1. The source of these data is thought to be the work of Jones. Ideally the blade geometry produced from the calculations should match the known design of Oxford (1965), rotated by 6^{o}, but the respective blade angle plots shown on Figure 8.1 show some discrepancy.

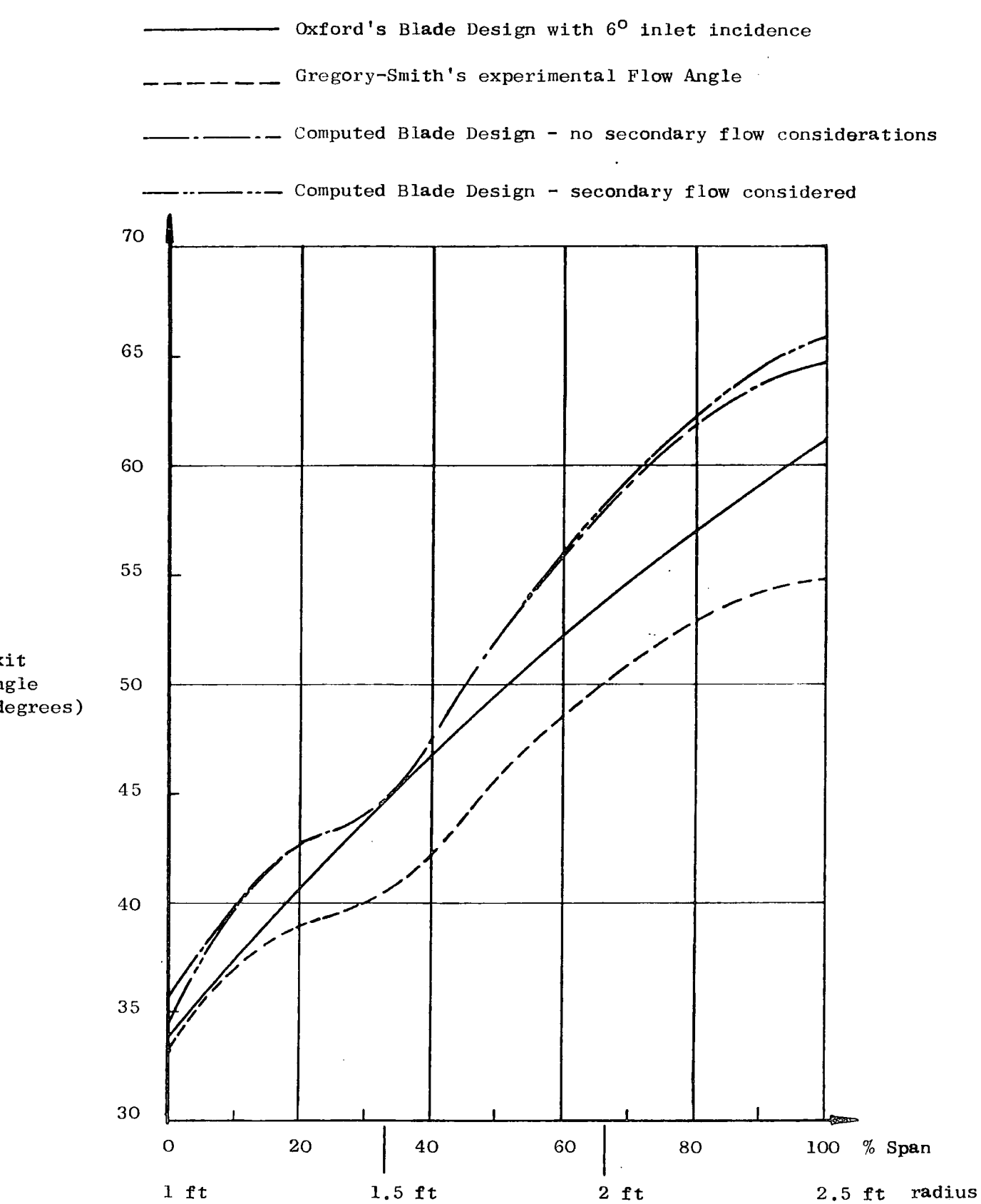

FIGURE 8.1: GUIDE VANE DESIGN COMPUTED FROM GREGORY-SMITH'S FLOW ANGLES

The cause of this discrepancy has been traced to the estimation of deviation angle. Howell's deviation correlation (reference: Dixon (1975)) was used in the present work, but in his original blade design Oxford (1965) used that due to Carter. Both these rules were formulated similarly for the design of compressor cascades, wherein fluid is decelerated, though they include different modifications to their formulae to allow the calculation of deviation in guide vane nozzles, such as the present application, and turbine cascades.

Oxford applied Carter's method to the design of the inlet guide vanes, and the deviation values he obtained may be contrasted with those for the 'nominal' deviation of Howell, viz:

	Howell, δ^*	Carter, δ (from Oxford (1965))
Hub	2.265^o	1.183^o
Mean	5.712^o	2.700^o
Tip	9.462^o	4.183^o

The deviation angles predicted by Howell's rule may not be meaningfully adjusted for the departure from nominal operating conditions, because this aspect of the method is applicable only to cascades which reduce the swirl angle and decelerate the flow, such as compressor cascades.

Figure 8.2 shows the deviation angles tabulated above, applied to the guide vane exit angle in the rotated position used by Gregory-Smith (1970). Also plotted is a smoothed profile for the experimental exit flow angle given by Gregory-Smith. It is seen that neither rule has predicted the actual deviation accurately; Carter's method underestimates it, and Howell's gives an over-estimate. The discrepancy between the actual and the computed blade exit angle plots on Figure 8.1 (and Figure 8.6) is caused by the inability of Howell's deviation rule

Oxford's Blade Design with 6° inlet incidence

Gregory-Smith's experimental flow angle (smoothed)

Flow Angle predicted with Carter's deviation rule

Flow Angle predicted with Howell's deviation rule

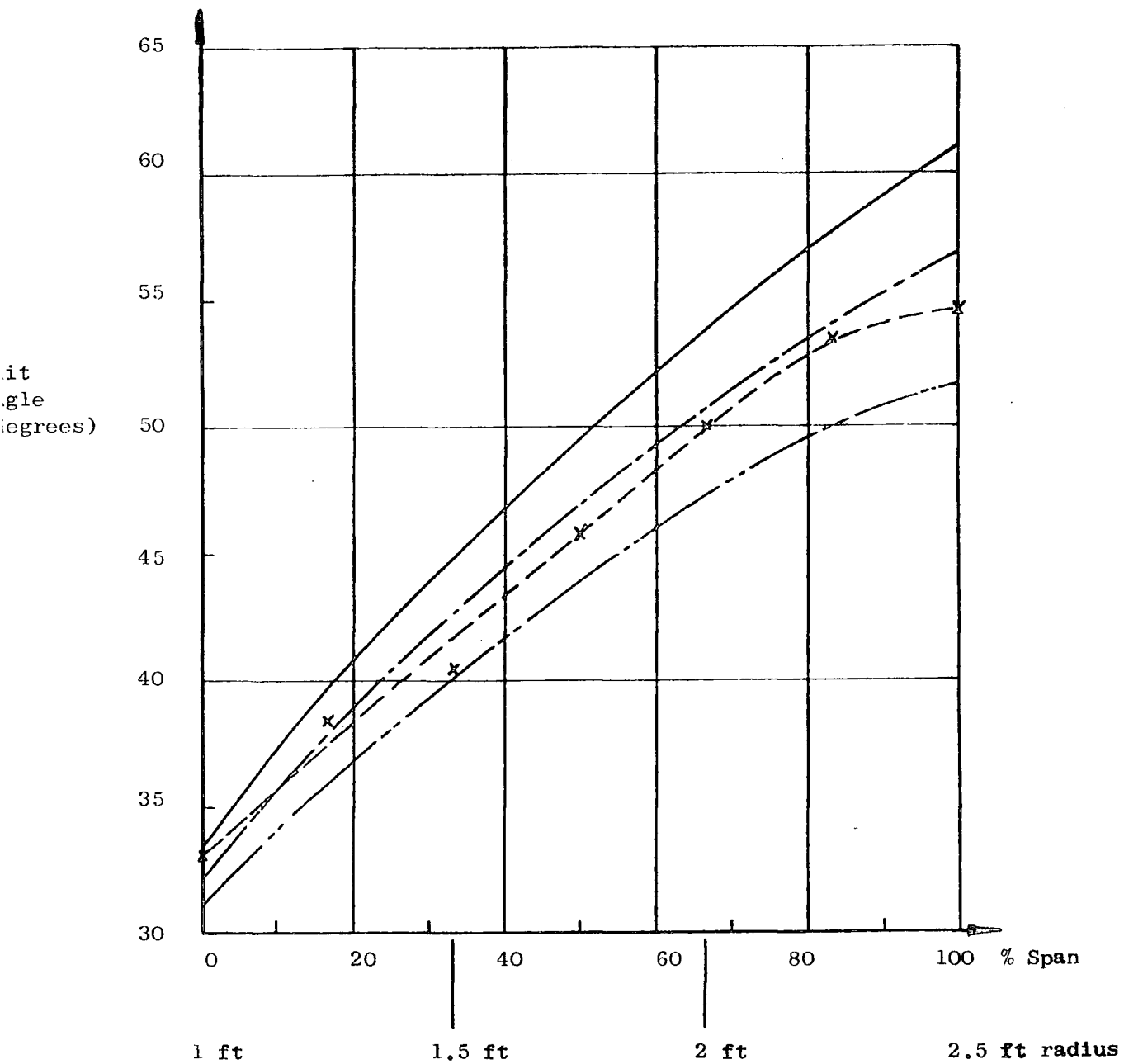

FIGURE 8.2: FLOW DEVIATION CALCULATIONS

to predict the angular difference between the blade exit angle and the experimental flow angle.

The uneven pattern in the flow angle between the hub and midspan indicates that the experimental data may be considerably in error, and the unevenness is reflected in the computed blade exit angle distribution. Figure 8.6 shows a blade design assuming a smoothed flow angle profile.

It is worth noting that the deviation rules of both Howell and Carter are formulated for linear cascades. The secondary flow effects which occur in annular cascades (Glynn and Marsh (1980)), may be found using a computer program developed by Gregory-Smith (1977), once an initial blade shape has been designed and flow field calculations have been performed. For the example modelled here subsequent secondary flow calculations indicated a contribution to the flow angle of over $+1^{o}$ at the hub, passing through zero to about $-.8^{o}$ at the tip. Since the flow angles used to reconstruct the blade shape were experimental results, they must already contain these secondary flow effects, which are not considered in the usual deviation rules. Thus a more realistic blade profile may be designed by removing the secondary flow contribution from the flow angle distribution and then redesigning the blade, calculating the deviation as if for a linear cascade. This second-generation blade geometry is also shown in Figure 8.1. For the exit angle profile, the difference from Oxford's (1965) blade design is now small (less than 1^{o}) at the hub, but the secondary flow allowance enhances the discrepancy towards the tip, where it is nearly 5^{o}, with an estimated deviation of 11^{o} there.

The computer program used the method described in Section 5.4 to stack the various aerofoil sections designed. Oxford's guide vanes were constructed to have a straight, though not radial, trailing edge, and with a constant axial chord in the design orientation.

8.3 Downstream Axial Velocity Profiles

By performing aerodynamic calculations on the inlet guide vanes, the operation of the computer program was checked against Gregory-Smith's (1970) graphical plots of experimental axial velocity profiles at distances of 0.5 inch and 11.2 inch downstream of the inlet guide vanes.

The upstream air flow was uniform and non-swirling; the axial velocity there was not given, and so it was estimated by graphically integrating the downstream velocity profiles. Small modifications were necessary after the first attempts at reproducing the velocity profiles because the original integration took no account of varying air density. Within the accuracy of this procedure, the upstream axial velocity was found to be 20.0 m/s, which may be a fortuitously round number since the original experiments were measured in imperial units.

Given that one calculation station is set on the blade trailing edge, the positioning of another 0.5 inch behind it in the 18 inch span duct would give a local grid aspect ratio of 36. Relaxation factors generated there would be small (Section 6.8) and the calculations would therefore require many iterations. The intrablade axial grid spacing for a blade of about 6 inch axial chord would be around 0.6 inch, with 10% spacing, but for the first and second parts of the three-stage solution scheme (Section 6.9) not all of the intrablade stations are used, giving correspondingly larger aspect ratios. A similar treatment could be developed for the duct grid, but in its absence the easier solution was to relocate the close downstream station permanently a little further away, and then interpolate results there and at the blade trailing edge to estimate the velocity profile 0.5 inch behind the blade. The station was set 1.8 inches (about 0.3 chord lengths) downstream, giving an aspect ratio of 10.

The blade exit flow angle variation was known ab initio, and so despite the questionable blade design results the mean stream surface

flow treatment could be performed accurately in the aerodynamic calculations; furthermore there was no need to correct the flow angle for secondary flow effects retrospectively.

The loss model in the theory comes into its own in a multi-stage machine where appreciable radial gradients of entropy are developed over several stages. Although annulus wall boundary layers were studied by Gregory-Smith (1970), no loss data are presented for the inlet guide vanes. The computed velocity profiles were therefore produced assuming lossless flow.

Figures 8.3 and 8.4 show, at 0.5 inch and 11.2 inch downstream respectively, the comparisons of the computed axial velocity profiles with Gregory-Smith's (1970) experimental results. The joggle centred at about 30% span in the computed profile immediately behind the blade would appear to match the uneven flow angle variation at that point in Gregory-Smith's (1970) blade exit flow angle data, shown in Figure 8.1. Other than this effect, the calculated result follows the experimental data closely over most of the span. The greatest error, 4%, occurs near the hub.

For the station further downstream the computed profile again crosses the line of experimental data at about 30% span, with the predicted velocity less than the experimental at radii inside this point and greater than the experimental at larger radii. The reduction of the experimental axial velocity over the outermost 15% of the span is not apparent in the computed result.

More accurate velocity distributions were computed following smoothing of the original blade exit flow angle data from Gregory-Smith (1970). These are considered in Section 8.5, but one more aspect of the calculation method was investigated during the above-described trials, and an account of this is first given below.

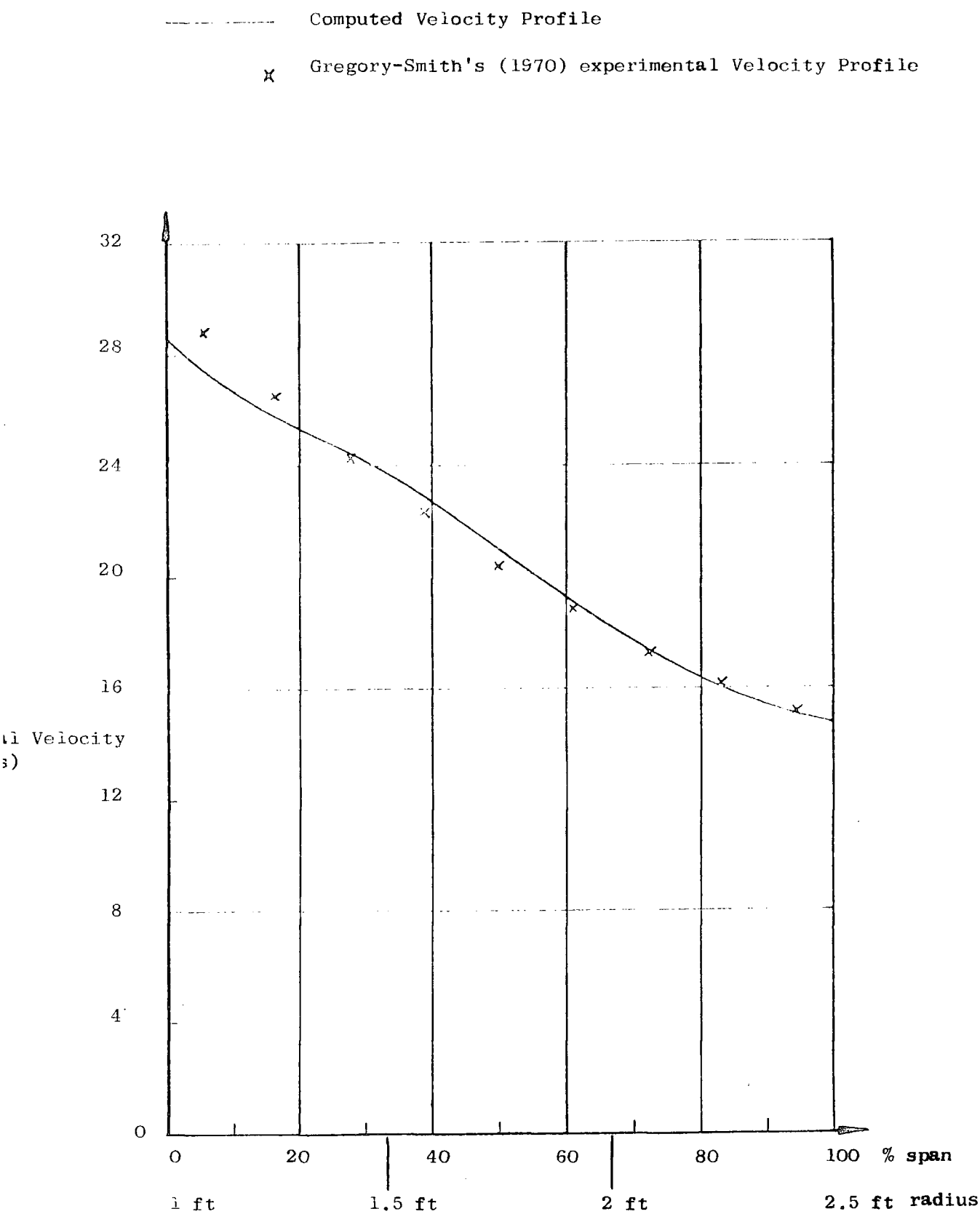

GURE 8.3: AXIAL VELOCITY 0.5 INCH DOWNSTREAM OF INLET GUIDE VANES, USING EXIT FLOW ANGLE DISTRIBUTION OF GREGORY-SMITH (1970)

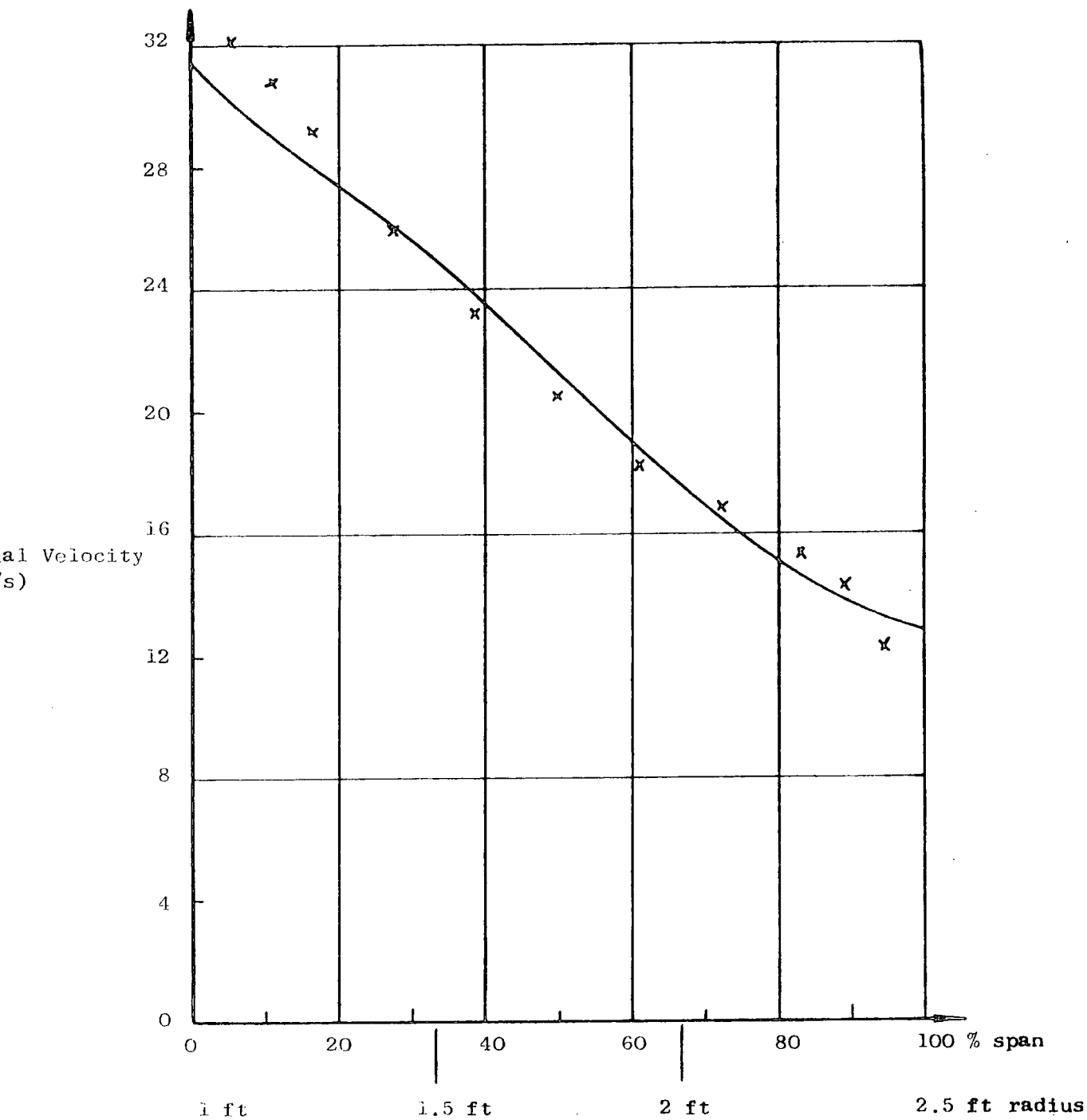

FIGURE 8.4: AXIAL VELOCITY 11.2 INCH DOWNSTREAM OF INLET GUIDE VANES, USING EXIT FLOW ANGLE DISTRIBUTION OF GREGORY-SMITH (1970)

8.4 Effects of Relocating the Relaxation Factors

As discussed in Section 6.7 the relaxation factors are usually applied to the calculation of stream function values from the velocity profiles, though they could alternatively be used in the subsequent calculations of streamline slope or of the radius of curvature of the streamlines. Comparative trials were conducted to perform the calculations described in Section 8.3 with Stow's (1971) relaxation factors applied in each of two ways: firstly the usual application of the factors in the stream function calculation, and secondly using them instead in the determination of slope values. In both cases the three-stage scheme of Section 6.9 was used for intrablade analysis, demanding for convergence at each stage that the greatest meridional velocity change be less than 1%. During these trials the $\cos^2 \beta$ relaxation on changes in the term L(r) of equation 6.1 was being applied only within blade rows - subsequently its use was extended to duct calculations as well. The comparative run times, in terms of the number of flow field marches required, are tabulated in Figure 8.5.

For this example the transfer of the relaxation factors to the slope calculation reduced the amount of calculation required by over 30% and produced very similar results. The number of iterations to convergence for Stage 3 with the relaxation imposed on the stream function calculations was not determined properly because the restriction on the changes in the velocity profile (Section 6.4) was being invoked in the Stage 3 calculations: the maximum allowed change, which was reduced as the number of iterations performed increased, dropped below the convergence criterion (1%), giving a false indication of a converged solution. This procedure was modified subsequently to avoid such situations, but other changes to the program had by then been made, and a direct comparison with the other data in Figure 8.5 was no longer possible.

FIGURE 8.5: EFFECT ON RUN TIME OF RELOCATION OF RELAXATION FACTORS

Stage	Intrablade Axial Chord Step	Cumulative Marches To Convergence. Relaxation Applied To Calculation Of:		
		Stream Function (Note 1)	Slope (Note 1)	Slope (Note 2)
1	50% chord	14	8	7
2	20% chord	25	16	15
Secondary Flow Angle Adjustment	20% chord	26	17	16
3	10% chord	?	39	31

Notes: 1. Blade Exit Flow Angle data from Gregory-Smith (1970)
2. Blade Exit Flow Angle data as (1) but smoothed between hub and midspan

8.5 Smoothed Flow Angle Data

The uneven distribution of blade exit flow angle between the hub and midspan in Gregory-Smith's (1970) tabulated data (Figure 8.1) was thought to be the cause of the similarly-placed disturbances on the computed blade exit angle profile (Figure 8.1) and the downstream axial velocity distribution (Figures 8.3 and 8.4).

The blade design and aerodynamic analysis were repeated using the subjectively smoothed blade exit flow angle profile depicted in Figure 8.6. The blade angle variations shown on this Figure appear with the ripple smoothed out, though the overall design still shows the departure from Oxford's (1965) original attributed to the methods of estimating deviation.

Compared with Figure 8.3, Figure 8.7 shows much better simulation, near the hub, of Gregory-Smith's (1970) experimental axial velocity results, and Figure 8.8 shows a smoother velocity profile than Figure 8.4, though the errors at the hub and tip are almost identical to those previously produced. Boundary layers on the annulus walls developed in practice and by this point they had increased to thicknesses of approximately 1 inch on each wall, so that about 10% of the duct span was affected. The effective narrowing of the usable duct may be responsible for the steeper experimental radial gradient of velocity.

These results were produced using the program with the relaxation factors applied to the slope calculation, and convergence times to 1% on meridional velocity were now a little faster than those using the original data. Figure 8.5 shows the number of flow field marches required, for comparison with the tests using unsmoothed flow angle data.

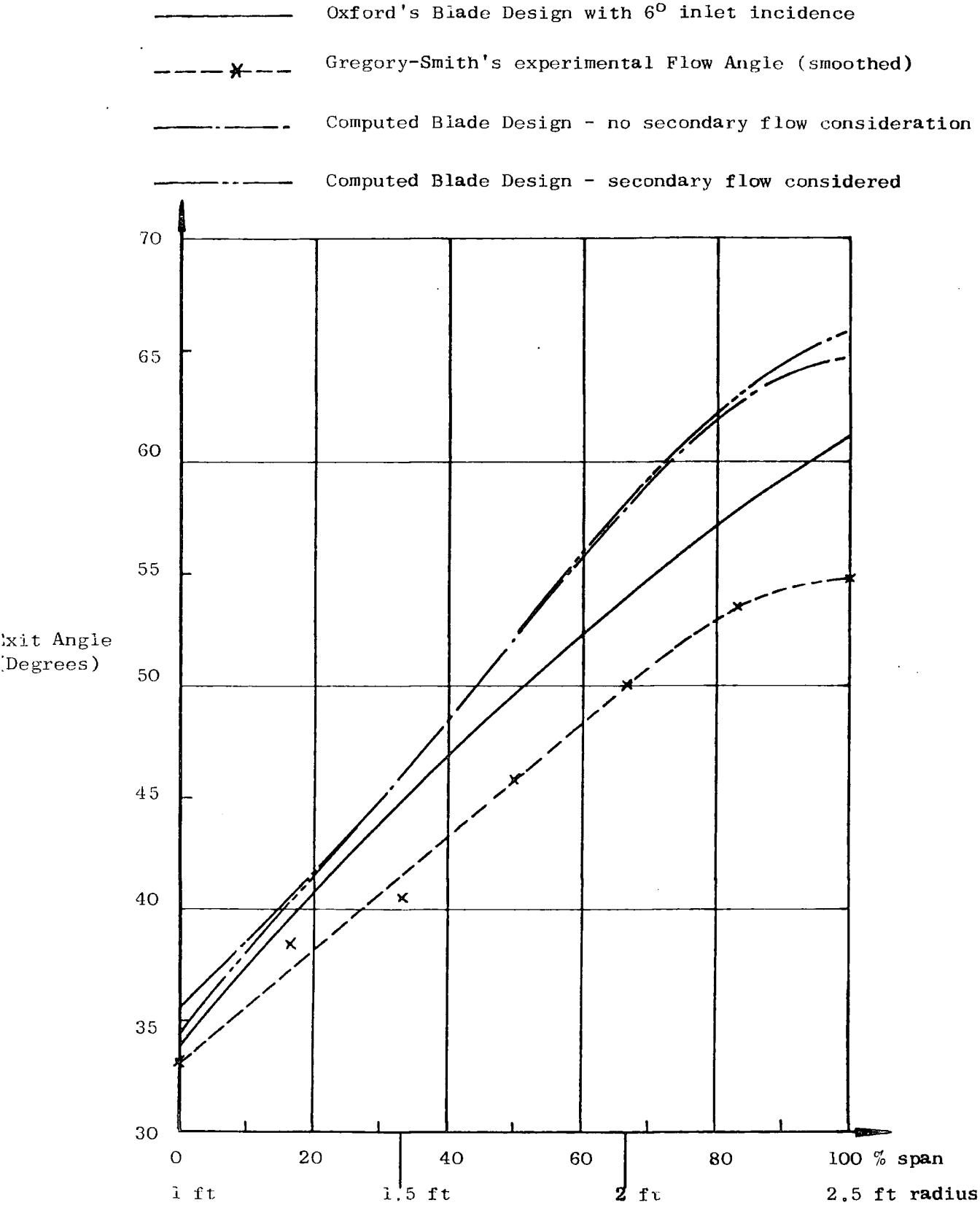

FIGURE 8.6: BLADE REDESIGN WITH SMOOTHED FLOW ANGLE DATA

———— Computed Velocity Profile

✕ Gregory-Smith's (1970) Experimental Velocity Profile

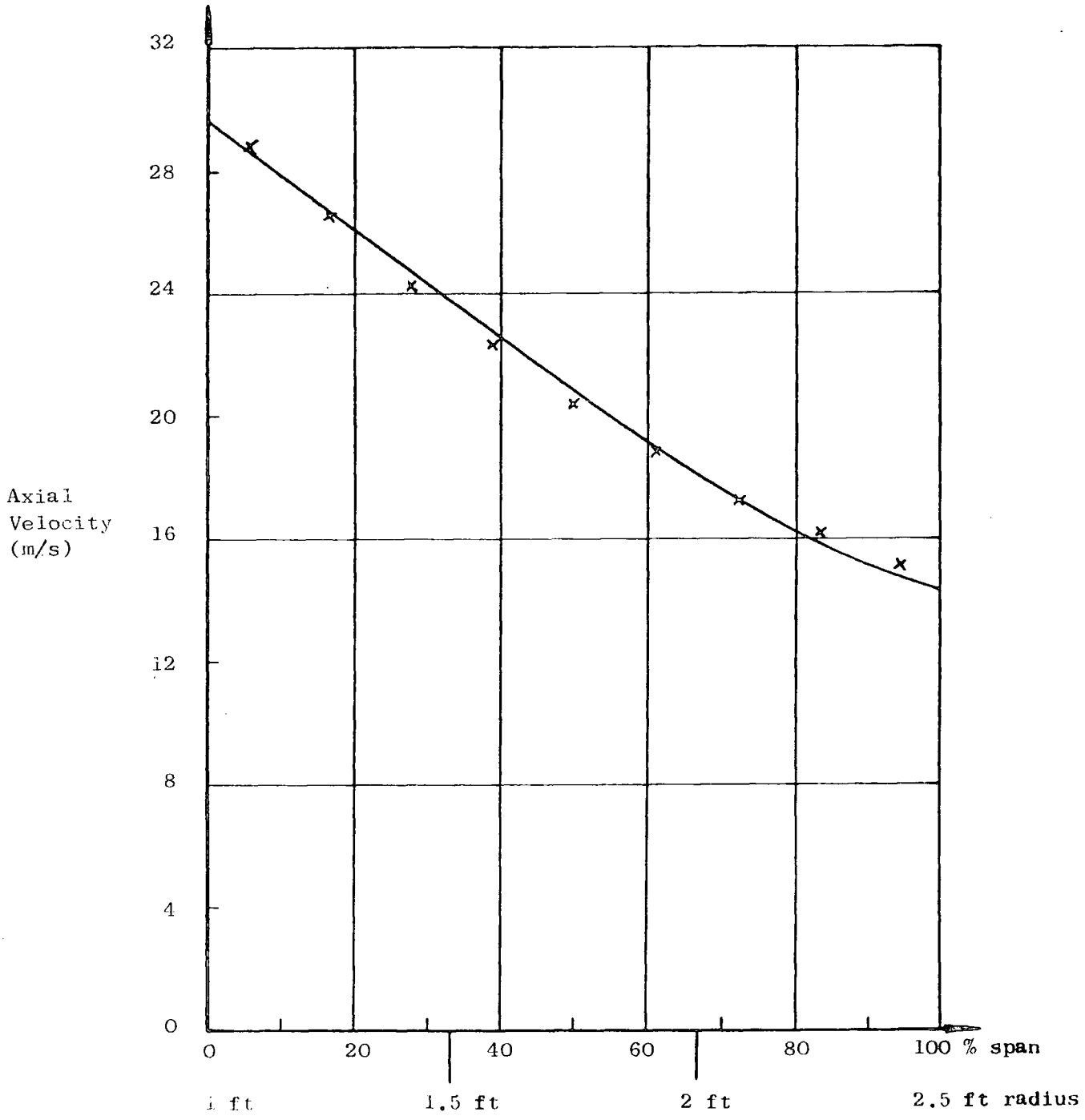

FIGURE 8.7: AXIAL VELOCITY 0.5 INCH DOWNSTREAM OF INLET GUIDE VANES, USING SMOOTHED EXIT FLOW ANGLE DISTRIBUTION

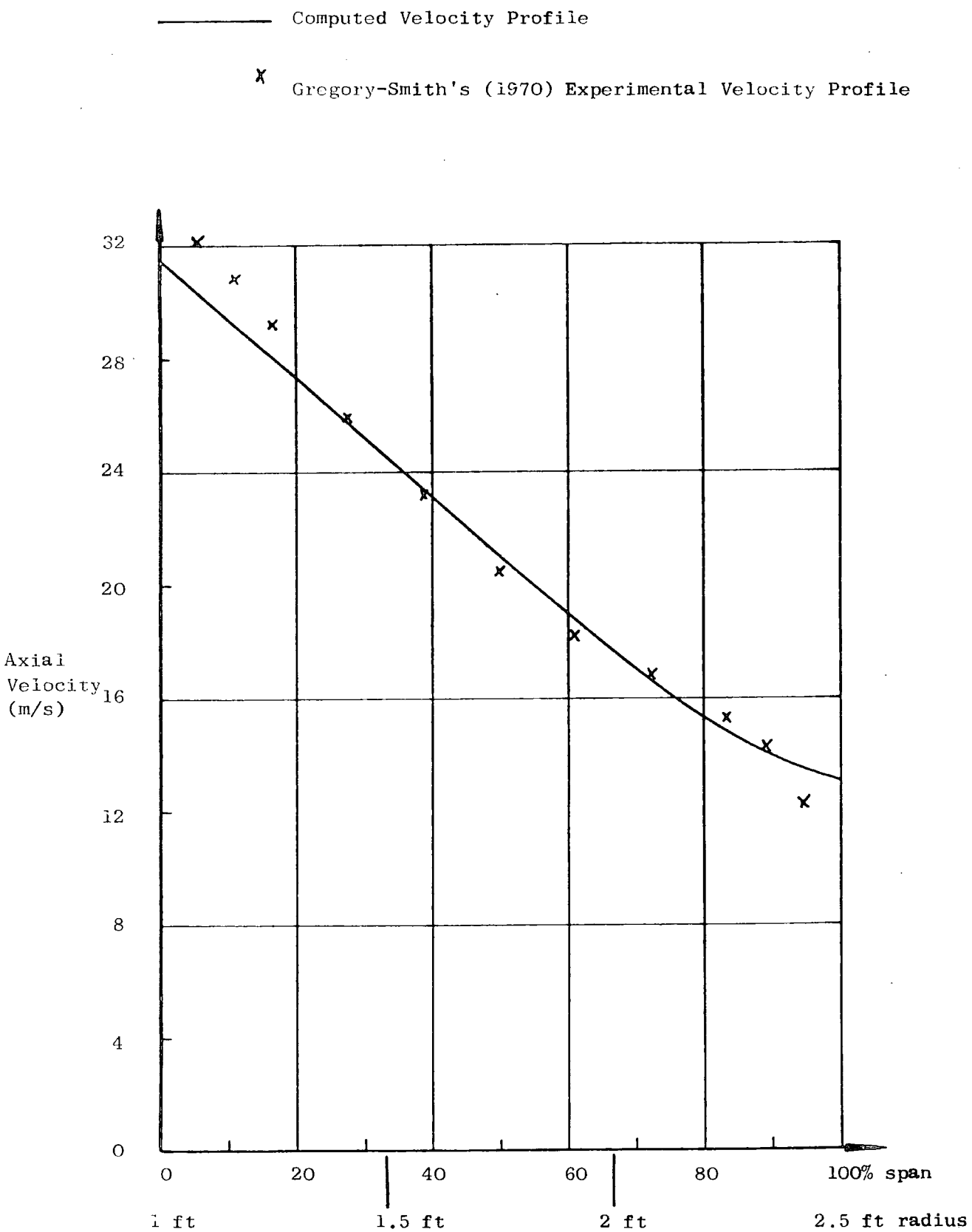

FIGURE 8.8: AXIAL VELOCITY 11.2 INCH DOWNSTREAM OF INLET GUIDE VANES, USING SMOOTHED EXIT FLOW ANGLE DISTRIBUTION

8.6 Conclusions From Modelling the Rig of Oxford and of Gregory-Smith

The geometry of a set of inlet guide vanes was reconstructed using experimental flow angle data. Several parameters, such as the system of stacking different aerofoil sections, may have been different in the original design by Oxford (1965), but a discrepancy of up to 5^{o} in the blade exit angle between the real and the computer-modelled blades is attributed to the estimation of the exit flow deviation from methods developed for compressor cascade design.

Good agreement was obtained between experimental axial velocity data and computed values across the duct span at two locations downstream of the row of blades, one close to the trailing edge, the other some distance away. The comparison of the results was improved by smoothing a ripple in some basic data, the blade exit flow angle distribution given by Gregory-Smith (1970).

Faster convergence was obtained by applying the relaxation factors to the slope calculations rather than to the determination of the stream function, the more conventional approach.

8.7 The Compressor of Fahmi

As is also noted in Section 10.6.2, there is little material published in the open literature on multi-stage machines which also contains sufficient information to test a computer program of the kind developed in the present work. The work of Fahmi (1968) includes reasonably full definitions of the blade design, and also some flow loss data, in addition to experimental velocity profiles. Fahmi tested a low-speed axial-flow compressor containing only three blade rows: inlet guide vanes, rotor and stator. He conducted experiments with sets of blades of 3 inch and of 6 inch chord, to vary the blade aspect ratio, and also varied the air flowrate.

The selected test case modelled with the present computer program was that with the blade rows of longer chord operating at their design flowrate. For each of the three blade rows, the true chord was 6 inches at all radii, but the axial component of the chord varied because of the blade twist. The hub and tip radii of the parallel-walled duct were 18 inches and 24 inches respectively, giving blade aspect ratios of the order of unity. The finest intrablade grid used in the computations would therefore have an aspect ratio of ten, or not much larger, a value not expected to cause convergence problems by demanding very small relaxation factors (Section 6.8).

Inlet and outlet blade angles, the number of blades and the profile types (all C4) were all supplied in Fahmi's (1968) data. The experimental blades incorporated circular arc camber lines; the present computer program was capable of generating only parabolic camber lines but a reasonably true shape was produced by specifying the ratio $a/c = 0.5$. The designed cross-sections of the actual inlet guide vanes were stacked radially at the leading edge, and the rotor and stator cross-sections were stacked radially at the mid-chord. Although each blade row could be replicated as viewed in an (r, z) plane, only one option was available in the computer program for the relative circumferential positioning of aerofoil cross-sections: the centres of mass of all the sections of a blade were set to lie at the same circumferential co-ordinate. The computed values of the lean angle λ were thus unrealistic.

In the absence of more detailed information, the maximum blade thickness was entered as 0.1 chord lengths at all radii for all blades.

8.8 Axial Velocity Profiles Following Each Blade Row

Upstream of the guide vanes, the axial velocity profile adopted for the aerodynamic calculations was not uniform, but was based on the

experimental form given by Fahmi (1968), with reduced velocity near the walls. The computer program could not handle stationary flow and so the axial velocity at the walls was not prescribed as zero. The small experimental swirl component was included in the flow data for the computer program. Assuming no meridional curvature or slope of the flow at the inlet calculation station, the static pressure there is very nearly constant with radius; the swirl component of velocity in this example has very little centripetal effect. However, the total pressure profile contains a radial variation to match the varying dynamic head of the flow.

Blade row loss data provided by Fahmi (1968) include both theoretical and experimental values. No experimental data are given for the inlet guide vanes, and those for the rotor indicate an unrealistic negligible loss at the condition modelled here, so the theoretical predictions were employed in the computed simulation.

Figure 8.9 shows radial distributions of axial velocity following each blade row. The results at exit from the rotor and from the stator are in fairly good agreement with Fahmi's (1968) test data, but the profile at exit from the guide vanes does not follow the test points at all well. However, examination of the computed intrablade results at the rotor leading edge shows a predicted axial velocity increasing considerably with radius. The axial velocity profile obtained behind the guide vane exit is influenced by the upstream propagation of such effects through the short inter-row space and into the guide vanes. The program would appear to predict a more sensitive reaction than that observed in practice.

Figure 8.10 shows the computed exit flow angles relative to each blade row, which all accord well with the design values of Fahmi (1968), though no secondary flow calculations were undertaken in this application of the computer program. For the inlet guide vanes, the measured flow

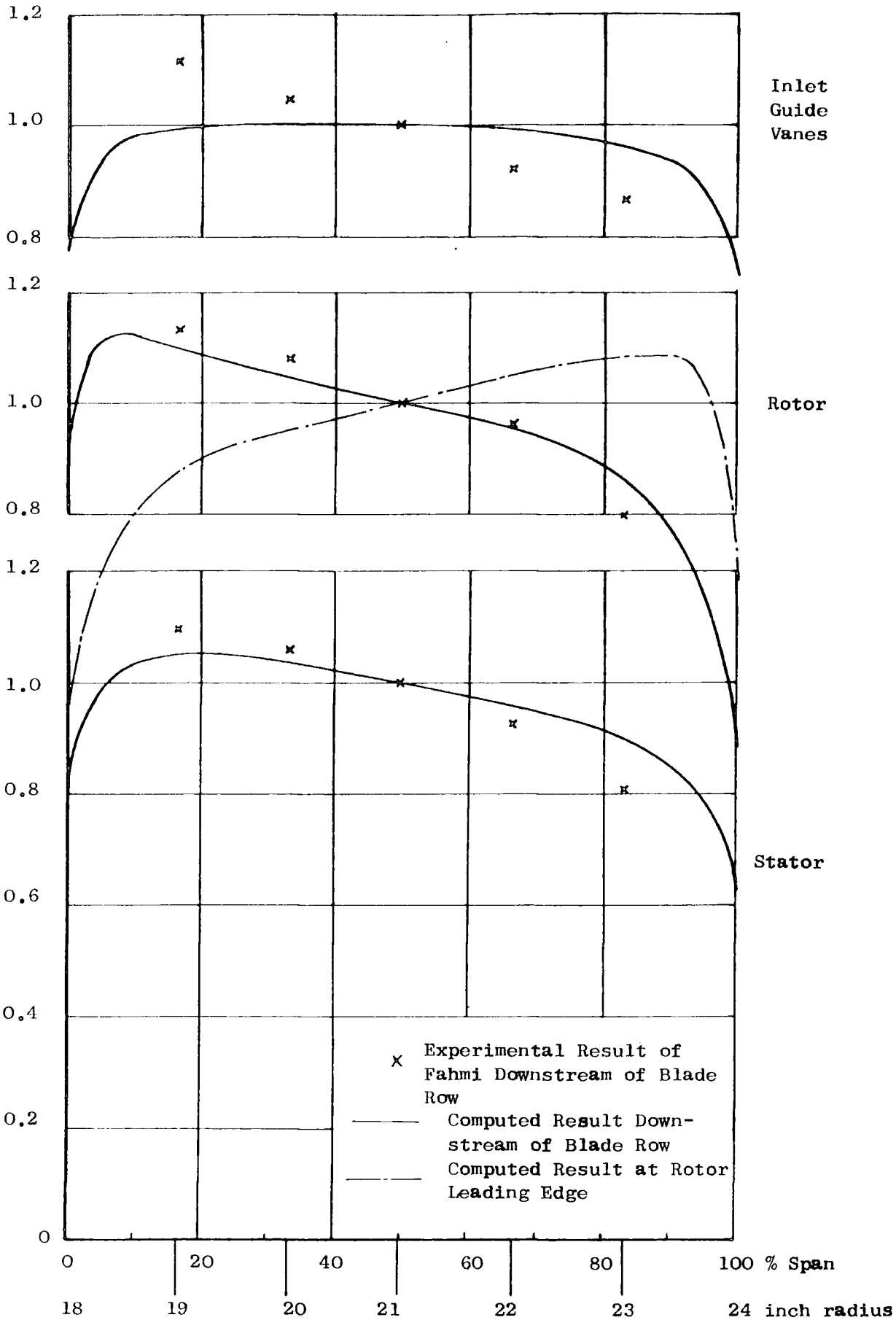

FIGURE 8.9: AXIAL VELOCITY PROFILES FROM SIMULATION OF THE COMPRESSOR OF FAHMI (1968)

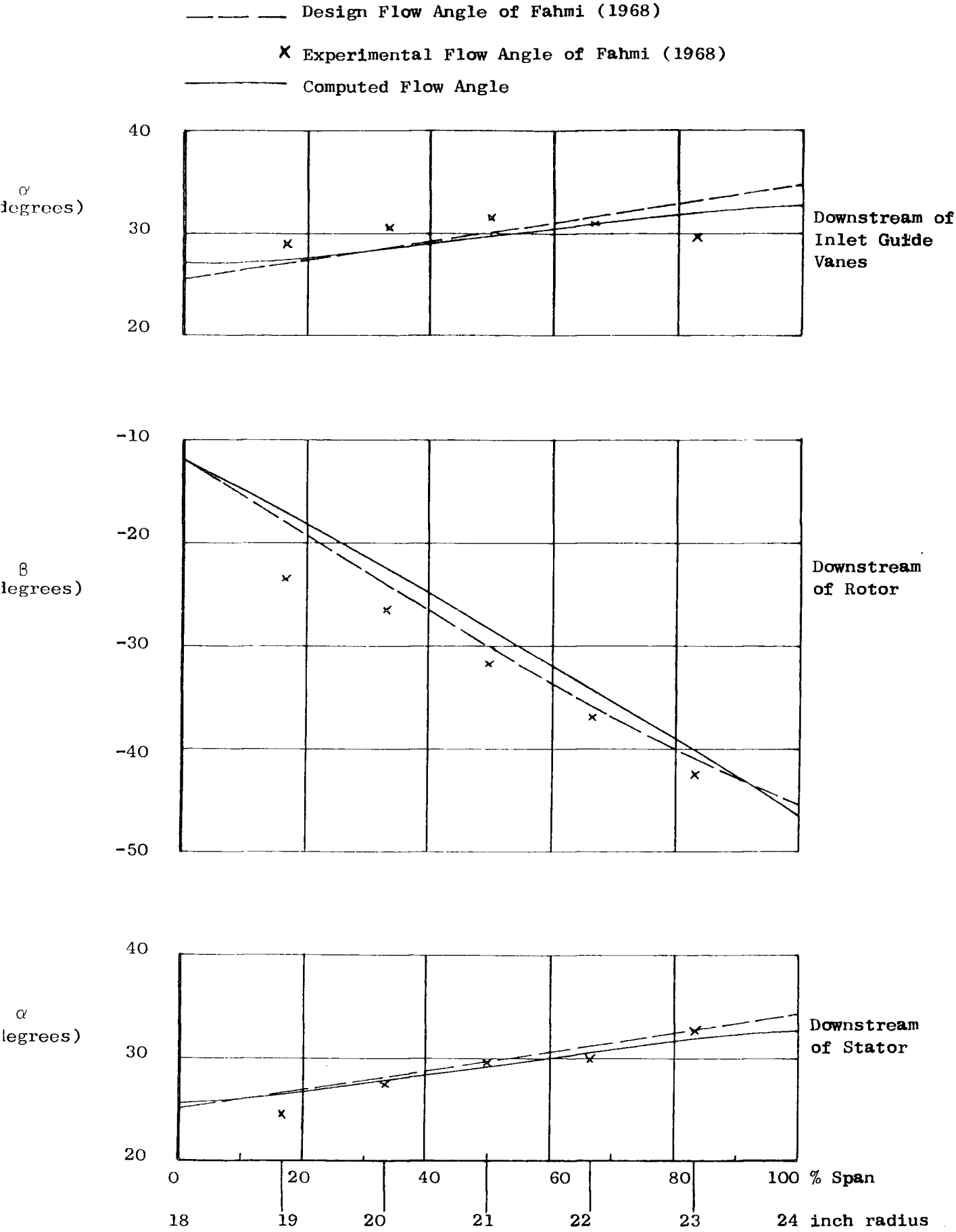

FIGURE 8.10: BLADE-RELATIVE EXIT FLOW ANGLES FROM SIMULATION OF THE COMPRESSOR OF FAHMI (1968)

angles near the hub are higher than expected, and rather lower than expected towards the tip. From mid-span to tip the experimental flow angle variation follows closely a 'free-vortex' distribution.

The computed axial velocity profiles following the rotor and the stator (Figure 8.9) are not as greatly inclined as the experimental data, but the measured flow angles do differ from the design predictions, by up to 6^{o} in the case of the rotor.

8.9 Numerical Considerations

The computer program requires a duct calculation station just upstream of each blade row and another following each row. They indicate the presence of a blade row and its type (stator or rotor). For the example used here this resulted in two closely-spaced calculation stations being placed in the half-inch duct length between each pair of blade rows. It was these stations, rather than the intrablade stations, which produced the smallest relaxation factors in the solution process. By extending the inter-row spacing to 50 mm, faster convergence could be obtained. In place of such undesirable modifications to the geometry of the problem being considered, the program should be improved by eliminating the necessity for such duct calculation stations.

Calculations assuming a uniform velocity profile at inlet to the compressor converged in little over a quarter of the number of iterations required for the solution with the experimental profile. Difficulties had been encountered with the sharp changes in properties near the duct walls, associated with the lowering of the axial velocity there.

One problem arose in the interpolation of property values from upstream data, for example in tracing total pressure values along a loss-less streamline. Referring to Figure 8.11, the data points A, B, C and D show the total pressure and dimensionless stream function values held

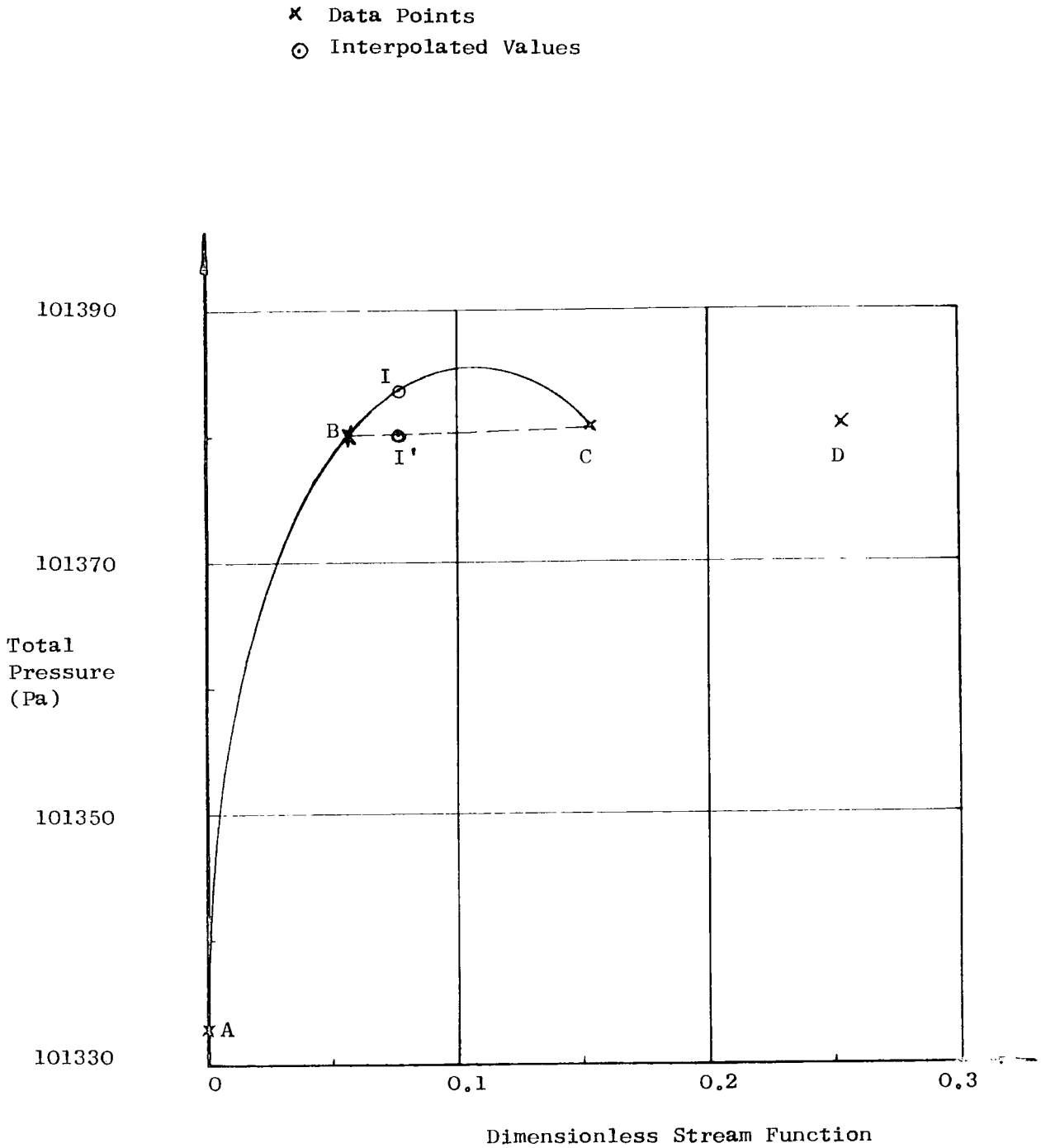

FIGURE 8.11: INTERPOLATION PROBLEM NEAR DUCT WALL

at four grid points equally spaced radially at the inlet calculation station, where flow conditions must be defined by the user. Point A is on the hub wall of the duct; the low total pressure there is indicative of the low speed flow along the wall.

Because of the proximity of a blade row downstream, for example, some redistribution of the flow occurs between the inlet and the second stations, so that at the grid points on the second station different stream function values will be stored from those at the first station. An interpolation scheme was used in the computer program for evaluating certain fluid properties from their values upstream on the same streamlines, i.e. by following stream function values. For a grid point where the stream function value is that of I and I' on Figure 8.11, a parabola is constructed through points A, B and C, and the interpolated total pressure value is taken as that at I, which for the case depicted lies above the total pressure at B and C, and indeed above the maximum inlet station total pressure, at the duct mid-span. Erroneous values of entropy and of the term $\frac{\partial s}{\partial r}$ are subsequently found at I, affecting the predicted velocity profile over the innermost part of the span.

For such ill-conditioned cases where the interpolated point I lies outside the range of B and C, a simple linear interpolation is used, resulting for the example shown in the total pressure value at I'. However, a better alternative or additional method would be to introduce a calculation grid whose radial distribution may be defined by the user, to allow more grid points to be placed in regions of great change of fluid behaviour, such as near the duct walls, whereby information may be stored in more detail.

The formation of the meridional velocity profile at each calculation station (Section 6.4) is begun at the mid-span and progressively extrapolated towards the duct walls, using the radial gradient of

velocity determined at the latest completed grid point. Thus a severe drop-off in velocity near the walls is not reproduced unless the calculation procedure senses the high gradient there; this may be achieved by again incorporating a radially adjustable calculation grid.

The average calculation time for this test example was 0.15 second per calculation station (including intrablade stations) per flow field march, on an IBM 370/168 computer.

8.10 Conclusions from Modelling Fahmi's Compressor

The flow through a three-row axial compressor has been modelled with a degree of success. The original blade designs could not be reproduced exactly as there are insufficient options in the design procedures in the computer program. The axial velocity profile downstream of the inlet guide vanes was not well reproduced.

Multistage machines may be modelled by the program, but some improvements may usefully be made: the elimination of the need for duct calculation stations adjacent to every blade row; and the introduction of a calculation grid with a user-defined radial distribution.

CHAPTER 9

Three-Dimensional Flow

9.1 Introduction

In the initial part of his analysis, Wu (1952) includes the variations of fluid properties with both circumferential position and with time, though in presenting a calculation procedure he eliminates the time variable and considers only steady flow.

The assumption of axisymmetric flow introduced in Chapter 2 of this thesis implies that no flow variations exist with respect to the circumferential co-ordinate, and in the case of a turbomachine with relative motion of the blade rows, no variation with time either.

Turbomachine flow models suitable for computing have increased in complexity over recent years as computers have become faster and larger, and considerable progress has been made in removing the commonly-made assumption of axisymmetric flow. In the context of this Chapter the asymmetry considered is that occurring in each circumferential passage from the suction surface of one blade to the pressure surface of its neighbour, rather than uneven distribution of flow around the annulus as a whole.

Full three-dimensional calculations performed following Wu's (1952) approach require families of intrablade stream surfaces, types S1 and S2, which were described in Section 2.6; the axisymmetric solution used just one representative S2 surface. The calculations to produce the axisymmetric solution represent only one iteration in a longer procedure in which the families of S1 and S2 surfaces must be allowed to interact to find a converged three-dimensional result.

The two blade surfaces bounding the intrablade flow passage generally differ in shape, and thus the family of S2 stream surfaces between them must form a transition from one surface shape to the other. The fluid

properties and velocities also vary circumferentially, and so the S1 stream surfaces are twisted, and not surfaces of revolution.

9.2 A Survey of Existing Calculation Methods

Krimerman and Adler (1978) report complete three-dimensional calculations for centrifugal flow impellers, using a lossless subsonic model in a finite element technique. The analysis of such single-rotor machines is a suitable application of a three-dimensional flow calculation method, but the computing time to analyse a multi-stage axial flow machine would be very considerable. Furthermore, the circumferentially-varying flow from the exit of one axial blade row is usually directed into a subsequent row which is rotating relative to the first. To an observer on the second row of blades, such approaching flow appears to vary with time, an effect which is not being considered here, and so the assumption must be made that between adjacent blade rows circumferential variations in the flow are mixed out, and the flow at any blade entry is axisymmetric. This means that the S1 surfaces at blade entry appear as chords of circles concentric with the machine axis. Within the blade row, behind the leading edge, the S1 surfaces may become twisted.

Many authors approximate the entire S1 surfaces to surfaces of revolution, and not just at the blade leading edges. Bosman and El-Shaarawi (1977), Novak and Hearsey (1977), Veuillot (1977), Hirsch and Warzee (1978) and Spurr (1980) follow this approach, usually with a mean S2 stream surface guessed initially from considerations of blade geometry, but modified as the calculations proceed, with the interaction of data from S1 and S2 surface calculations. This type of procedure is commonly known as the Quasi-Three-Dimensional solution.

Various choices of the initial 'mean' stream surface appear in the works of Bosman and El-Shaarawi (1977), Novak and Hearsey (1977) and Veuillot (1977), but Horlock and Marsh (1971) conclude that although

an axisymmetric flow model can represent overall flow changes through a blade row, averaged properties within the blade row cannot all be matched locally by only one, mean,stream surface.

Hirsch and Warzee (1978) set out a method which, as they say, is restricted to the use of surfaces of revolution for the S1 surfaces, unless extended by performing secondary flow calculations. They derive averaged equations of motion for which no S2 surface choice is required, by specifying that the data used for each term of the equations must be a 'mass-averaged' value across the blade-to-blade passage. Denoting the averaged value of a variable q over the passage width by a bar superscript, Hirsch and Warzee (1978) define a 'mass-average' value, denoted by a tilda superscript, as

$$\tilde{q} = \overline{\rho q} / \overline{\rho} \quad .$$

When several mass-averaged values are multiplied together to produce each term of the main equation, extra terms are included to allow for the differences between the products of mass-averages and mass-averages of products. These extra terms, called 'interaction' terms, are simpler than those obtained from working with passage-averaged terms only.

However, the mass passing any point in the flow field is dependent not only upon the local fluid density, but also on the axial velocity and, within a blade row, on the local blockage factor. Thus the 'mass-averaged' value of q should be defined as

$$\tilde{q} = (\overline{\rho B V_z q}) \; / \; (\overline{\rho B V_z})$$

which may give a different set of interaction terms.

Smith (1966) originated a similar procedure assuming a linear pitchwise variation of every property, and introduced a series of extra terms called G-functions in the radial equation of motion.

Hirsch and Warzee (1978) use a finite element calculation method. Bosman and El-Shaarawi (1977) incorporate the Consistent Loss Model of

Chapter 3 and of Bosman and Marsh (1974), but in a finite difference Matrix Throughflow solution. The Time-Marching methods of Veuillot (1977) and Spurr (1980) allow transonic flow, but the models used are lossless.

Spurr (1980) acknowledges the serious disadvantage in assuming the S1 surfaces to be surfaces of revolution, and Novak and Hearsey (1977) discuss the incorporation of twisted blade-to-blade surfaces through the relation between $\frac{\partial \varepsilon}{\partial \theta}$ and the streamwise vorticity.

9.3 Wu's Power Series Analysis, and Vorticity

Wu (1952) outlines a method by which the circumferential variation of fluid properties within a blade row may be determined without recourse to any assumption about the shapes of S1 stream surfaces. Given the flow pattern and the value of some general property $q\ (\theta_m)$ on the mean S2 stream surface, then the value $q(\theta)$ of the property a short angular distance away can be obtained by a Taylor Series:

$$q(\theta) = q(\theta_m) + (\theta-\theta_m)\,q'(\theta_m) + \frac{(\theta-\theta_m)^2}{2}\,q''(\theta_m) + \frac{(\theta-\theta_m)^3}{3}\,q'''(\theta_m) + \ldots$$

Wu reports that only the first few terms of the series need be found to give accurate results, but this does require calculation of the θ-derivatives of q.

Starting from the definitions of the r, θ and z components of vorticity, ξ, Wu (1952) derives equations for the circumferential gradients of the velocity components, using the special derivatives following the mean stream surface which are readily found from the axisymmetric solution:

$$\frac{1}{r}\frac{\partial W_m}{\partial \theta} = \frac{F_m^2}{F^2}\left[\frac{F_r}{F_m r}\frac{\overline{\partial}(rV_m)}{\partial r} + \frac{F_z}{F_m r}\frac{\overline{\partial}(rV_m)}{\partial z} - \frac{D(\ln B)}{Dt} + \frac{F_z}{F_m}\xi_r - \frac{F_r}{F_m}\xi_z\right] \quad \ldots (9.1)$$

$$\frac{1}{r}\frac{\partial W_z}{\partial \theta} = \frac{1}{r}\frac{\overline{\partial}(rV_m)}{\partial z} + \xi_r + \frac{F_z}{F_m}\frac{1}{r}\frac{\partial W_m}{\partial \theta} \quad \ldots (9.2)$$

$$\frac{1}{r}\frac{\partial W_r}{\partial \theta} = \frac{1}{r}\frac{\overline{\partial}(rV_m)}{\partial r} - \xi_z + \frac{F_r}{F_m}\frac{1}{r}\frac{\partial W_m}{\partial \theta} \quad \ldots (9.3)$$

In equation 9.1, the term

$$\frac{D(\ln B)}{Dt} = W_r \frac{\partial(\ln B)}{\partial r} + W_z \frac{\partial(\ln B)}{\partial z} .$$

The ratios of the body force components in equations 9.1 to 9.3 may all be expressed as functions of the flow angles λ and μ, but the form of their blade-to-blade variation must be assumed in some way.

Wu (1952) proposed that the analysis be applied to flow with zero absolute vorticity only, and it is known that equations like 9.1 to 9.3 have been used at Rolls-Royce to estimate circumferential variation, ignoring the vorticity terms. Came and Marsh (1974) analyse the secondary flow in linear cascades, applying Kelvin's circulation theorem to determine the vorticity within the blade row from known upstream values of both the streamwise and perpendicular vorticity components. Glynn and Marsh (1980) extend the method to annular cascades. Kelvin's circulation theorem as applied in these papers should strictly be limited to reversible incompressible flow, but is generally a good approximation for other applications; the effect of compressibility is considered by Marsh (1976). A simple numerical example following Glynn and Marsh (1980) to determine the intrablade secondary vorticity yielded values of the vorticity components in equations 9.1 to 9.3 which were insignificant compared to other terms. However, secondary flow effects can affect the flow angle at exit from a blade row, as discussed in connection with the blade design of Section 8.2.

9.4 The Problem of Flow Deviation

The calculation method proposed by Wu (1952) has not been described in mathematical detail because although it would provide sufficiently accurate blade-to-blade flow variations very rapidly without some of the stream surface constraints of other methods, there appears to be a fundamental problem concerning the circumferential distribution of the flow

angle μ (related to β), which appears in equations 9.1 to 9.3 as a body force ratio.

The flow angle in general varies from β_a on one blade surface to β_b on the other across the blade passage, about a mean value $\bar{\beta}$, as discussed by Horlock and Marsh (1971) and shown in Figure 9.1. In the many-bladed cascade model, β_a and β_b are very nearly identical, but the pitchwise profile of Figure 9.1 still exists, falling below $\bar{\beta}$ towards the mid-pitch.

The value $\tan \bar{\beta}$ is used for the axisymmetric analysis and because of flow angle deviation it need not lie between the values on the blade surfaces, $\tan \beta_a$ and $\tan \beta_b$. Wu (1952) suggests that the Power Series method may be used to extend the flow field outwards from the mean stream surface, but it is clear from Figure 9.1 that the three angles $\bar{\beta}$, β_a β_b provide insufficient data to determine the curve joining β_a and β_b across the passage.

Novak and Hearsey (1977) realise that the Taylor Series type of blade-to-blade technique cannot recognise the off-cascade momentum change which occurs on the mean streamline towards the leading and trailing edges, but obtain surprisingly realistic information for centrifugal impellers. The experimental deviation is considerable, as indicated in Figure 8.1 by the departure of the mixed-out downstream flow angle from the blade exit angle for Oxford's (1965) inlet guide vanes. This suggests that for axial flow cascades, which have high pitch:chord ratios, compared with the equivalent tip spacing:channel length of centrifugal impellers, blade-to-blade flow variations may not be found realistically by extending calculations circumferentially from the mean stream surface.

The form of mean stream surface developed in Chapter 4 for intra-blade analysis allows the progressive application of circumferential curvature along the streamline path, and is considered to be an improvement

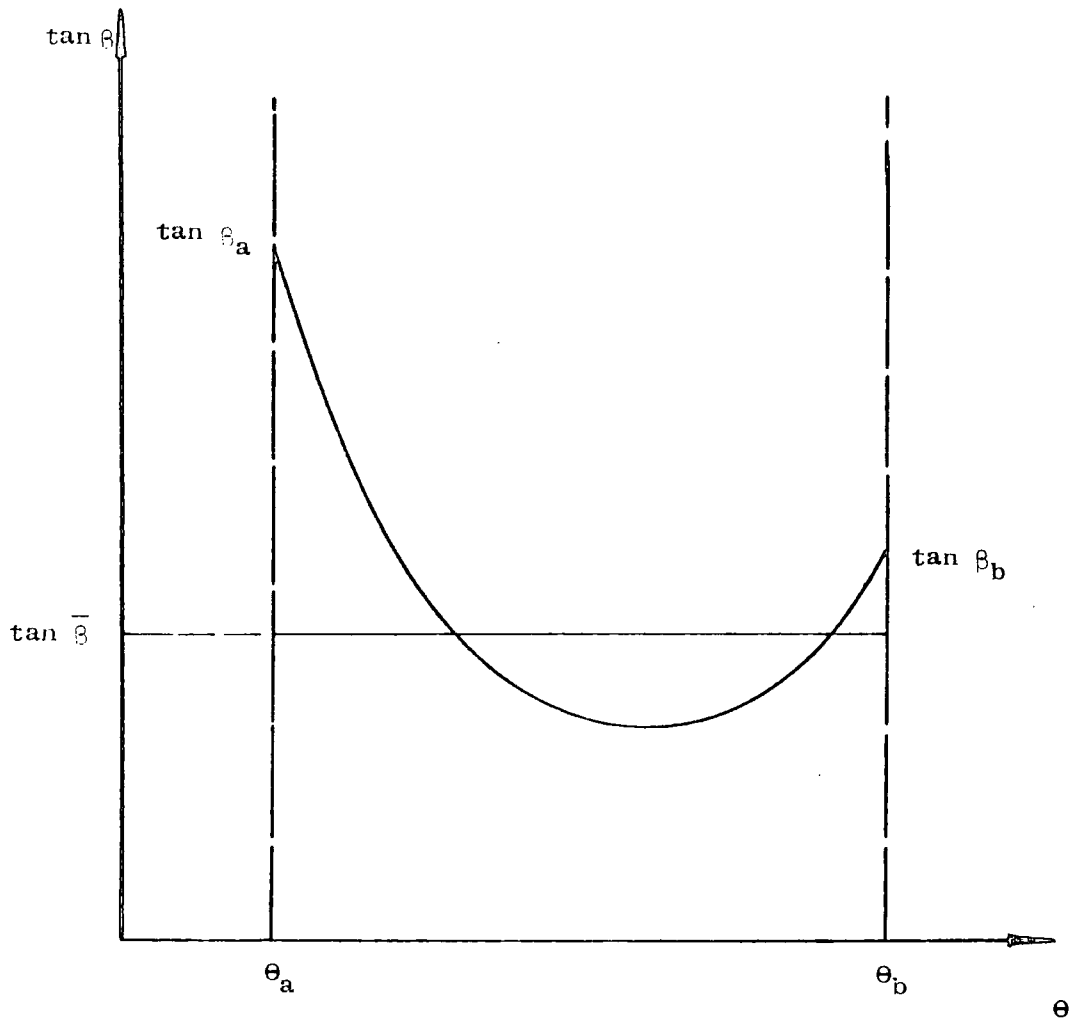

FIGURE 9.1: BLADE-TO-BLADE VARIATION OF FLOW ANGLE

over many intrablade analyses using mean stream surfaces based on the blade geometry only, since these were shown to indicate sudden radial redistribution of the flow. Bosman and El-Shaarawi (1977) use a geometrically-defined initial guess for the mean S2 surface, and iterate between producing improved S1 and S2 solutions, retaining surfaces of revolution for the S1 shapes throughout. They remark that the major change in the S2 surface occurs in the first interaction with the S1 surfaces; it would be of interest to discover whether the reshaped S2 surface is at all like that produced by the considerations of Chapter 4.

9.5 Conclusions

The quasi-three-dimensional techniques of other workers involve the calculation of the fluid flow on a series of S1 surfaces, which are held to be surfaces of revolution. Attempts to relax this condition, by applying to an axisymmetric solution Wu's (1952) circumferential extension of the flow field via a Taylor Series, would appear to be unsuitable for axial-flow machines because of the uneven distribution across the blade-to-blade passage of the angular momentum imparted to the fluid; this appears as a considerable pitchwise variation of flow angle.

A more promising method of removing the restriction on S1 shape may be to use the quasi-three-dimensional solution as a starting point for secondary flow calculations, as mentioned by Novak and Hearsey (1977) and Hirsch and Warzee (1978). The time-marching method developed by Spurr (1980) for quasi-three-dimensional calculations in axial flow steam turbines presents an alternative path.

Full three-dimensional calculations will become feasible in multi-stage axial machines as computers are developed which are both faster and with sufficient storage, but such an application to turbomachines

with relative motion of the blade rows is of dubious value unless the variation of flow with time can also be incorporated. Results produced may then become difficult to understand meaningfully.

CHAPTER 10

CONCLUSIONS, AND RECOMMENDATIONS FOR FUTURE WORK

10.1 Theory

The loss model proposed by Horlock (1971) has been successfully incorporated into the equations of motion for axisymmetric flow. The principal equation of motion is presented in a form providing for easy modification of Streamline Curvature calculation methods based on the former analysis of Marsh (1970). The modification is achieved by replacing four terms in the conventional radial equation of motion by four new terms which transform the equation to that in the N-direction with the consistent loss model included. The version for use within blade rows is expressed in terms of the special derivatives along the mean stream surface, and these derivatives, together with body forces applied to the fluid to represent the blade row torque and the frictional flow loss, account for all the circumferential derivatives of velocity appearing in the initial formulation of the equations of motion, equations 3.2.

The basic assumptions made in Chapter 3 about the fluid and the system analysed are:

(i) The fluid is a perfect gas

(ii) losses may be modelled by a force opposing the relative flow velocity vector, so in the sense that no rheological tensor cross-coupling terms are considered, the fluid is assumed to be Newtonian

(iii) the flow is steady relative to each blade row

(iv) the flow is axisymmetric

(v) rotors rotate with constant angular velocity

(vi) the flow is adiabatic, i.e.

(a) no energy is transferred by heat to or from the environment

(b) there is no inter-streamline energy migration.

Assumptions (ii) and (vi,b) are made to satisfy criticisms raised by Hong (1980) concerning the loss model used here.

Equations 3.15 and 3.18 provide the radial gradients of the meridional velocity. A redistributed velocity profile indicates a repositioning of the streamlines, and so terms within these equations cannot change value instantaneously. This condition applies equally to those terms which are derivatives of fluid properties so that, for these, not only the property value but also its first derivative must be continuous with streamline path length. The terms $\frac{\partial B}{\partial m}$, $\frac{\partial s}{\partial m}$ and $\frac{\partial}{\partial m}(rV_u)$ appearing in equation 3.15 must generally all be continuous, unless their multiplying factors are zero, and this continuity must be observed particularly at blade entry and exit. The term $\frac{\partial}{\partial m}(rV_u)$ was found to be sufficiently influential that attention was required to ensure that at blade entry and exit the circumferential curvature of the streamlines was not changed suddenly, as otherwise sharp changes were predicted in the radial position of streamlines. The streamline path through a blade row viewed in the (θ,z) plane was modified by an empirically-developed method to create transition curves within the blade.

For the examples analysed, the effects of abrupt changes in $\frac{\partial B}{\partial m}$ and $\frac{\partial s}{\partial m}$ were not troublesome. The leading and trailing edge cusps extending up- and down-stream applied to blade rows in the techniques of some authors may obviate problems from the gradient of blockage term. The entropy changes through a blade row are related to the flow losses, and the distribution undoubtedly varies from one application to another, in a manner not well defined.

10.2 Blade Design

The procedures for designing blade geometry arose from a need to determine the blockage factor B within blade passages, and are sufficient

for the purposes of demonstrating the accompanying aerodynamic analysis but as was found in Chapter 8 the calculation of flow deviation angle is not sufficiently refined. For the applications presented, the use of conical design surfaces for the aerofoil cross-sections is reasonable, though methods of transformation from linear cascades onto more generally-shaped surfaces of revolution are available (Bez (1978)). Only one option for the stacking of the blade cross-sections is available in the computer program. Aerofoil thickness data are applied to the camber lines to find not only the blockage factor B, but also the blade surface distributions of the angles μ and λ.

Calculation stations are required in the duct immediately upstream and downstream of the blade row. This results in close axial spacing of the stations if the inter-row distance is short. The program may be modified to eliminate the requirement for some or all of these stations, which as presently used cause small local relaxation factors to be generated, and consequently many flow field marches are required to reach converged flow solutions.

10.3 Numerical Techniques

A computer program has been developed in the PL/1 language by which axisymmetric subsonic flow field solutions may be found using a development of the usual streamline curvature method of repeatedly solving the principal equations of motion. Profiles of the meridional velocity are computed along each of several calculation stations spanning the duct from the hub to the tip wall by integrating equation 3.15 or 3.18 from the mid-span to the hub and tip walls. Using the form of equation 6.1, the functions K(r) and L(r) are evaluated from previous results and held constant while successive values of meridional velocity at the duct centre are tried until the calculated mass flowrate past the calculation station matches that at the duct inlet.

The greatest errors in the velocity profile may be expected towards the edges of the span because of the cumulative inaccuracy in the numerical integration performed along the calculation station. The velocity distribution being constructed by extrapolation from the latest known grid point, using the radial gradient calculated there, some detail is lost at the duct walls if the flow pattern in the input data changes rapidly close to walls; the modelling of the low speed flow in boundary layers is a case in point. The radial spacing of the calculation grid should be made adjustable so that closely-spaced grid points may be used to retain such flow detail.

For the entire flow field being analysed, the meridional velocity value at each grid point is stored. During the next calculation march through the flow field, each meridional velocity value is not allowed to change by more than a certain proportion, to avoid problems of wildly oscillating velocity profiles during the first few marches which may even include negative velocities, i.e. regions of reverse flow.

Sweptback calculation stations in duct flow and intrablade stations generally curved in the meridional plane may be used, since the station velocity profile is formed considering local velocity gradients both radially and axially. The mass flowrate calculation allows for the local geometrical effects of non-radial stations and non-axial streamlines.

Streamline slope is determined from the changing distribution of stream function between successive calculation stations, and the curvature of the streamlines is subsequently found from the changing slopes. The slope values were found by a simple quadratic fit through points of equal stream function on three adjacent calculation stations, following the method of Denton (1978). The curvatures were evaluated in a similar manner but using the slope values as data for the curve fit. This detail was inspired by the methods of Shaalan and Daneshyar (1972) and gives a

simple curve fit with some weighting of the original stream function data as far as two calculation stations upstream and two downstream.

To maintain stability of the converging overall solution, it is usual to apply relaxation factors to the calculation of stream function distributions from the mass flowrate profiles, whereby only a proportion of the indicated change in stream function between one flow field march and the next is applied. It was found however that solution convergence was accelerated if the same relaxation factors were applied not to the determination of stream function values from mass flowrate, but to the next step in the calculation sequence, the calculation of streamline slopes from the stream function distributions. Additionally it proved helpful to relax, by a factor related to the flow swirl, the changes from march to march of the function L(r) in the principal equations in a manner similar to that used by Denton (1978).

The optimum relaxation factor values are dependent on the aspect ratio of the calculation grid, and become small in the closely-spaced intrablade grids generated by the program. Very long times to convergence may be expected if all the calculation stations within a blade row are used from the start, and so a three-stage solution technique was developed in which blade rows are treated with successively finer grids, the solution of each previous stage providing initial estimates of the flow at the newly-introduced extra calculation stations.

Secondary flows within blade passages are not computed by the program developed; Gregory-Smith's (1977) program may be used for this purpose. The swirl angle changes it indicates may be stored, and applied before entry to the final stage of the three part solution described. The magnitude of these changes is of the order of a few degrees.

The small relaxation factors generated in high aspect ratio grids may produce only small flow field changes, even when the solution is far from converged. At the point in the calculations where the relaxation factors are applied, the discrepancy arising is checked, since only when a truly converged solution is achieved will the unrelaxed and the stored values of slope agree closely. Test cases indicate that the error detected in an unconverged solution may be pessimistic compared with the overall subsequent slope changes applied from then until a sufficiently converged solution is produced.

10.4 Applications

Examples of flow were used for testing the computer program for which the radial distribution of axial velocity was predictable. In each case, uniform unswirled upstream flow was passed through a stator blade row within a cylindrical-walled duct to produce flow with a swirl angle distributed according to some simple function of radius. The analytical axial velocity profiles were reproduced to good accuracy in the far downstream flow, where meridional streamline slope and curvature had settled to zero. Small errors are attributed to the radial repositioning of streamlines after exit from the blade row, and these errors were greater for cases modelling compressible flow than for those assuming incompressible flow.

A test example given by Hirsch (1976) of incompressible flow within a 'swan-necked' transition duct was successfully modelled to show that the program could handle problems with flared wall duct geometry and with sweptback calculation stations.

Experimental data were obtained from the works of Oxford (1965) and Gregory-Smith (1970), using the same apparatus, and of Fahmi (1968). A blade design based on Gregory-Smith's experimental guide vane exit flow

angle figures was not an exact reproduction of the actual blades used, designed by Oxford; the discrepancy in blade exit angle was as much as 5^{o} near the tip. This was because the programmed method of calculating flow deviation over-estimated the deviation found in practice, and Oxford's original design used different deviation calculations, which under-estimated the effect. The axial velocity profile close behind the blade trailing edges was simulated well, after smoothing the original flow angle data used (Gregory-Smith (1970)). The computed velocity profile further downstream departed from the experimental profile near the duct edges, but this is attributable to the considerable thickness of the annulus wall boundary layer by this distance downstream, an effect not modelled in the program.

The three-row compressor of Fahmi (1968) was modelled to demonstrate the ability to perform multi-row calculations. The axial velocity profile following the inlet guide vanes was not well reproduced, but the predicted velocity distributions behind the rotor and stator agree rather better with experimental results. The flow entering the compressor was non-uniform, as found in practice, and the flow through the blade rows was assumed to be irreversible, following loss predictions by Fahmi (1968). The numerical inadequacies in the computer program regarding the treatment of highly non-uniform portions of velocity profiles have been mentioned in Sections 8.9 and 10.3.

10.5 Three-Dimensional Flow

No firm proposals are put forward concerning the calculation of the blade-to-blade property variations in axial flow turbomachines. The full three-dimensional methods recently applied to centrifugal impellers are not suitable for multi-stage axial machines as present computer running times would be excessive. The mean fluid flow from an axial blade row incurs considerable flow angle deviation, indicating

that simple premises about the form of the blade-to-blade variations are unsuitable, e.g. Smith's (1966) assumption of linear variation across the passage of each fluid property.

Methods involving quasi-three-dimensional calculations using S1 surfaces which are constrained to be surfaces of revolution are proposed by several authors, e.g. Bosman and El-Shaarawi (1977), Novak and Hearsey (1977), Spurr (1980). In a machine with blade rows moving relative to one another it is necessary to assume axisymmetric flow and circular arc S1 surface shapes at entry to every blade row (unless time-variation of the flow is allowed), but the local flow behaviour within the blade row would be better determined if the S1 surfaces were allowed to twist in shape.

Wu (1952) analyses a method of obtaining blade-to-blade property variations without needing to define any S1 surface shape. A power series is formed with the first, second, etc. , θ-derivatives of each property, and these in turn are found from radial and axial gradients upon the mean S2 surface. The θ-derivatives of velocity are determined from an analysis based on vorticity definitions. The vorticity terms which appear in the resulting equations for the blade-to-blade velocity gradients are typically small compared with other terms, and may even be neglected. However, Wu (1952) envisages the mean S2 solution as the starting point for extending the flow field outwards, and this returns the problem to that of defining the blade-to-blade variation of the flow angles, the mean S2 surface not being representative of the mid-passage flow.

10.6 Future Work

10.6.1 Introduction

Recommendations made here for future study in the field of turbomachine flow calculation methods arise from two sources: those topics

included in the original wide brief at the start of the present work, but incompletely covered or not touched upon; and those arising from the analytical and computational work presented here.

10.6.2 Coverage of Original Brief

It was intended that the research programme could cover:

(i) Improvements in the streamline curvature method by examining the possibility of including:

  (a) the effects of the circumferential variations in flow and fluid properties,

  (b) a model for the annulus wall boundary layer,

  (c) secondary flow, using the new approach developed at Durham,

  (d) mixing of wakes

  (e) improved loss models.

(ii) A re-examination of alternative approaches to turbomachinery flow calculations, including time marching through-flow and McCune's work on transonic flow.

Preliminary requirements for part (i) (a) have been extensively covered, with the development of a method of intrablade axisymmetric flow calculation, including a mean S2 surface shape which conforms to the blade loading requirements at the leading and trailing edges. The blade design procedures also determine the surface shapes of the blades. The extension to blade-to-blade property calculations has not been achieved, beyond the acceptance of present quasi-three-dimensional techniques with their limitations, and the important problem to be faced appears to be the determination of the form of the flow angle variations across the blade passage, in view of the considerable mean flow deviation present in axial blade rows.

The annulus wall boundary layer, (i) (b), has not been considered in the development of a flow model, though the work of Gregory-Smith (1970)

indicates that it may become significantly thick and affect the main-stream flow behaviour. Horlock (1968) examines the experimentally-observed result that within a multi-stage axial compressor the boundary layer growth does not continue beyond about the second stage, but reaches a steady state.

Secondary flow calculations have been performed using a computer program of Gregory-Smith (1977); it would be advantageous to include such calculations automatically within the streamline curvature technique, even for the axisymmetric solution, as blade flow angles may be changed noticeably. The vorticity components found in the process would be needed in Wu's (1952) proposals for blade-to-blade calculations.

Part (i) (d), the mixing of wakes in the duct downstream of a row of blades, has been alluded to in the context of re-forming axisymmetric flow before entry to the next blade row. The vorticity components which appear in the blade wake, the trailing shed and trailing filament vorticities, are analysed by Came and Marsh (1974) for linear cascades, and should be derived for annular cascades as a development of that paper and of the work of Glynn and Marsh (1980) on intrablade secondary flow in annular cascades. In the wake behind a blade row, the mixing may be considered to be that of the distributed secondary vorticity with the trailing shed and trailing filament vorticities, but the mixing length is expected to be an empirical result based on experimental observations. From such considerations may be estimated the time variation of flow entering downstream blade rows.

The Consistent Loss Model forms a major contribution of the present work, and is shown to produce usable equations for the Streamline Curvature calculation method. However, the use of the loss model is best illustrated by analysing the flow in multi-stage machines with pressure loss data available; significant radial gradients of entropy may be expected in the latter stages and the use of the new loss model

will predict a different flow pattern there from other analyses. Suitable published experimental data are sparse; Chauvin and Weyer (1976) comment on the reluctance of research organisations to publish results. The requirement is for detailed data on intrablade losses, and the effects on the behaviour of multi-stage machines. The three-row axial compressor used as a test case in the present work does not fully test the loss model incorporated.

Regarding part (ii), research on Time-Marching Through-flow methods, with blade-to-blade calculations, has been conducted by Spurr (1980), overlapping in time with the present studies which have concentrated on the application of the Streamline Curvature approach. Spurr shows that the partial differential equations used in the Streamline Curvature analysis are elliptic for subsonic flow solutions, but hyperbolic for supersonic solutions. The Time-Marching approach allows transonic calculations by introducing into the flow unsteadiness with time, to give the same, hyperbolic, form to the equations in both subsonic and supersonic applications. The calculation method is conceived as stepping forward in time from an original flow field estimate. The method is lossless, and so more suited to modelling turbines, which are less sensitive to irreversiblities than are compressors, but it may be a promising path to pursue for the purposes of three-dimensional calculations.

10.6.3 Aspects of the Present Work

Theoretical studies may be possible to predict the extent of inter streamline energy migration in irreversible flows, and to express this in terms of the entropy loss and the change in total enthalpy (or rothalpy) along a streamline.

The transition curves imposed on the intrablade mean stream surface shape at blade entry and exit warrant further investigation because

their use implies that the mechanical blade loading is considerably higher in some regions and lower in others than otherwise assumed. It may be possible to deduce the loading pattern experimentally from cascades of blades instrumented for surface pressure measurement, or constructed with a segmented blade so that the loading on each segment may be measured.

The blade design procedure can be bettered by allowing more general design surface shapes, requiring iteration with the aerodynamic analysis to follow true streamlines. Flow deviation angles need to be estimated more accurately, particularly for blade rows which accelerate the flow such as inlet guide vanes, for which the departure from Howell's nominal operating condition cannot be estimated by his deviation method. The requirement in the program of duct calculation stations adjacent to blade rows should be removed.

Further analysis is required on the stability and convergence of the numerical techniques propounded here. The application of the relaxation process to the slope calculation may not yet be the optimum method and the relaxation factors themselves need to be re-analysed for use in their new location. The calculation grid should be improved so that the radial distribution of grid points at each station is defined by the user, and not limited to being uniformly spaced across the duct span.

It should be a straightforward matter to incorporate the secondary flow analysis into the Streamline Curvature program to estimate intra-blade flow angle adjustments.

The program needs to be proved more fully in regions of high loss and in multi-stage applications. The lack of suitable test data has been mentioned in Section 10.6.2.

The best approach to three-dimensional developments may be to plan for the introduction of computers sufficiently fast that full three-dimensional calculations may be performed, with the inlet flow to each blade row assumed axisymmetric. Beyond this, the understanding must

be advanced of the fluid mechanics involved in unsteady flow, boundary layers, flow losses and blade wakes, so that realism of the flow models may be improved; the complexity of available calculation methods will then be justified, and the expected computing power will be fully utilised.

APPENDIX A

The Calculation of Stagnation (Total) Property Values

A.1 Introduction

The stagnation value of a fluid property is its value if brought to rest reversibly and adiabatically, i.e. isentropically, relative to an observer, and if in a force field, relative also to some datum for potential energy level. Thus the stagnation value is the sum of the thermodynamic value (independent of an observer's velocity or position) and the components due to the relative kinetic and potential energies.

A.2 Entropy

Since by definition the fluid is assumed to be brought to rest isentropically, the stagnation entropy has the same value as the property static entropy, irrespective of an observer's velocity or position, or the strength of any force field.

A.3 Enthalpy

For a fluid flowing steadily and changing from state 1 to state 2, the steady-flow energy equation, per unit mass of fluid, may be written in the following manner:

Energy transfer by:			Changes in:		
Heat	Work		Enthalpy	Kinetic Energy	Potential Energy
$\dot{Q}$	$- \dot{W}_x$	$=$	$h_2 - h_1$	$+ \frac{1}{2}(W_2^2 - W_1^2)$	$-\int_{x_1}^{x_2} J \, dx$

where $\dot{Q}$ is rate of energy transfer by heat

$\dot{W}_x$ is rate of energy transfer by work

x is displacement from some datum within a force field

J is a function denoting strength of a force field acting upon the fluid, + ve J acting in the +ve x direction.

If the process 1 → 2 be that which brings an element of fluid to rest reversibly and adiabatically at the datum level, then

$$\dot{Q} = 0; \quad \dot{W}_x = 0.$$

When at rest,

$$W_2 = 0; \quad x_2 = 0.$$

Hence the change in enthalpy

$$h_2 - h_1 = \tfrac{1}{2} W_1^2 + \int_{x_1}^{0} J \, dx.$$

A.3.1 Stationary Observer

To an observer stationary on the earth, the J force (per unit mass) is the acceleration due to the earth's gravity, denoted g, and taking x as increasing with vertical distance above the earth,

$$J = -g.$$

g may be taken as constant over the small changes of height from the bottom to the top of a typical jet engine. Thus using suffix o to denote stagnation values,

$$h_o = h + \tfrac{1}{2} V^2 + g x,$$

where V is the fluid velocity relative to the stationary observer.

Furthermore for the purposes of this thesis, changes in gx encountered are small compared to other terms, and the potential energy change in the gravity field is neglected in the assumption of axial symmetry of flow properties. Thus in stationary blade rows and in ducts,

$$h_o = h + \tfrac{1}{2} V^2.$$

A.3.2 Observer Rotating at Angular Velocity ω

An observer on a blade row rotating at uniform angular velocity ω experiences a centripetal acceleration and the function J is in the form of an acceleration $(-\omega^2 r)$ in the r direction, whose magnitude varies with radius.

Thus the potential energy of a fluid element, taking the axis of rotation as zero datum, is

$$\int_r^0 r\omega^2 \, dr = -\tfrac{1}{2}\omega^2 r^2$$

If the fluid velocity be W relative to the rotating observer, the stagnation enthalpy relative to him, termed the rothalpy I, is

$$I = h + \tfrac{1}{2} W^2 - \tfrac{1}{2}\omega^2 r^2.$$

Denoting radial, circumferential and axial components of V and W by the suffices r, u and z respectively,

$$W_r = V_r$$

$$W_u = V_u - \omega r$$

$$W_z = V_z$$

Thus $I = h + \tfrac{1}{2}(V_r^2 + (V_u - \omega r)^2 + V_z^2 - \omega^2 r^2)$

$$\therefore \quad I = h + \tfrac{1}{2} V^2 - \omega r V_u.$$

$$\therefore \quad I = h_o - \omega r V_u.$$

Clearly when $\omega = 0$, $I = h_o$.

For any steady adiabatic flow, even if irreversible the summation of stagnation enthalpy over the entire mass flowrate passing any axial location is the same as at any other location. Where work transfer occurs, i.e. within rotors, it is the integral of rothalpy which remains constant. In reversible flow, or irreversible flow with no heat transfer within the fluid itself, the value of stagnation enthalpy (or of rothalpy) is constant along individual streamlines, and then

$$\left.\begin{aligned} &\frac{Dh_o}{Dt} = 0 \quad \text{(Ducts and stators)} \\ \text{or} \quad &\frac{DI}{Dt} = 0 \quad \text{(Rotors)} \end{aligned}\right\} \qquad \ldots \text{A.1}$$

In irreversible heat-conducting flow which is shearing, fluid friction transfers energy by heat from one streamline to another, and though the overall stagnation enthalpy (or rothalpy) level of the working

fluid is unchanging, equations A.1 no longer hold. This effect is referred to by Chauvin and Weyer (1976) as 'inter-streamline energy migration'. In assuming equations A.1 to be valid along irreversible streamlines, Bosman and Marsh (1974) and Horlock (1971) must also assume that no energy is transferred by heat within the fluid. Few real fluids exhibit this behaviour and Hong (1980) objects to such applications of equations A.1, but concedes that to do otherwise raises difficulties which are presently insurmountable.

A.4 Temperature

Assuming that the working fluid is a perfect gas, C_p and C_v may vary with temperature, but the difference is constant, the gas constant R:

$$C_p - C_v = R.$$

Further assuming that C_p is constant over the range of temperature of interest, then from its definition, i.e.

$$C_p = \left(\frac{\partial h}{\partial T}\right)_p,$$

the relationship between temperature changes and enthalpy changes may be obtained:

$$\Delta T = \Delta h/C_p$$

If the datum for temperature changes is chosen as absolute zero,

$$T = h/C_p.$$

Similarly for stagnation temperatures:

(i) in the stationary frame of reference

$$T_o = h_o/C_p \ ;$$

(ii) relative to a rotor

$$T_{o_{rel}} = I/C_p.$$

This last equation uses the definition of the stagnation condition as being the fluid at rest and on the axis of rotation. The temperature measured by a rotating observer at the radius of the original streamline, denoted $T_o'_{rel}$, is

$$T_o'_{rel} = (h + W^2/2)/C_p,$$

which does not include the effect of the radial shift through the centripetal force field.

A.5 Pressure

For a compressible gas, the simple form of Bernoulli's equation does not hold, but stagnation values of pressure, p_o, may be found from the temperature values, as follows.

Consider the following equation for entropy:

$$s_o - s = C_p \ln\left(\frac{T_o}{T}\right) - R \ln\left(\frac{p_o}{p}\right) .$$

For the isentropic process used to define stagnation property values

$$s_o - s = 0.$$

$$\therefore \quad \ln\left(\frac{p_o}{p}\right) = \frac{C_p}{R} \ln\left(\frac{T_o}{T}\right)$$

Now $$\frac{C_p}{R} = \frac{\gamma}{\gamma - 1}$$

Thus $$p_o = p\left(\frac{T_o}{T}\right)^{\gamma/(\gamma-1)}$$

A.6 Density

Density values are easily found from the perfect gas equation

$$\rho = \frac{p}{RT},$$

or for stagnation values

$$\rho_o = \frac{p_o}{RT_o} .$$

APPENDIX B

Co-ordinate Systems

B.1 r, θ, z Co-ordinates

The co-ordinates r, θ, z represent the usual radial, circumferential and axial cylindrical co-ordinates shown in Figure B.1.

r is taken as zero at the axis of rotation and increases with distances away from this centre. It has units of length.

θ has an arbitrary zero, and increases in the direction of rotation of rotors. Its units are dimensionless angles, so that circumferential distance is the product rθ.

z has an arbitrary zero position, and increases parallel to the machine axis in the direction of overall fluid flow.

B.2 m Co-ordinate

The meridional direction, co-ordinate m, is the streamline path projected onto a (r,z) plane of constant θ as in Figure B.2, so that for example

$$W_m^2 = W_r^2 + W_z^2.$$

There is no component of circumferential velocity in W_m.

For the general property q, the special derivatives (Appendix C) are related by

$$W_m \frac{\bar{\partial} q}{\partial m} = W_r \frac{\bar{\partial} q}{\partial r} + W_z \frac{\bar{\partial} q}{\partial z}$$

Components of quantities such as velocity, Mach Number, or vorticity, are denoted by the suffixes r, u, z or m and taken as positive in the same sense as the co-ordinates.

B.3 N, n, S Co-ordinates

The steamwise co-ordinate S is aligned to the relative velocity vector $\underline{W}$.

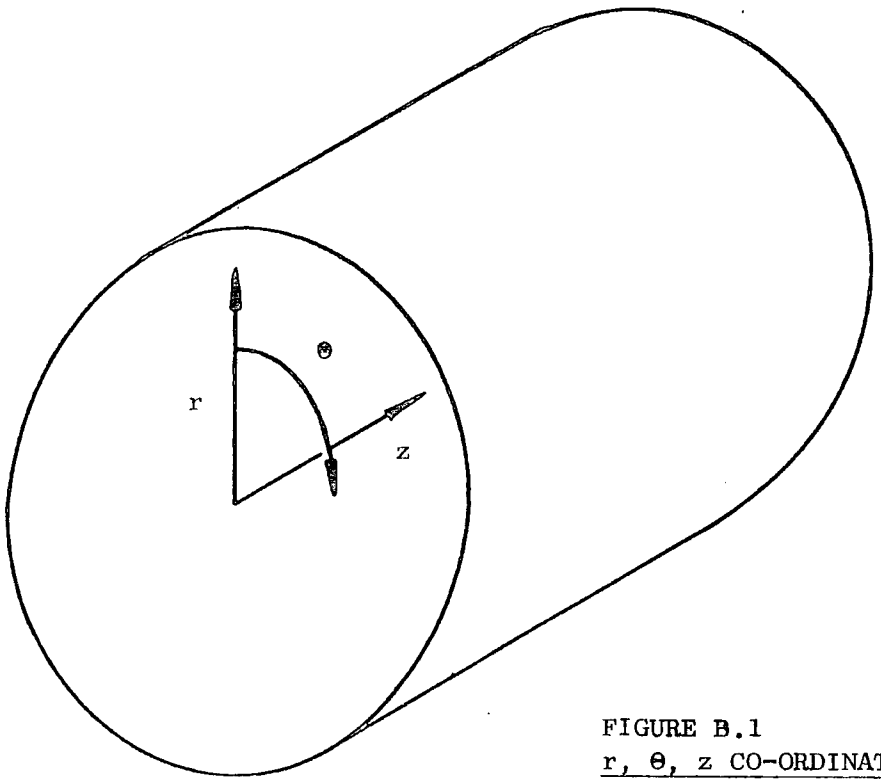

FIGURE B.1
r, θ, z CO-ORDINATES

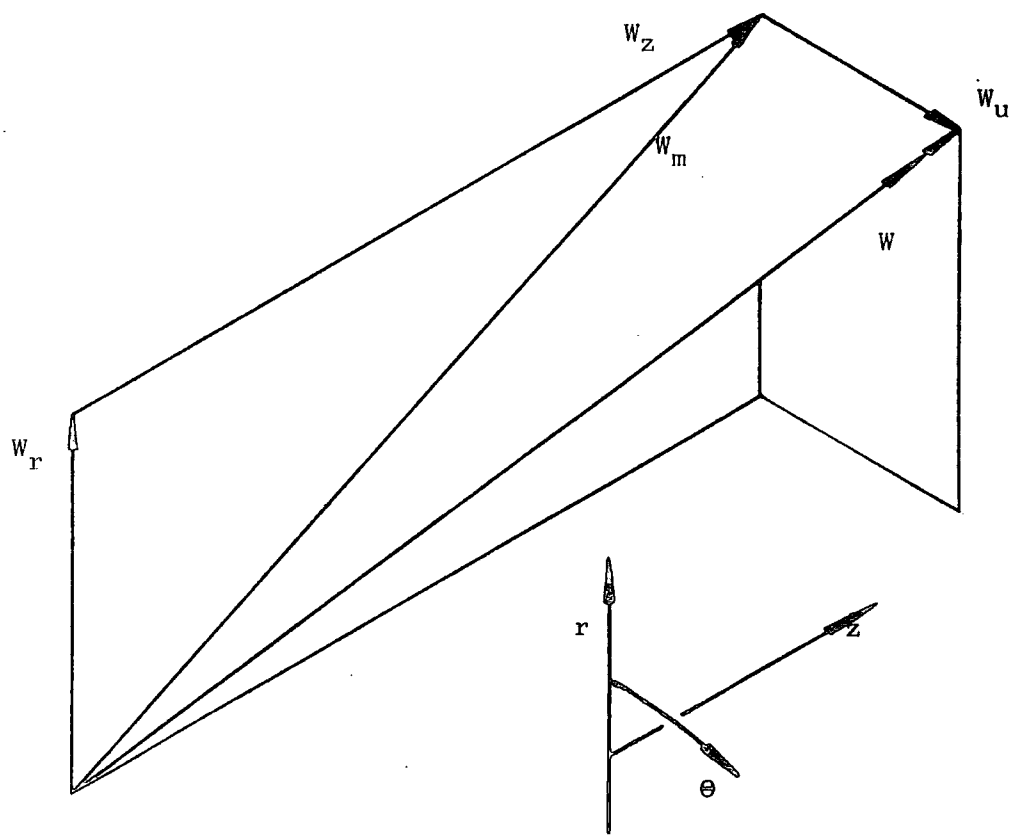

FIGURE B.2: MERIDIONAL CO-ORDINATE

Lying in the same type '2' stream surface is the N co-ordinate, normal to the flow.

The co-ordinate n is perpendicular to the stream surface, and is thus normal to both S and N co-ordinates.

N, n and S all have units of length and are shown in Figure B.3.

The positive directions of N, n and S are arbitrary, but it is convenient to set them such that

$$\frac{\partial S}{\partial z}, \quad \frac{\partial N}{\partial r} \text{ and } \frac{\partial n}{\partial \theta}$$

are all positive.

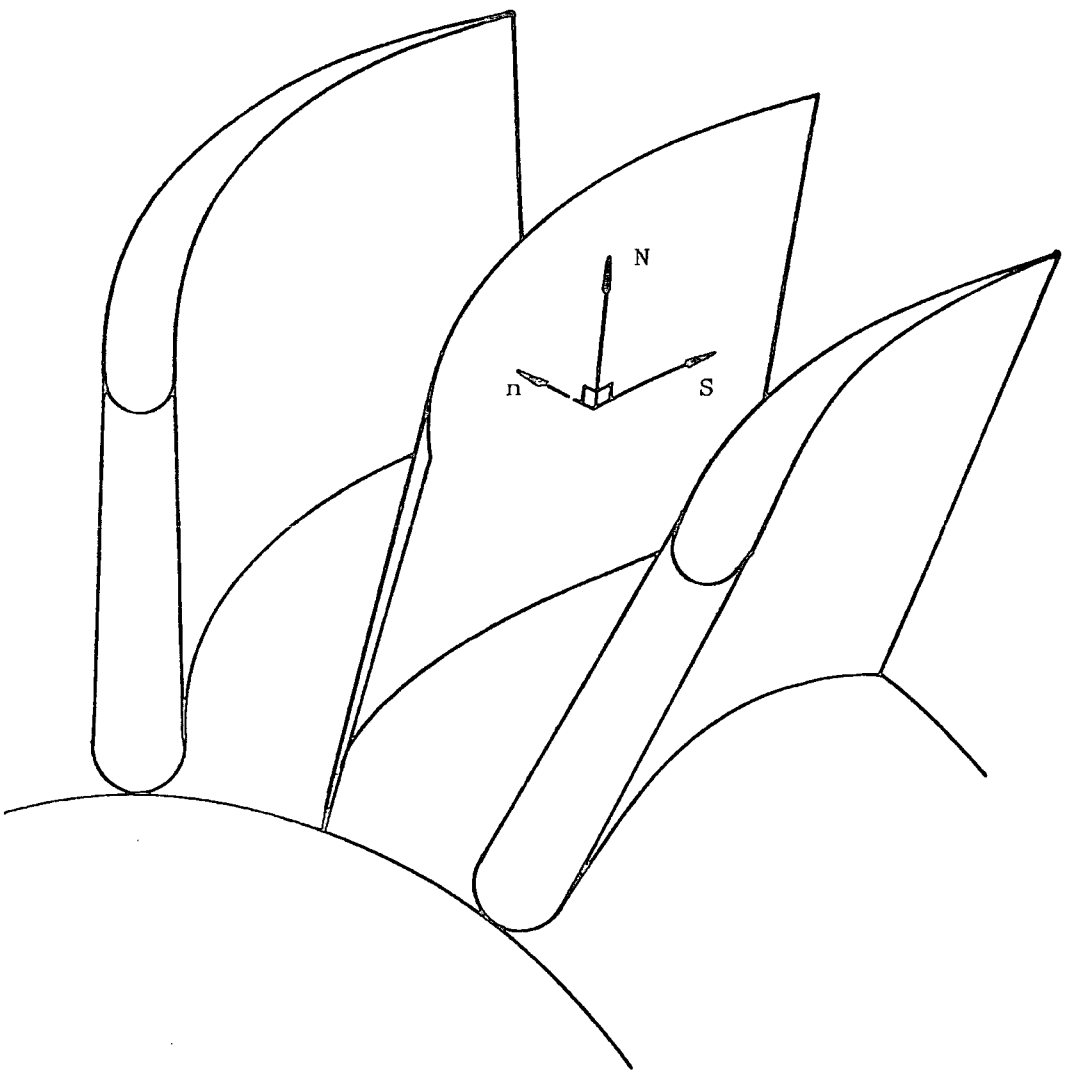

FIGURE B.3: N,n,S CO-ORDINATES

APPENDIX C

The Use of the Special Derivative

C.1 Special Derivatives on a Stream Surface

Let a stream surface be defined by

$$f(r,\theta,z) = 0.$$

If $\underline{\nu}$ is the unit vector normal to this surface, then

$$\frac{\nu_r}{\partial f/\partial r} = \frac{\nu_u}{\frac{1}{r}\partial f/\partial \theta} = \frac{\nu_z}{\partial f/\partial z} \quad .$$

If, for some property q, $\frac{\bar{\partial} q}{\partial r}$ and $\frac{\bar{\partial} q}{\partial z}$ are partial deriviaties taken along tne stream surface, then

$$\frac{\bar{\partial} q}{\partial r} = \frac{\partial q}{\partial r} - \frac{\nu_r}{r\nu_u}\frac{\partial q}{\partial \theta}$$

and

$$\frac{\bar{\partial} q}{\partial z} = \frac{\partial q}{\partial z} - \frac{\nu_z}{r\nu_u}\frac{\partial q}{\partial \theta} \quad .$$

The special derivative $\frac{\bar{\partial} q}{\partial r}$ is the rate of change of q with r on the stream surface at constant z, whereas $\frac{\partial q}{\partial r}$ is the rate of change of q with r at constant z and θ.

The vectors $\underline{\nu}$ and $\underline{F}$ both act in the n-direction in the N,n,S co-ordinate system, so that the components of $\underline{\nu}$ are proportional to the respective components of $\underline{F}$.

C.2 The Introduction of Special Derivatives in Forming Equations 3.3

No assumptions about axisymmetry have been made in obtaining equations 3.3 from equations 3.2. This may be demonstrated as follows, first re-analysing the θ-derivative of pressure.

$$\frac{dp}{\rho} = dh - Tds$$

and $$dh = dI - d\left(\frac{W^2}{2} - \frac{U^2}{2}\right)$$

$$\therefore \quad \frac{1}{\rho}\frac{\partial p}{\partial \theta} = \frac{\partial I}{\partial \theta} - T\frac{\partial s}{\partial \theta} + \frac{1}{2}\frac{\partial (U^2)}{\partial \theta}$$

$$-\frac{1}{2}\frac{\partial}{\partial \theta}\left(W_u^2 + W_r^2 + W_z^2\right) .$$

U is the blade speed, so $\frac{\partial U^2}{\partial \theta} = 0$.

$$\therefore \quad \frac{1}{\rho}\frac{\partial p}{\partial \theta} = \frac{\partial I}{\partial \theta} - T\frac{\partial s}{\partial \theta} - \left[W_u\frac{\partial W_u}{\partial \theta} + W_r\frac{\partial W_r}{\partial \theta} + W_z\frac{\partial W_z}{\partial \theta}\right] .$$

Following Wu (1952, equations 67 and 68), $\frac{\partial W_r}{\partial \theta}$ and $\frac{\partial W_z}{\partial \theta}$ may be replaced to give

$$\frac{1}{\rho}\frac{\partial p}{\partial \theta} = \frac{\partial I}{\partial \theta} - T\frac{\partial s}{\partial \theta} - \left[W_u\frac{\partial W_u}{\partial \theta} + W_r\left(\frac{\overline{\partial}(rV_u)}{\partial r} - r\xi_z + \frac{F_r}{F_u}\frac{\partial W_u}{\partial \theta}\right)\right.$$

$$\left. + W_z\left(\frac{\overline{\partial}(rV_u)}{\partial z} - r\xi_r + \frac{F_z}{F_u}\frac{\partial W_u}{\partial \theta}\right)\right]$$

$$= \frac{\partial I}{\partial \theta} - T\frac{\partial s}{\partial \theta} - \left[\frac{\partial W_u}{\partial \theta}\left(W_u - W_u\frac{F_u}{F_u}\right) + W_r\frac{\overline{\partial}(rV_u)}{\partial r}\right.$$

$$\left. + W_z\frac{\overline{\partial}(rV_u)}{\partial z} + r\left(W_z\xi_r - W_r\xi_z\right)\right] .$$

Evaluating the special derivatives,

$$\frac{1}{\rho}\frac{\partial p}{\partial \theta} = \frac{\partial I}{\partial \theta} - T\frac{\partial s}{\partial \theta} - \left[W_r\left(\frac{\partial (rV_u)}{\partial r} - \frac{\nu_r}{r\nu_u}\frac{\partial (rV_u)}{\partial \theta}\right)\right.$$

$$\left. + r\left(W_z\xi_r - W_r\xi_z\right) + W_z\left(\frac{\partial (rV_u)}{\partial z} - \frac{\nu_z}{r\nu_u}\frac{\partial (rV_u)}{\partial \theta}\right)\right]$$

$$= \frac{\partial I}{\partial \theta} - T\frac{\partial s}{\partial \theta} - \left[W_r\frac{\partial (rV_u)}{\partial r} + W_z\frac{\partial (rV_u)}{\partial z} + \frac{W_u}{r}\frac{\partial (rV_u)}{\partial \theta}\right.$$

$$\left. + r\left(W_z\xi_r - W_r\xi_z\right)\right] .$$

From the definitions of vorticity of Wu (1952),

$$\frac{1}{\rho}\frac{\partial p}{\partial \theta} = \frac{\partial I}{\partial \theta} - T\frac{\partial s}{\partial \theta} - \left[\frac{W_u}{r}\frac{\partial (rV_u)}{\partial r} + W_z\left(\frac{\partial (rV_u)}{\partial z} + \frac{\partial W_z}{\partial \theta} - \frac{\partial (rV_u)}{\partial z}\right)\right.$$

$$\left. + W_r\left(\frac{\partial (rV_u)}{\partial r} - \frac{\partial (rV_u)}{\partial r} + \frac{\partial W_r}{\partial \theta}\right)\right] .$$

$$\therefore \frac{1}{\rho}\frac{\partial p}{\partial \theta} = \frac{\partial I}{\partial \theta} - T\frac{\partial s}{\partial \theta} - \left[W_r\frac{\partial W_r}{\partial \theta} + \frac{W_u}{r}\frac{\partial (rV_u)}{\partial \theta} + W_z\frac{\partial W_z}{\partial \theta}\right] .$$

This is the desired form for the circumferential pressure gradient.

The body force $\underline{F}$ is defined by

$$\underline{F} = \frac{-1}{\rho r \nu_u}\frac{\partial p}{\partial \theta}\underline{\nu} ,$$

so that its components are

$$F_u = \frac{-\nu_u}{\rho r \nu_u}\frac{\partial p}{\partial \theta} = \frac{-1}{r\rho}\frac{\partial p}{\partial \theta} ,$$

$$F_r = \frac{-\nu_r}{\rho r \nu_u}\frac{\partial p}{\partial \theta}$$

and $$F_z = \frac{-\nu_z}{\rho r \nu_u}\frac{\partial p}{\partial \theta} .$$

Equations 3.2 may be analysed using the results for $\frac{\partial p}{\partial \theta}$ and for the components of $\underline{F}$, to produce equations 3.3. The procedure is similar for each equation; equation 3.2a is taken as an example:

$$\frac{W_u}{r}\left[\frac{\partial (rV_u)}{\partial r} - \frac{\partial V_r}{\partial \theta}\right] - W_z\left[\frac{\partial V_r}{\partial z} - \frac{\partial V_z}{\partial r}\right] = \frac{\partial I}{\partial r} - T\frac{\partial s}{\partial r} - D_r .$$

Using special derivatives gives

$$\frac{W_u}{r}\left[\overline{\frac{\partial}{\partial r}}(rV_u) + \frac{\nu_r}{r\nu_u}\frac{\partial (rV_u)}{\partial \theta} - \frac{\partial V_r}{\partial \theta}\right] - W_z\left[\overline{\frac{\partial V_r}{\partial z}} + \frac{\nu_z}{r\nu_u}\frac{\partial V_r}{\partial \theta} - \overline{\frac{\partial V_z}{\partial r}} - \frac{\nu_r}{r\nu_u}\frac{\partial V_z}{\partial \theta}\right]$$

$$= -\overline{\frac{\partial I}{\partial r}} + \frac{\nu_r}{r\nu_u}\frac{\partial I}{\partial \theta} - T\left[\overline{\frac{\partial s}{\partial r}} + \frac{\nu_r}{r\nu_u}\frac{\partial s}{\partial \theta}\right] - D_r .$$

$$\therefore \frac{W_u}{r}\frac{\partial(rV_u)}{\partial r} - W_z\left[\frac{\partial V_r}{\partial z} - \frac{\partial V_z}{\partial r}\right] = \frac{\partial I}{\partial r} - T\frac{\partial s}{\partial r} - D_r$$

$$-\left[\frac{W_u}{r}\left(\frac{\nu_r}{r\nu_u}\frac{\partial(rV_u)}{\partial\theta} - \frac{\partial V_r}{\partial\theta}\right) - W_z\left(\frac{\nu_z}{r\nu_u}\frac{\partial V_r}{\partial\theta} - \frac{\nu_r}{r\nu_u}\frac{\partial V_z}{\partial\theta}\right)\right.$$

$$\left. - \frac{\nu_r}{r\nu_u}\frac{\partial I}{\partial\theta} + T\frac{\nu_r}{r\nu_u}\frac{\partial s}{\partial\theta}\right] .$$

The contents of square bracket on the right hand side become

$$\frac{-\nu_r}{r\nu_u}\left[\frac{\partial I}{\partial\theta} - T\frac{\partial s}{\partial\theta} - \frac{W_u}{r}\frac{\partial(rV_u)}{\partial\theta} - W_z\frac{\partial V_z}{\partial\theta} + W_z\frac{\nu_z}{\nu_r}\frac{\partial V_r}{\partial\theta} + W_u\frac{\nu_u}{\nu_r}\frac{\partial V_r}{\partial\theta}\right]$$

$$= \frac{-\nu_r}{r\nu_u}\left[\frac{\partial I}{\partial\theta} - T\frac{\partial s}{\partial\theta} - W_r\frac{\partial V_r}{\partial\theta} - \frac{W_u}{r}\frac{\partial(rV_u)}{\partial\theta} - W_z\frac{\partial V_z}{\partial\theta}\right]$$

$$= \frac{-\nu_r}{r\nu_u}\frac{1}{\rho}\frac{\partial p}{\partial\theta}$$

$$= F_r .$$

$$\therefore \frac{W_u}{r}\frac{\partial(rV_u)}{\partial r} - W_z\left[\frac{\partial V_r}{\partial z} - \frac{\partial V_z}{\partial r}\right] = \frac{\partial I}{\partial r} - T\frac{\partial s}{\partial r} - D_r - F_r$$

which is equation 3.3a.

APPENDIX D

Blade Geometry

D.1 Blade Nomenclature

Angles marked in Figure D.1 are positive for rotor rotation to the left.

α_1 = fluid inlet angle

α_1' = blade inlet angle

α_2 = fluid outlet angle

α_2' = blade outlet angle

i = inlet incidence angle, $\alpha_1 - \alpha_1'$

δ = flow deviation angle, $\alpha_2 - \alpha_2'$

τ = stagger angle

υ = blade camber angle, $\alpha_1' - \alpha_2'$

N = number of blades

s = pitch of blades, $2\pi r/N$

c = chord length

b = maximum camber

a = location of maximum camber along chord line

t = blade thickness perpendicular to chord line

D.2 Howell's Deviation Rule

The deviation, δ, is introduced in Chapter 4. Given a required fluid outlet flow angle, it is necessary to find the deviation before the blade exit angle may be determined. Using the star superscript to denote Howell's 'nominal' operating conditions,

$$\delta^* = m\upsilon\left(\frac{s}{c}\right)^n ,$$

where for compressor cascades: $n = 0.5$, $m = 0.23\left(\frac{2a}{c}\right)^2 + \frac{|\alpha_2|}{500}$

(α_2 in degrees)

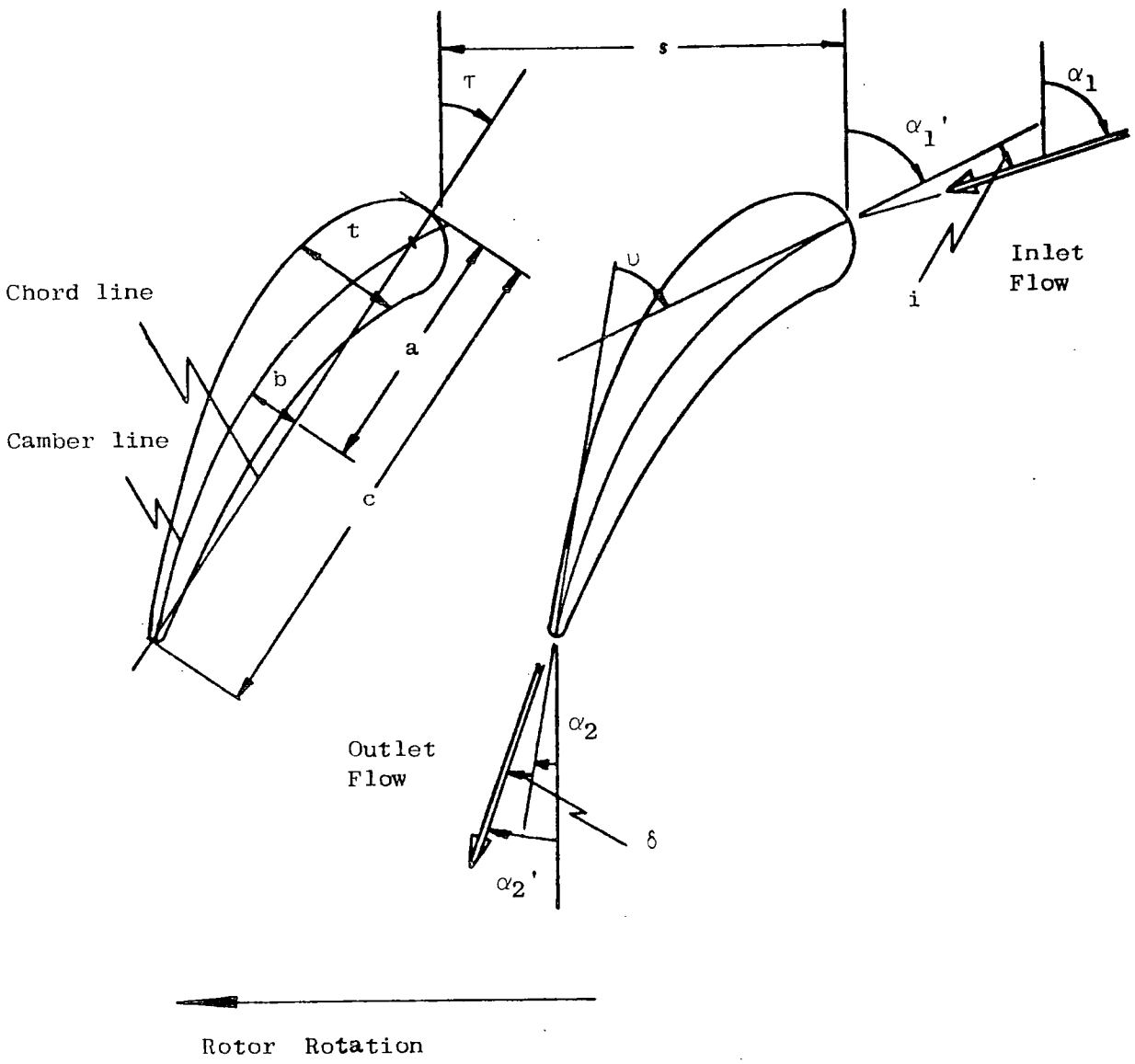

FIGURE D.1: BLADE NOMENCLATURE

and for inlet guide vanes and turbine cascades: $n = 0.1$, $m = 0.19$.

'a' is the distance along the chord line to the point of maximum camber. For circular arc camber lines $\frac{a}{c} = 0.5$; for parabolic camber lines $0.25 < \frac{a}{c} < 0.75$, but is normally set at about 0.4.

Howell's blade design method provides graphical adjustments to the deviation for operating conditions other than the 'nominal', but because the flow incidence is included as a variable, the nominal conditions may be satisfied by a range of cambers and associated staggers; the judgement of the designer is called for here. The computer program must be given the blade inlet angle.

The sign of the calculated deviation is inspected to ascertain that the effect of applying the deviation will be to lessen the turning caused by the blades.

APPENDIX E

Blade Design

E.1 Parabolic Camber Line Design

The blade inlet and exit angles which must be matched in designing a blade camber line, are given as angles from the axial direction. A parabolic camber line constructed using the η and ζ directions (Section 5.5) as the co-ordinate axes will be part of a parabola symmetrical about the η or ζ axis. The alternatives available from such geometry may not be suitable for practical blade design; for example, Figure E.1 shows a parabolic camber line for a blade row wherein the swirl is to be reduced to zero.

There is higher curvature towards the trailing edge than at the leading edge, making the blade row susceptible to flow separation from its convex surface.

By specifying the ratio a/c (Appendix D), the relative curvatures near the ends may be controlled in the design, but this extra parameter redefines the direction in the (η, ζ) plane of the axis of symmetry of the parabola.

The camber line may be designed by first constructing it on a parabola symmetrical about the η axis, matching the ratio a/c and only the difference between the blade inlet and exit angles, i.e. the camber angle υ. The whole construction is then rotated in the (η, ζ) plane so that the blade angles themselves are correct.

Figure E.2 shows the process diagramatically. Angles A and B are subtended between the ends of the camber line and the straight chord line. Clearly,

$$\sigma_1 - \sigma_2 = \upsilon = A - B.$$

Figure E.3 shows a construction of Rolls-Royce (undated) to determine A and B and hence the rotation required to produce the design camber line.

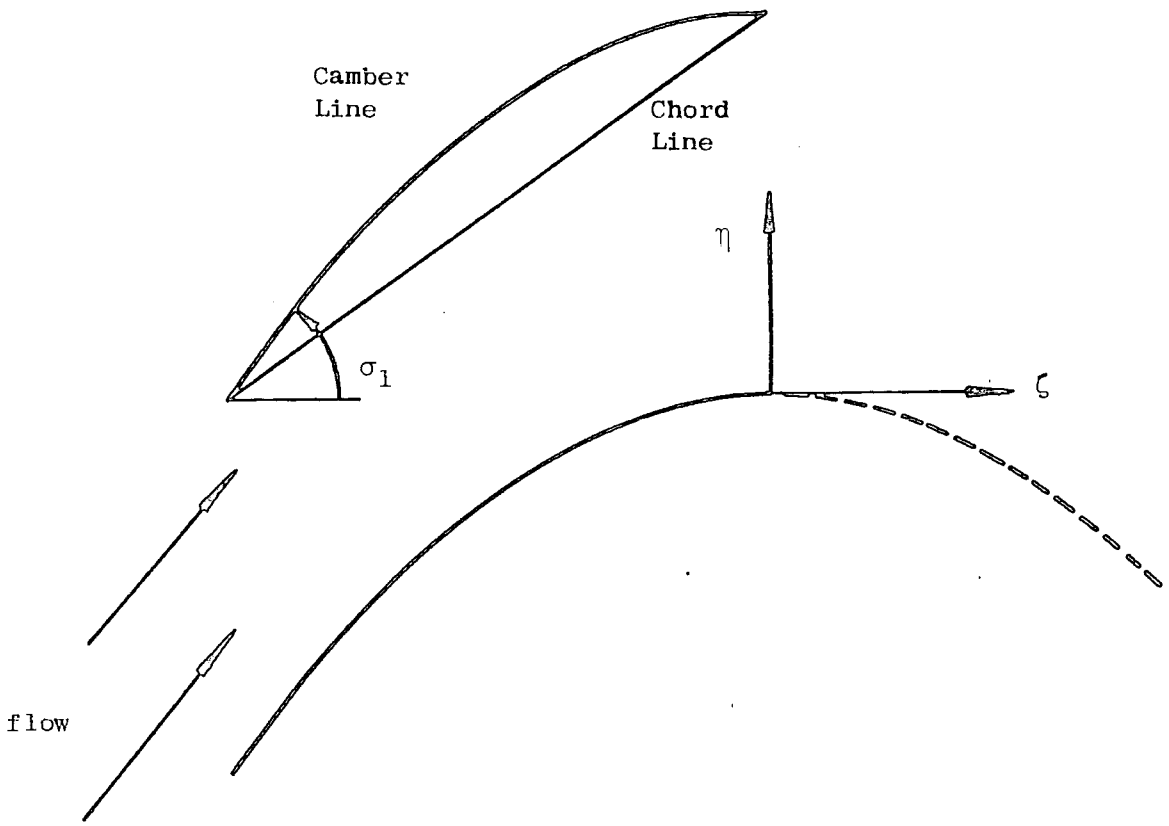

FIGURE E.1 : UNSUITABLE PARABOLIC CAMBER LINE

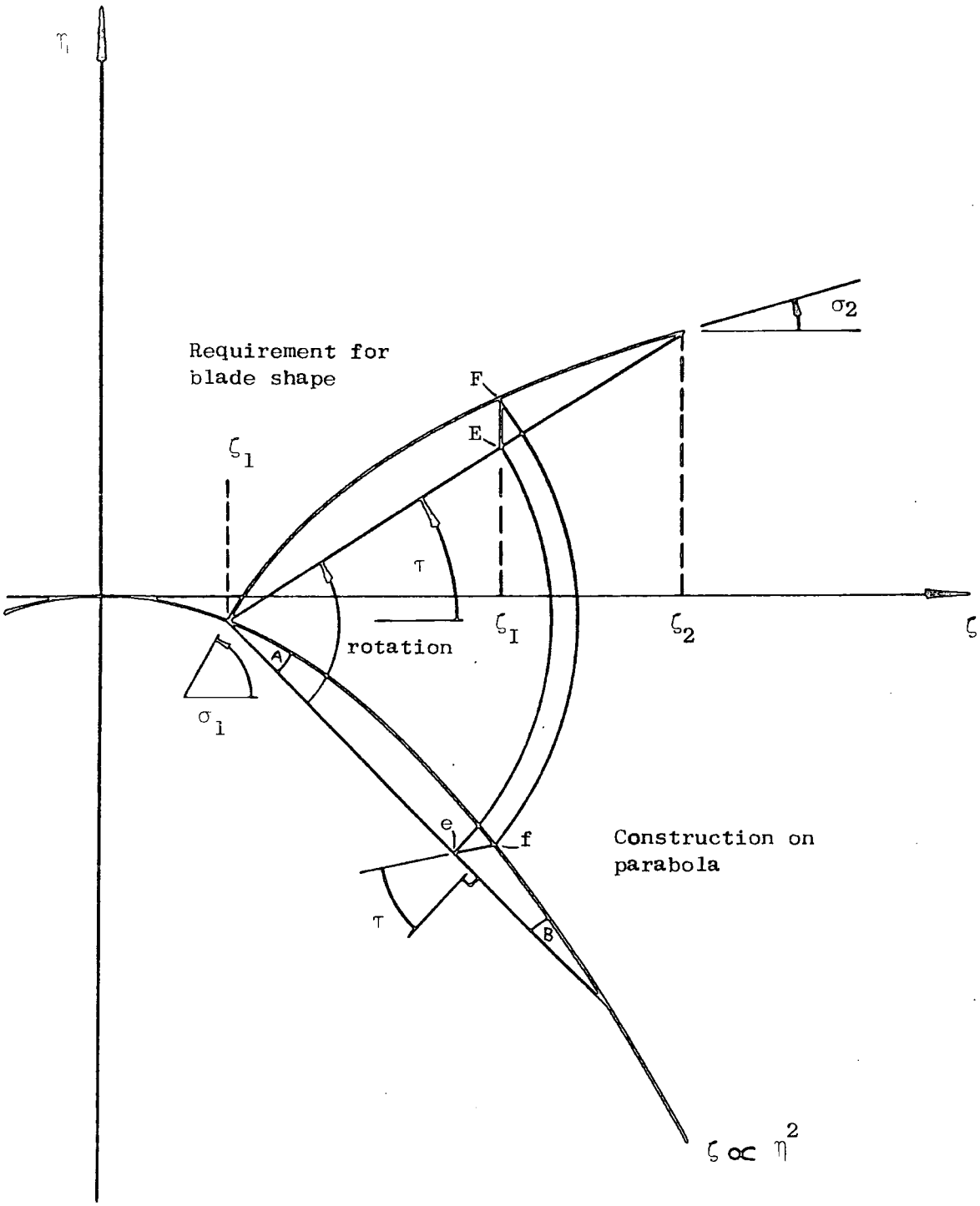

FIGURE E.2: CAMBER LINE DETERMINATION

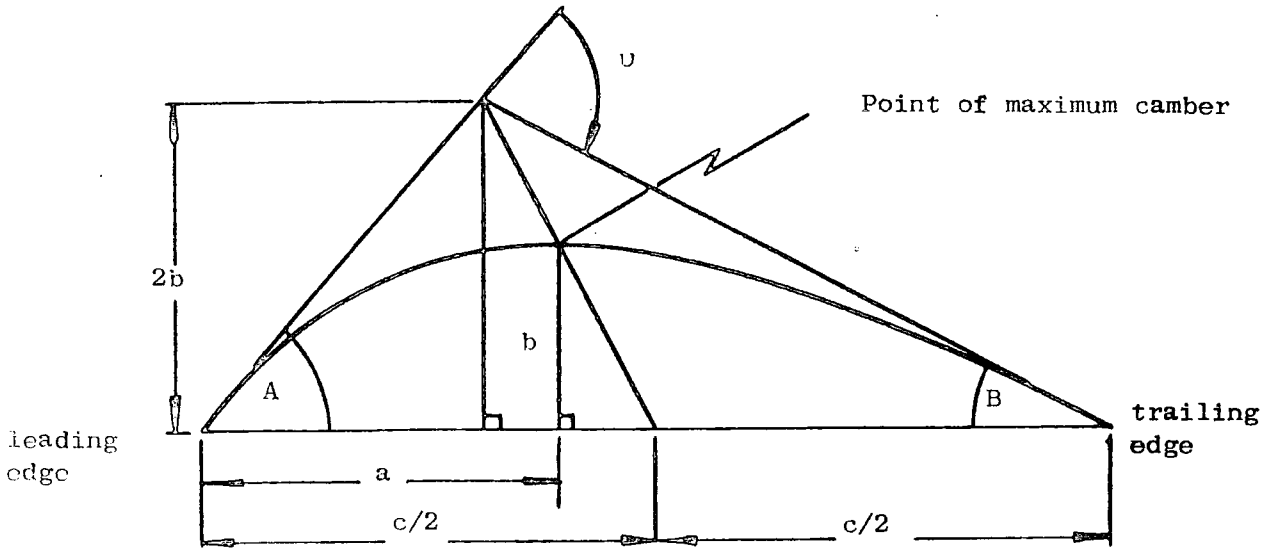

FIGURE E.3: SETTING a/c

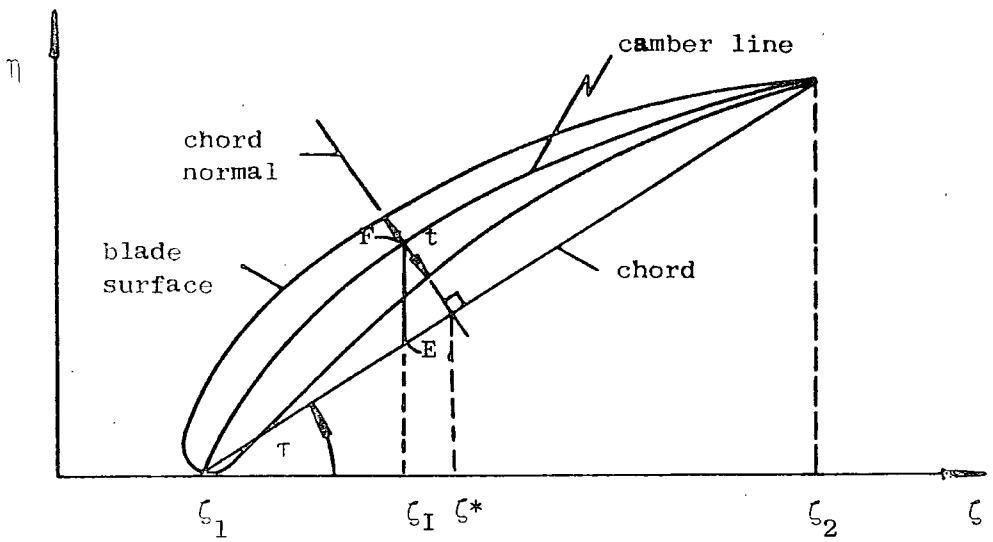

FIGURE E.4: APPLICATION OF BLADE THICKNESS

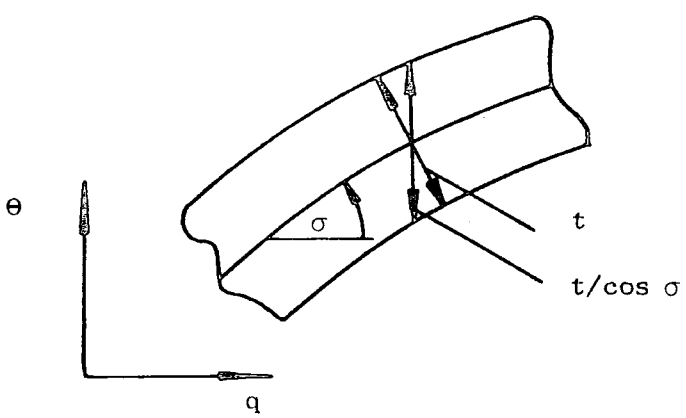

FIGURE E.5:
CIRCUMFERENTIAL COMPONENT OF BLADE THICKNESS

From the geometry of Figure E.3,

$$\tan A = \frac{2b}{2a - \frac{c}{2}} = \frac{4\,b/c}{4\,a/c - 1}$$

where $$\frac{4b}{c} = \frac{-1}{\tan v} \pm \sqrt{\frac{1}{\tan^2 v} + \left(\frac{4a}{c} - 1\right)\left(3 - \frac{4a}{c}\right)}$$

Referring to Figure E.2, points (ζ_1, η_1) and (ζ_2, η_2) are found as ends of the chord line. In determining intermediate loci on the camber line, e.g. point F, the corresponding value at f on the symmetrical parabola is more easily found. Values on the straight chord lines e and E are also simply found. The lengths ef and EF being equal, the displacement at F can be calculated.

E.2 The Application of Aerofoil Thickness Distribution Data to the Transformed Aerofoil

The specification of an aerofoil profile includes the variation of the material thickness with distance along the chord line. The maximum thickness, t_{max}, is given as a proportion of the chord line length, e.g. $\frac{t_{max}}{c} = 0.1$, and the value of t/t_{max} is given every few per cent of chord line length.

If ζ_I is the mapped q value of a grid point at which the thickness is desired, then t/t_{max} must be found, not at $\zeta = \zeta_I$, but at some other value $\zeta = \zeta^*$, where the chord-normal, through ζ_I on the camber line, intersects the chord. Figure E.4 shows this construction.

The length EF being known from the considerations of Section E.1,

$$\zeta^* - \zeta_I = EF \sin\tau \cos\tau \ .$$

Figure E.5 shows that if the local blade angle is σ, then the circumferential component of thickness is $t/\cos\sigma$. For a row of N blades, the "Blockage Factor" B, at radius r is then

$$B = 1 - \frac{Nt/\cos\sigma}{2\pi r} \ .$$

REFERENCES

Bez, H. (1978) On The Conformal Mapping Program in Q305. Rolls-Royce Ltd., TGR 90127.

Bosman, C. and El-Shaarawi, M.A.I. (1977) Quasi-Three-Dimensional Numerical Solution of Flow in Turbomachines. Journal of Fluids Engineering, Trans. A.S.M.E. Series I, Vol. 99, pp. 132-140.

Bosman, C. and Marsh, H. (1974) An Improved Method for Calculating the Flow in Turbo-machines, Including a Consistent Loss Model. J. Mech. Eng. Sci., Vol. 16, No. 1, pp. 25 - 31.

Came, P.M. and Marsh, H. (1974) Secondary Flow in Cascades: Two Simple Derivations for the Components of Vorticity. J. Mech. Eng. Sci., Vol. 16, No. 6, pp. 391-401.

Chauvin, J. and Weyer, H. (1976) Turbomachinery Through-Flow Calculation Methods - Technical Evaluation Report. AGARD-CP-195, Through-flow Calculations in Axial Turbomachinery, Köln.

Cohen, H., Rogers, G.F.C., and Saravanamuttoo, H.I.H. (1972) Gas Turbine Theory, 2nd Ed., Longman.

Cohen, H. and White, E.M. (1943) The Theoretical Determination of the Three Dimensional Flow in an Axial Compressor, with Special Reference to Constant Reaction Blading. A.R.C. Rep. No. 6842.

Denton, J.D. (1978) Throughflow Calculations for Transonic Axial Flow Turbines. Journal of Engineering for Power, Trans. ASME Series A, Vol. 100, pp. 212-218.

Dixon, S.L. (1975) Fluid Mechanics, Thermodynamics of Turbo-Machinery. 2nd Ed., Pergamon.

Fahmi, G.J.S. (1968) The Performance of Two Axial-Flow Compressors of Differing Blade Aspect Ratio. University of Liverpool Department of Mechanical Engineering. Also, Gas Turbine Collaborative Committee Paper No. Aero 700.

Frost, D.A. (1972) A Streamline Curvature Through-Flow Computer Program for Analysing the Flow Through Axial-Flow Turbomachines. A.R.C. R. & M. No. 3687.

Glynn, D.R. and Marsh, H. (1980) Secondary Flow in Annular Cascades. International Journal of Heat and Fluid Flow, Vol. 2, No. 1, pp. 29-33.

Gregory-Smith, D.G. (1970) Annulus Wall Boundary Layers in Turbo-Machines. Ph.D. Thesis, Cambridge University.

Gregory-Smith, D.G. (1977) Secondary Flow Program Q348R for Annular Cascades. Description and Users' Guide. Rolls-Royce Ltd., TRR 90191.

Hirsch, Ch. (1976) Finite Element Method for Through-Flow Calculations. AGARD-CP-195, Through-flow Calculations in Axial Turbomachinery, Köln.

Hirsch, Ch., and Warzee, G. (1978). An Integrated Quasi-Three-Dimensional Finite Element Calculation Program for Turbo-Machinery Flows. ASME Paper 78-GT-56.

Hong Hejing (1980) Aerodynamic Calculations Using S2 Stream-Surface Flow of Non-Radial Calculation Station in Turbomachine Blade Passage. Engineering Thermo-physics in China, Vol. 1, pp. 111 - 129, translated by Rumford Publishing Co., Inc.

Horlock, J.H. (1958) Axial Flow Compressors. Butterworth

Horlock, J.H. (1966) Axial Flow Turbines. Butterworth

Horlock, J.H. (1968) End Wall Effects in Ultimate Steady Flow In An Axial Flow Compressor. Gas Turbine Collaborative Committee, Paper No. 625.

Horlock, J.H. (1971) On Entropy Production in Adiabatic Flow in Turbomachines. Journal of Basic Engineering, Trans. ASME Series D, Vol. 93, pp. 587 - 593.

Horlock, J.H. (1978) Actuator Disc Theory. McGraw-Hill.

Horlock, J.H. and Marsh, H. (1971) Flow Models for Turbomachines. J.Mech. Eng. Sci., Vol. 13, No. 5, pp. 358 - 368.

Jones, R.W. (1969) Three-Dimensional Flow in Annular Cascades. Ph.D. Thesis, Cambridge University.

Krimerman, Y. and Adler, D. (1978) The Complete Three-Dimensional Calculation of the Compressible Flow Field in Turbo Impellers. J.Mech.Eng.Sci., Vol. 20, No. 3 pp. 149 - 158.

Marsh, H. (1968) A Digital Computer Program for the Through-flow Fluid Mechanics in an Arbitrary Turbomachine Using a Matrix Method. A.R.C. R&M No. 3509.

Marsh, H. (1970) The Through-flow Analysis of Axial Flow Compressors. Cambridge University Engineering Department Report, CUED/A-Turbo/TR11.

Marsh, H. (1971) The Uniqueness of Turbomachinery Flow Calculations Using the Streamline Curvature and Matrix Through-Flow Methods. J. Mech. Eng. Sci., Vol. 13, No. 6, pp. 376 - 379.

Marsh. H. (1976) Secondary Flow in Cascades - The Effect of Compressibility. A.R.C. R&M No. 3778.

Novak, R.A. (1966) Streamline Curvature Computing Procedures for Fluid-Flow Problems. ASME Paper 66-WA/GT-3.

Novak, R.A. and Hearsey, R.M. (1977) A Nearly Three-Dimensional Intrablade Computing System for Turbomachinery. Journal of Fluids Engineering, Trans. ASME Series I, Vol. 99, pp. 154-166.

Oxford, J.T.B. (1965) A Rotating Cascade Wind Tunnel and a Rotating Aerofoil in Rotational Flow. Vols. I and II, Ph.D. Thesis, Cambridge University.

Petit Bois, G. (1961) Tables of Indefinite Integrals. Dover.

Rolls-Royce Ltd. (undated) Design Rules and Aids DRA21.

Shaalan, M.R.A. and Daneshyar, H. (1969) Methods of Calculating Slope and Curvature of Streamlines in Fluid Flow Problems. Cambridge University Engineering Department Report, CUED/A-Turbo/TR2.

Shaalan, M.R.A. and Daneshyar, H. (1972) A Critical Assessment of Methods of Calculating Slope and Curvature of Streamlines in Fluid Flow Problems. Proc. Inst. Mech. Eng., Vol. 186, No. 70, pp. 891 - 896.

Silvester, M.E. and Hetherington, R. (1966) Three-Dimensional Compressible Flow Through Axial Flow Turbomachines. Contained in: Numerical Analysis - an Introduction, Academic Press.

Smith, L.H. (1966) The Radial-Equilibrium Equation of Turbomachinery. Journal of Engineering for Power, Trans. ASME Series A, Vol. 88, pp. 1 - 12.

Spurr, A. (1980) A Computational and Experimental Study of Fully Three-Dimensional Transonic Flow in Turbomachinery. Ph.D. Thesis, University of Southampton.

Stow, P. (1971) An Optimum Relaxation Factor for the Method of Streamline Curvature. Rolls-Royce Ltd., TGR 90051.

Veuillot, J.-P. (1977) Calculation of the Quasi Three-Dimensional Flow in a Turbomachine Blade Row. Journal of Engineering for Power, Trans. ASME Series A, Vol. 99, pp. 53 - 62.

Wilkinson, D.H. (1970) Stability, Convergence, and Accuracy of Two-Dimensional Streamline Curvature Methods Using Quasi-orthogonals. Proc. Inst. Mech. Eng., Vol. 184, Part 3G(1), No. 35, pp. 108 - 119.

Wood, M.D. and Marlow, A.V. (1967) The Use of Numerical Methods for the Investigation of Flow in Water Pump Impellers. Proc. Inst. Mech. Eng., Vol. 181, Part 1, No. 29, pp. 725 - 748 and amendments.

Wu, Chung-Hua. (1952) A General Theory of Three-Dimensional Flow in Subsonic and Supersonic Turbomachines of Axial, Radial and Mixed-Flow Types. Trans. ASME, November 1952, pp. 1363 - 1380.